Electrical Parameters Extraction of 3D Structures

By

Mohamed Ouda

A Thesis

Submitted to the Faculty of Graduate Studies

in Partial Fulfilment of the Requirements

for the Degree of

Doctor of Philosophy

Department of Electrical and Computer Engineering

University of Manitoba

Winnipeg, Manitoba, Canada 1996

ISBN 0-612-16225-7

Canada

Name _____

Dissertation Abstracts International and *Masters Abstracts International* are arranged by broad, general subject categories. Please select the one subject which most nearly describes the content of your dissertation or thesis. Enter the corresponding four-digit code in the spaces provided.

Electrical, Electromagnetic
SUBJECT TERM

0554
SUBJECT CODE

UMI

Subject Categories

THE HUMANITIES AND SOCIAL SCIENCES

COMMUNICATIONS AND THE ARTS
Architecture 0729
Art History 0377
Cinema 0900
Dance 0378
Fine Arts 0357
Information Science 0723
Journalism 0391
Library Science 0399
Mass Communications 0708
Music 0413
Speech Communication 0459
Theater 0465

EDUCATION
General 0515
Administration 0514
Adult and Continuing 0516
Agricultural 0517
Art 0273
Bilingual and Multicultural 0282
Business 0688
Community College 0275
Curriculum and Instruction 0727
Early Childhood 0518
Elementary 0524
Finance 0277
Guidance and Counseling 0519
Health 0680
Higher 0745
History of 0520
Home Economics 0278
Industrial 0521
Language and Literature 0279
Mathematics 0280
Music 0522
Philosophy of 0998
Physical 0523
Psychology 0525
Reading 0535
Religious 0527
Sciences 0714
Secondary 0533
Social Sciences 0534
Sociology of 0340
Special 0529
Teacher Training 0530
Technology 0710
Tests and Measurements 0288
Vocational 0747

LANGUAGE, LITERATURE AND LINGUISTICS
Language
- General 0679
- Ancient 0289
- Linguistics 0290
- Modern 0291

Literature
- General 0401
- Classical 0294
- Comparative 0295
- Medieval 0297
- Modern 0298
- African 0316
- American 0591
- Asian 0305
- Canadian (English) 0352
- Canadian (French) 0355
- English 0593
- Germanic 0311
- Latin American 0312
- Middle Eastern 0315
- Romance 0313
- Slavic and East European 0314

PHILOSOPHY, RELIGION AND THEOLOGY
Philosophy 0422
Religion
- General 0318
- Biblical Studies 0321
- Clergy 0319
- History of 0320
- Philosophy of 0322

Theology 0469

SOCIAL SCIENCES
American Studies 0323
Anthropology
- Archaeology 0324
- Cultural 0326
- Physical 0327

Business Administration
- General 0310
- Accounting 0272
- Banking 0770
- Management 0454
- Marketing 0338

Canadian Studies 0385
Economics
- General 0501
- Agricultural 0503
- Commerce-Business 0505
- Finance 0508
- History 0509
- Labor 0510
- Theory 0511

Folklore 0358
Geography 0366
Gerontology 0351
History
- General 0578
- Ancient 0579
- Medieval 0581
- Modern 0582
- Black 0328
- African 0331
- Asia, Australia and Oceania 0332
- Canadian 0334
- European 0335
- Latin American 0336
- Middle Eastern 0333
- United States 0337

History of Science 0585
Law 0398
Political Science
- General 0615
- International Law and Relations 0616
- Public Administration 0617

Recreation 0814
Social Work 0452
Sociology
- General 0626
- Criminology and Penology ... 0627
- Demography 0938
- Ethnic and Racial Studies 0631
- Individual and Family Studies 0628
- Industrial and Labor Relations 0629
- Public and Social Welfare 0630
- Social Structure and Development 0700
- Theory and Methods 0344

Transportation 0709
Urban and Regional Planning 0999
Women's Studies 0453

THE SCIENCES AND ENGINEERING

BIOLOGICAL SCIENCES
Agriculture
- General 0473
- Agronomy 0285
- Animal Culture and Nutrition 0475
- Animal Pathology 0476
- Food Science and Technology 0359
- Forestry and Wildlife 0478
- Plant Culture 0479
- Plant Pathology 0480
- Plant Physiology 0817
- Range Management 0777
- Wood Technology 0746

Biology
- General 0306
- Anatomy 0287
- Biostatistics 0308
- Botany 0309
- Cell 0379
- Ecology 0329
- Entomology 0353
- Genetics 0369
- Limnology 0793
- Microbiology 0410
- Molecular 0307
- Neuroscience 0317
- Oceanography 0416
- Physiology 0433
- Radiation 0821
- Veterinary Science 0778
- Zoology 0472

Biophysics
- General 0786
- Medical 0760

EARTH SCIENCES
Biogeochemistry 0425
Geochemistry 0996
Geodesy 0370
Geology 0372
Geophysics 0373
Hydrology 0388
Mineralogy 0411
Paleobotany 0345
Paleoecology 0426
Paleontology 0418
Paleozoology 0985
Palynology 0427
Physical Geography 0368
Physical Oceanography 0415

HEALTH AND ENVIRONMENTAL SCIENCES
Environmental Sciences 0768
Health Sciences
- General 0566
- Audiology 0300
- Chemotherapy 0992
- Dentistry 0567
- Education 0350
- Hospital Management 0769
- Human Development 0758
- Immunology 0982
- Medicine and Surgery 0564
- Mental Health 0347
- Nursing 0569
- Nutrition 0570
- Obstetrics and Gynecology .. 0380
- Occupational Health and Therapy 0354
- Ophthalmology 0381
- Pathology 0571
- Pharmacology 0419
- Pharmacy 0572
- Physical Therapy 0382
- Public Health 0573
- Radiology 0574
- Recreation 0575
- Speech Pathology 0460
- Toxicology 0383

Home Economics 0386

PHYSICAL SCIENCES
Pure Sciences
Chemistry
- General 0485
- Agricultural 0749
- Analytical 0486
- Biochemistry 0487
- Inorganic 0488
- Nuclear 0738
- Organic 0490
- Pharmaceutical 0491
- Physical 0494
- Polymer 0495
- Radiation 0754

Mathematics 0405
Physics
- General 0605
- Acoustics 0986
- Astronomy and Astrophysics 0606
- Atmospheric Science 0608
- Atomic 0748
- Electronics and Electricity 0607
- Elementary Particles and High Energy 0798
- Fluid and Plasma 0759
- Molecular 0609
- Nuclear 0610
- Optics 0752
- Radiation 0756
- Solid State 0611

Statistics 0463

Applied Sciences
Applied Mechanics 0346
Computer Science 0984
Engineering
- General 0537
- Aerospace 0538
- Agricultural 0539
- Automotive 0540
- Biomedical 0541
- Chemical 0542
- Civil 0543
- Electronics and Electrical 0544
- Heat and Thermodynamics ... 0348
- Hydraulic 0545
- Industrial 0546
- Marine 0547
- Materials Science 0794
- Mechanical 0548
- Metallurgy 0743
- Mining 0551
- Nuclear 0552
- Packaging 0549
- Petroleum 0765
- Sanitary and Municipal 0554
- System Science 0790

Geotechnology 0428
Operations Research 0796
Plastics Technology 0795
Textile Technology 0994

PSYCHOLOGY
General 0621
Behavioral 0384
Clinical 0622
Developmental 0620
Experimental 0623
Industrial 0624
Personality 0625
Physiological 0989
Psychobiology 0349
Psychometrics 0632
Social 0451

THE UNIVERSITY OF MANITOBA

FACUTY OF GRADUATE STUDIES

COPYRIGHT PERMISSION

ELECTRICAL PARAMETERS EXTRACTION OF 3D STRUCTURES

BY

MOHAMED OUDA

A Thesis/Practicum submitted to the Faculty of Graduate Studies of the University of Manitoba in partial fulfillment of the requirements for the degree of

DOCTOR OF PHILOSOPHY

Abstract

An efficient two-stage technique for the calculations of the capacitance and the conductance matrices of three-dimensional structures is developed. This technique minimizes the computational cost and memory storage requirements of the classical Integral Equation Method (IEM). By using this technique, the cost of analyzing a structure, consisting of m conductors, is reduced by an order of m^2. In addition, the memory storage requirement is reduced to that required for the solution of the largest conductor in the structure. The results obtained show the reduction of the computational cost and memory storage requirements. Furthermore, the results obtained using the two-stage method compare well with those obtained using the classical IEM.

In addition, a two-step approximate method is used for the extraction of the frequency dependent inductance and resistance matrices of three-dimensional structures. This two-step method is based on the Partial Element Equivalent Circuit (PEEC) method and the filaments approximation. The self inductance and resistance of each conductor in isolation are calculated using the PEEC method. The mutual inductances among the conductors are approximated using filaments approximation. Similarly, the computational cost is reduced by an order of m^2, for a structure consisting of m conductors. The memory storage requirement is reduced to that required for the solution of the largest conductor in the structure. Results

obtained using this method compare well with those obtained using the classical PEEC method.

Furthermore, the electrical parameters of some printed circuit board (PCB) structures obtained using the two-stage technique and the two-step approximate method are employed in the calcultations of crosstalk, ground-noise and radiated emissions. PCB structures are modelled using transmission line and lumped-circuit modelling. Transmission line modal analysis and HSPICE circuit simulator are used, in frequency and time domains, to obtain the voltage and current distributions on the traces of PCBs. The radiated fields are then calculated in the frequency domain using a simple radiation model.

Acknowledgements

Praise be to Allah for giving me the ability to carry out this work.

I would like to express my sincere gratitude to my supervisor, A. Sebak, for his advice, continuous encouragement and the many helpful discussions throughout the course of this research.

The assistance of A. Wexler in developing insight into the numerical computation problems that faces the industry is also greatly appreciated.

In addition, the helpful discussions with G. Bridges throughout the course of this research is highly appreciated.

I would also like to thank C. Schneider for his help in the generation of FASTCAP comparison data. Finally, I would like to acknowledge the financial assistance of the University of Manitoba and MICRONET.

Table of Contents

Abstract i

Acknowledgements iii

Chapter Page

List of Figures viii

List of Tables xii

1. Introduction 1

2. Literature Review 5

2.1 Statement of the Problem 6

2.1.1 The Capacitance and Conductance Matrices 6

2.1.2 The Inductance and Resistance Matrices 6

2.2 Integral Equation Method (IEM) 7

2.2.1 Capacitance Calculation 7

2.2.2 Inductance Calculations 9

2.2.3 The Geometry Dependent Green's Function 10

2.2.4 The Interface Integral Equation Approach 11

2.3 Partial Element Equivalent Circuit Method 14

2.4 Finite Element Method (FEM) 16

2.4.1 Capacitance Calculations 16

2.4.2 Inductance Calculations 17

2.5 Finite Difference Method (FDM) 19

2.6 Methods for Special Geometries 20

Chapter Page

2.7 Methods for Reducing Cost and Memory Requirements 21
2.8 Methods for Solving Large Electromagnetic Problems. 23
2.9 Signal Integrity Analysis 25
2.10 Conclusion 26

3. The Capacitance of Perfectly Conducting Structures 27
3.1 Statement of the Problem 28
3.2 Analysis 29
3.2.1 The Equivalent Charge Formulations 29
3.2.2 The Integral Equation Discretization 30
3.2.3 Point Matching Testing 31
3.3 The Two-Stage Method 33
3.4 Computational Time and Memory Storage Requirements 39
3.5 Results and Comparison 40
3.6 Numerical Considerations 49
3.6.1 The Surface Discretization 49
3.6.2 Evaluation of the Integrals 50

4. The Capacitance and Conductance Matrices 54
4.1 Statement of the Problem 55
4.2 Analysis 55
4.2.1 The Equivalent Charge Formulations 56
4.2.2 The Integral Equation Discretization 58
4.2.3 Point Matching Testing 59
4.2.4 Galerkin Testing 60
4.3 The Two-Stage Method 62
4.4 Computational Time and Memory Storage 67

Chapter Page

4.5 Results and Comparison 68

5. Frequency Dependent Inductance and Resistance Matrices . . . 73

5.1 Integral Equation Formulations 74

5.1.1 Nodal Analysis Formulation 78

5.1.2 Mesh Analysis Formulation 79

5.2 The Two-Step Solution 81

5.3 **Results and Comparison** 84

5.4 Generalization of the Algorithm 92

5.4.1 Inclusion of Ground Plane 92

5.4.2 Evaluation of the Partial Resistance 94

5.5 Volume Element Discretization 95

5.5.1 Meshing For Low Frequencies 96

5.5.2 Meshing For High Frequencies 97

6. Application 98

6.1 Frequency-Domain Transmission Line Analysis 99

6.1.1 Incorporating the Terminal Conditions 103

6.2 Lumped-Element Approximation 104

6.3 Frequency-Domain to Time-Domain Transformation 106

6.4 Crosstalk Analysis 108

6.4.1 Frequency-Domain Crosstalk Analysis 110

6.4.2 Time-Domain Crosstalk Analysis 118

6.5 Ground-Noise Calculations 122

6.6 Radiation Model 127

6.6.1 Formulations 128

6.6.2 Results and Comparison 129

Chapter Page

7. Conclusion 136

List of Figures

Figure		Page
2.1	*Charge distribution on the interfaces.*	8
2.2	*Volume meshing for the inductance calculation using the PEEC method*	15
3.1	*Normalized charge distribution on the upper plate of dimensions* 10 × 10 *m positioned on the Z=1 plane at unity potential and separated by 1 m from another identical plate positioned at Z=0 plane at zero potential.*	35
3.2	*Normalized charge distribution on one plate of dimensions* 10 × 10 *m positioned on the Z=0 plane at unity potential.*	35
3.3	*A structure consisting of two conductors*	36
3.4	*The capacitance of two transmission lines as a function of distance between the lines obtained using IEM and the two-stage method. The length of the line is 15cm*	44
3.5	*Cross section of the charge distribution on the upper plate of the geometry shown above obtained using the iterative method and the classical IEM.*	47
3.6	*Cross section of the charge distribution on plate one of the geometry shown above obtained using the iterative method and the classical IEM.*	48
4.1	*A structure consisting of two conductors*	56
4.2	*(a) An example of two conductor. (b) and(c) Discretization for the first stage solution.*	63
4.3	*Two traces over a dielectric with* $\hat{\epsilon}_r = 3(1 - tan\delta)$, $tan\delta = 0.001$.	70
4.4	*A system of four pin connectors*	72
5.1	*(a) A two-straight sectioned conductor, (b) circuit model*	76

Figure **Page**

5.2 (a) *A two-straight sectioned conductor, (b) circuit model* 79

5.3 *Example of two conductors* 82

5.4 *One conductor discretized to filaments, (b) modelled as a circuit* . . . 82

5.5 *Resistance and inductance of transmission line* 87

5.6 *Inductance of two parallel conductors as a function of conductors separation.* 88

5.7 *The inductance of two parallel conductors as a function of the conductors length.* 91

5.8 *Discretization of a finite ground plane in a width scale of 0.5:1* 92

5.9 *Two traces over infinite ground plane. (a) Original structure, (b) equivalent structure by image theory.* 93

5.10 *(a)Conductor with curved segment. (b) Discretized straight segments* . 96

5.11 *Low frequency meshing that accounts for the proximity effect.* 96

5.12 (a) *Medium to high frequency meshing.* (b) *High frequency meshing* . 97

6.1 (a) *A circuit of multiconductor transmission lines* 99

6.2 (a) *Lumped Pi model, (b) Lumped T model* 105

6.3 (a) *A single-input single-output linear system in time-domain, (b) A single-input single-output linear system in frequency-domain (c) representation of the MTL as a single-input single-output linear system* 106

6.4 *General trapezoidal pulse train* 108

6.5 *Three traces over a dielectric of permittivity* ϵ_r*=3.7* 109

6.6 *Three-conductor transmission lines model of the PCB* 110

6.7 *Spice Pi model of the PCB* 111

6.8 *A comparison of the frequency-domain near-end crosstalk voltages, calculated by using HSPICE and the modal analysis method.* 112

Figure **Page**

6.9 *A comparison of the frequency-domain far-end crosstalk voltages, calculated by using HSPICE and the modal analysis method.* 112

6.10 *A comparison of the frequency-domain near-end crosstalk voltages, calculated for a separation d=10, 20 and 30 mils* 114

6.11 *A comparison of the frequency-domain far-end crosstalk voltages, calculated for a separation d=10, 20 and 30 mils* 114

6.12 *PCB structure consisting of five traces and ground trace* 115

6.13 *The frequency-domain near-end crosstalk voltages* 117

6.14 *The frequency-domain far-end crosstalk voltages* 117

6.15 *Trapezoidal pulse train* 118

6.16 *A comparison of the time-domain near-end crosstalk voltages, calculated by using HSPICE and the modal analysis method.* 119

6.17 *A comparison of the time-domain far-end crosstalk voltages, calculated by using HSPICE and the modal analysis method.* 119

6.18 *A comparison of the time-domain near-end crosstalk voltages, calculated for a separation d=10, 20 and 30 mils* 120

6.19 *A comparison of the time-domain far-end crosstalk voltages, calculated for a separation d=10, 20 and 30 mils* 120

6.20 *Time-domain near-end crosstalk voltages obtained using trapezoidal pulse train with three different rise/fall times.* 121

6.21 *Time-domain far-end crosstalk voltages obtained using trapezoidal pulse train with three different rise/fall times.* 121

6.22 *Two traces over a dielectric of permittivity* ϵ_r*=3.7* 122

6.23 *Lumped-circuit ground-noise model for a two-conductor transmission line.* 123

Figure **Page**

6.24 *A comparison of the frequency-domain ground-noise voltages, calculated for load resistances of* R_L *=5, 50, 100 and 200* Ω. 125

6.25 *A comparison of the time-domain ground-noise voltages, calculated for load resistances of* R_L *=5, 50, 100 and 200* Ω. 125

6.26 *A comparison of the frequency-domain ground-noise voltages, calculated for a separation d=10, 20 and 40 mils.* 126

6.27 *A comparison of the time-domain ground-noise voltages, calculated for a separation d=10, 20 and 40 mils.* 126

6.28 *Cross section of microstrip structure consisting of two traces and ground plane* 131

6.29 *Radiation model* 132

6.30 *Two conductors configuration used for radiation results* 132

6.31 *Near-field emissions versus the angle* θ *with* $\phi = 90^o$ *and* $r = 1\lambda$ . . . 133

6.32 *Near-field emissions versus the angle* θ *with* $\phi = 0^o$ *and* $r = 1\lambda$ 133

6.33 *Radiation pattern versus the angle* θ *with* $\phi = 90^o$ *and* $r = 10\lambda$ . . . 134

6.34 *Radiation pattern versus the angle* θ *with* $\phi = 90^o$ *and* $r = 10\lambda$ . . . 134

6.35 *Radiation pattern versus the angle* θ *with* $\phi = 90^o$ *and* $r = 10\lambda$ . . . 135

List of Tables

Table | Page

3.1 *Comparison between the two-stage method and the IEM.* 41

3.2 *Comparison between the two-stage method and FASTCAP.* 41

3.3 *Comparison between the capacitance matrix of a system of 4 pins, as shown above, obtained using the two-stage method and FASTCAP. The unit of the capacitances is pF.* 45

3.4 *Comparison between the capacitance matrix of a system of 6 conductors, shown above, obtained using the two-stage method and FASTCAP. The unit is fF.* 46

4.1 *Comparison between the capacitance and conductance matrices of the system shown in Fig.* 4.2. *The unit of the capacitances is fF and the conductance is mS.* 70

4.2 *Comparison between the capacitance matrix of a microstrip structure. The units of the capacitances are fF.* 71

4.3 *Comparison between the capacitance matrix of a system of 4 connectors, as shown in Fig. 4.3. The units of the capacitances are fF.* . . . 72

5.1 *Comparison between the inductance matrix of a system of 6 connectors, as shown, obtained using the two-step approach and the classical PEEC method. The unit of the inductances is nH.* 89

5.2 *Comparison between the inductance matrix of a microstrip structure, as shown above, obtained using the two-step approach and the classical PEEC method. The dimensions are mm and the units of the inductances are nH.* 90

Table **Page**

6.1 *The general capacitance matrix in fF and the general inductance matrix in nH.* 109

6.2 *The capacitance matrix in pF and the inductance matrix in nH for a separation d = 10, 20 and 30 mils* 113

6.3 *The capacitance matrix in fF, the inductance matrix in nH and the resistance in mΩ* 116

6.4 *The capacitance matrix in fF and the inductance matrix in nH for a separation d = 10, 20 and 40 mils* 123

6.5 *The capacitance matrix in pF, the inductance matrix in nH and the resistance in mΩ* 131

Chapter 1

Introduction

In computer-aided design and analysis of high performance integrated circuits, it is important to study the effects of packaging and interconnections on signal integrity. The coupling among the stray interconnection which have extremely small physical dimensions strongly affects the performance of circuits, such as in dynamic memory cells, chip carriers and packaging connectors [1]. Careful control of package parasitics leads to improved circuit performance. The objective of this thesis is to consider methods and develop new techniques for the extraction of the package parasitics and to study the application of these electrical parameters in the signal integrity and EMC analysis. The four quasi-TEM electrical parameters which completely describe multiconductor structures are capacitance, inductance, resistance and conductance matrices. A review of the main numerical techniques used for parasitic extraction, namely, the integral equation method, the partial element equivalent circuit method and the finite element method is presented in Chapter 2. In addition, some of the less general methods and those methods developed for special geometries are discussed. The application of each method to practical structures with reference to the literature is then outlined.

In the integral equation method (IEM), the problem is formulated in terms of the charge distribution on the boundary for the capacitance and conductance cal-

culations; and in terms of the current density for the inductance and resistance calculations. Therefore, for the capacitance and conductance calculations, only the interfacing surfaces need to be discretized into surface elements. The open region problem is automatically handled by the IEM analysis. In the partial element equivalent circuit method (PEEC), capacitances are obtained using a three-dimensional boundary element method and the inductances are calculated using a volume-element integral equation formulation and general circuit network theory. For the finite element method, the potential distribution throughout the region is obtained. Therefore it requires the discretization of the entire domain of interest, with a special treatment for the open region problem.

In general, the numerical calculation of the electrical parameters of arbitrary three-dimensional geometries is very costly and requires very large storage memory. Various attempts have been made to reduce the memory storage and computational time required to calculate these parameters. However, these attempts are usually made for special geometries [2, 3, 4, 5] or do not result in considerable savings in the computational cost [6], [7] or in memory requirements [1], [8].

In this thesis, two approaches are developed to minimize the computational cost and memory requirements for the numerical calculations of capacitance, conductance, inductance and resistance matrices of arbitrary three-dimensional structures.

The proposed approach for the capacitance calculation, based on the integral equation method, is presented in Chapter 3. The capacitance matrix of a three-dimensional multiconductor, embedded in a homogeneous dielectric medium, is calculated in two stages. In the first stage, the structure is divided into sections. Then,

the integral equation method is used to obtain the charge distribution on each section in isolation from all other sections. In the second stage, the charge distribution obtained in the first stage is used to calculate the change in the total charge stored on each conductor in the environment of the whole system. A comparison between the classical IEM and the proposed method with respect to the computational cost and memory storage requirements is included. This comparison shows that the computational time and memory storage are significantly reduced. Results obtained using the new method compare well with those based on other techniques.

In chapter 4, the two-stage method presented in chapter 3 is extended to the extraction of the capacitance and conductance matrices of conductors embedded in arbitrary dielectric materials. The capacitance and conductance matrices are calculated in two stages. In the first stage, the structure is divided into blocks. Each block consists of a single conductor and all the dielectric-dielectric interfaces. The IEM method is then used to separately solve for the charge distribution on each block, thus neglecting the effect of all other blocks in the structure. In the second stage, the coupling among the conductors is included with the application of the IEM to the whole structure.

The frequency-dependent inductance and resistance matrices extraction of three-dimensional multiconductor system is included in chapter 5. The inductance and resistance matrices are calculated in two step. In the first step, the partial elements equivalent circuit method, (PEEC) [9], is used to calculate the self inductance and resistance of each conductor in isolation of all other conductors in the system. Then, in the second step, The filaments approximation given by Grover [10] are used

to approximate the mutual inductances among the conductors. The results are included and compared with those obtained using the partial element equivalent circuits method applied to the whole structure.

In chapter 6, the electrical parameters obtained in the previous chapters are employed in the quasi-static calculation of crosstalk and ground-noise in printed circuit boards (PCBs). Furthermore, radiation emissions from traces in PCBs are calculated using the current distribution obtain in the crosstalk analysis.

The near-end and far-end crosstalk voltages on the transmission lines are calculated by modal analysis and lumped-element model which is analyzed using HSPICE [11]. Ground-noise is calculated using a lumped-element approximations model . The time-domain response of the system is obtained from the frequency-domain response using Fourier transformation algorithm and by the transient analysis using HSPICE. The radiated field is calculated using the current distributions obtained from the crosstalk analysis and a simple radiation model.

Finally, the conclusions of this work is included in Chapter 7.

Chapter 2

Literature Review

This chapter presents a review of numerical methods employed for the calculations of the capacitance, conductance, inductance and resistance matrices of an arbitrary multiconductor system. Multiconductor transmission line models can be generated using these parameters. These models can then be used to analyze various electrical circuit behaviors that can be classified as signal integrity problems such as crosstalk, ground noise and bounce, dispersion and susceptibility [12]. Furthermore, the currents and voltages obtained using the transmission line models can be used to calculate the electromagnetic radiation and the electrical circuits compliance with the electromagnetic compatibility (EMC) compliance standards.

Three principal numerical techniques, namely, the integral equation method, the partial element equivalent circuit method and the finite element method are considered. Some of the less general methods and methods for special geometries are also discussed. In addition, the application of each method to practical structures with reference to the literature is outlined. Furthermore, some attempts to reduce the memory storage and computational time required to calculate these parameters are included.

2.1 Statement of the Problem

Consider a system consisting of m arbitrary ideal conductors embedded in a multiple dielectric region. The objective is to determine the electrical parameters of the system and to include some of the application of these parameters in the signal integrity and EMC analysis.

2.1.1 The Capacitance and Conductance Matrices

The complex capacitance matrix of such a system is an $m \times m$ symmetric matrix $\hat{\mathbf{C}}$ that represents the capacitance and conductance matrices of the system. The real part of the complex matrix, $\mathrm{Re}(\hat{\mathbf{C}})$, is the capacitance matrix of the system; the imaginary part, $\mathrm{Im}(\hat{\mathbf{C}})$, represents the conductance matrix of the system, or the dielectric losses. The ij^{th} element of the matrix is the free charge on the i^{th} conductor when all conductors except the j^{th} conductor are grounded and the j^{th} conductor is charged to a potential of 1 V. Hence, the elements of the capacitance matrix can be determined by relating the free charges on the conductors to the potential of these conductors.

2.1.2 The Inductance and Resistance Matrices

The inductance of such a system is an $m \times m$ symmetric matrix $\mathbf{L}$, and the resistance is $m \times m$ diagonal matrix $\mathbf{R}$. The two matrices can be obtained from the $m \times m$ impedance matrix $\mathbf{Z}$, where $\mathbf{Z} = \mathbf{R} + jw\mathbf{L} = \mathbf{Y}^{-1}$. The ij^{th} element of the $\mathbf{Y}$ matrix is the amount of current that flows on the i^{th} conductor when all conductors except

the j^{th} conductor are grounded and the j^{th} conductor is charged to a potential of 1 V. Hence, the elements of the $\mathbf{Z}$ matrix can be determined by relating the currents on these conductors to the potentials of the conductors.

Calculating the capacitance, inductance and resistance matrices of multiconductor structures can be done using a variety of numerical techniques available in the literature. Some of these numerical techniques are presented next.

2.2 Integral Equation Method (IEM)

The integral equation method is the most widely applied method for the extraction of capacitance and inductance matrices. The main advantages of this method are; its efficiency, simplicity of data preparation and automatic handling of open regions. The conductor surface and dielectric-dielectric interfaces need to be discretized when the free space Green's function is employed. By using a geometry dependent Green's function, only the conductor surfaces need to be discretized. However, the IEM formulation results in a dense matrix. This formulation limits the number of elements that can be accommodated due to the long solution time and large memory storage requirements.

2.2.1 Capacitance Calculation

All the conductor surfaces and dielectric-dielectric interfaces are replaced by unknown charge distributions and a potential distribution equivalent to that of the original system [13], Fig. 2.1. The charges consist of free charges on the conductor

surfaces, free and polarization charges on the conductor-dielectric interfaces and polarization charges alone on the dielectric-dielectric interfaces. The potential at any point is due to the cumulative effects of all present charges. The potential at any point r arising from a unit source charge at r' is given by

$$\phi(r) = \frac{1}{\epsilon_0} \int_s G(r, r')\sigma(r')ds' \tag{2.1}$$

where $G(r, r')$ is a proper Green's function, $\sigma(r')$ is the unknown charge density and ϵ_0 is the permittivity of free space.

Once the charge density $\sigma(r')$ has been obtained, the total charge on each conductor, Q_T, can be calculated from

$$Q_T = \int_S \sigma(r')ds' \tag{2.2}$$

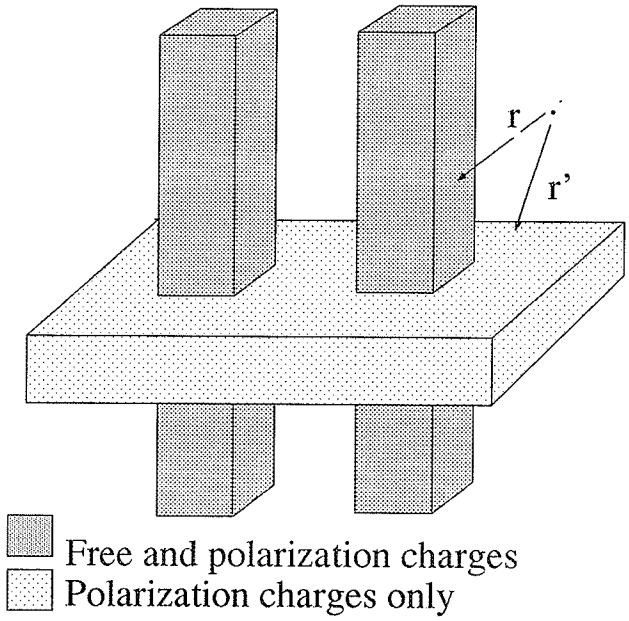

Figure 2.1: *Charge distribution on the interfaces.*

2.2.2 Inductance Calculations

The inductance matrix for a two-dimensional system, can be obtained directly from the capacitance matrix [14], using the following equation:

$$\mathbf{L} = \frac{1}{\mu_0 \epsilon_0}[\mathbf{C}_0]^{-1} \tag{2.3}$$

where L is called the lower bound inductance or the inductance at infinite frequency, μ_0 and ϵ_0 are the permeability and permittivity of the free space, respectively, and $[C_0]$ is the capacitance matrix obtained after removing all dielectric materials in the system; *i.e.*, the capacitance matrix for a system consisting of only perfect conducting materials.

The quasi-static analysis can be used to estimate the inductance as frequency dependent parameter. The vector integro-differential skin-effect equation is:

$$\frac{\mathbf{J}(r)}{\sigma} + \frac{jw\mu}{4\pi}\int_{v'} \frac{\mathbf{J}(r')}{\mid r - r' \mid} dv' = - \bigtriangledown \phi(r) \tag{2.4}$$

where $\mathbf{J}$ is the unknown current density, σ and μ are the conductivity and the permeability of the material, respectively, and ϕ is the potential imposed on the conductors.

The unknown current density distribution, $\mathbf{J}$, is to be evaluated for a given geometry and potential excitation ϕ. The inductance may be calculated from the following equations

$$\int_v \mathbf{A}.\mathbf{J}dv = LI^2 \tag{2.5}$$

$$[\int_v \mathbf{J}dv]^2 = I^2 \tag{2.6}$$

To solve (2.4), the homogeneous solution for **J** is evaluated; with the right hand side equals zero. Laplace's equation is then solved for ϕ for a given potential excitation, and hence $\nabla \phi$ is determined.

Practical systems with nonhomogeneous media can be handled by one of the following two approaches: A) The geometry dependent Green's function approach or B) The interface integral equation approach.

2.2.3 The Geometry Dependent Green's Function

The free-space Green's function may be modified to incorporate the effect of the dielectric-dielectric interfaces and the ground plane. Using this approach, only the conductor-dielectric interfaces need to be discretized and there is no need to truncate wide ground conductor and dielectric layers. Therefore, the interaction matrix is reduced in size and requires less time to be solved but each matrix element now takes additional computing time. However, the required Green's function can easily be found for some special systems such as: dielectric slab microstrip, homogeneous strip line configuration and other structures in which all dielectric interfaces and ground planes are planar, parallel, and infinite in extent. Green's function becomes very complicated as the number of layers increases. In general, finding the geometry dependent Green's function is difficult, making this approach impractical. The form of Green's function, for a special structure, may be determined from the interface boundary condition, together with image theory [15], transverse transmission line theory [16], or Fourier integrals [17].

The geometry dependent Green's function has been employed in various forms by many researchers. Weeks [15] approximated the surface charge density by piecewise-linear functions. He solved the Green's function for several transmission line configurations by applying a least squares minimization procedure to the integral equation. The capacitance of thin finite conductors on a dielectric sheet is calculated by Patel[17]. Taylor *et al.* [4] solved for the three-dimensional crossover capacitance between multilevel skewed circular lines above a ground plane. The charge density around the cylindrical conductor at any particular cross section was assumed constant. In addition, the dependence of the mutual capacitance on the intersection angle of the lines was investigated. Ning *et al.* [3] developed a three-dimensional boundary elements method for lines on a dielectric above a ground plane, in which the charge distribution is modeled by piecewise-linear trial functions. Thus the multiple integrals defining the system matrix elements were reduced to a single integral. Wu and Wu [2] employed structural symmetry and periodicity to reduce the number of unknowns in the problem; hence, reducing the memory storage requirements and computational cost. They introduced modified Green's functions which account for the symmetry and periodicity of the system.

2.2.4 The Interface Integral Equation Approach

The Green's function used in this approach is the simple free-space Green's function. A clear advantage of this approach over the geometry dependent Green's function technique is that this approach can handle systems with arbitrary configurations.

The main disadvantage is that the system matrix size is increased by the discretization of the dielectric-dielectric interfaces. In this approach all dielectric-dielectric interfaces are replaced by distributions of polarization charges that are considered to exist in free space. The following integral equation may be derived by applying the boundary conditions at the dielectric-dielectric interfaces

$$\frac{\epsilon_{r1}+\epsilon_{r2}}{2\epsilon_0}\sigma(r') - \frac{\epsilon_{r1}-\epsilon_{r2}}{\epsilon_0}\int \frac{\partial G(r,r')}{d\hat{n}}\sigma(r')dr' = 0 \tag{2.7}$$

where the direction of the normal $\hat{n}$ is into medium 2, and ϵ_{r1} and ϵ_{r2} are the permittivities of medium 1 and 2, respectively.

The interface integral equation approach has been used by various researchers. Two and three-dimensional microstrip configurations were investigated, by McDonald *et al.* [18] and [19], using variational solutions of the integral equations. The inclusion of special trial functions to handle singular field behavior near edges and corners improved convergences, especially when the functions are accurate. A simplified functional formula corresponding to the interface integral equation in two-dimensions is given by Jeng and Wexler [20]. They have treated three-dimensional problems by the same variational approach. This method allowed higher-order modelling of curved boundaries as well as higher-order polynomial trial functions for the unknown quantity [21]. The integration of the kernel over a curved boundary led to the finite error in the previous paper [21], and a technique using appropriately weighted Gaussian quadrature to integrate these kernels was detailed by Lean and Wexler [22]. In particular the handling of kernels with $ln \mid r \mid$ and r^{-1} behaviors is detailed.

Gopinath and Silvester [23] used an integro-differential skin-effect formulation to evaluate the inductance of arbitrary-shaped finite-length conducting strips over a ground plane. Smith and Cange [24] dealt with an open microstrip structure with finite-width dielectric in two-dimensions and investigated the effect of placing a signal line close to a dielectric edge. Wei *et al.* [25] calculated self and mutual capacitances and inductances of transmission line systems over an infinite ground plane, in two-dimensions. The dielectric interfaces allowed must be parallel to the ground plane. Three-dimensional structures were analyzed by Rao *et al.* [14] using a similar formulation. The charge was approximated using piecewise-constant trial functions on triangular subdomain with point matching for testing. The method of Wei *et al.* [25] was extended by Harrington and Wei [26] to account for shunt conductance. Series resistance was estimated by applying a perturbation method to each mode of the transmission line system. Venkatarman *et al.* [27] analyzed multiconductor transmission lines in multilayered lossy dielectric regions with a ground plane of finite extent. All surfaces and interfaces were considered as interfaces so that the interface equation alone would be sufficient to model a complete system. Interfaces of arbitrary orientation were allowed. Arbitrary geometries were modeled by Vekuda *et al.* [28] using just one boundary element method equation over multiple regions. The charge was approximated by linear discontinuous elements, and all integrations were done numerically with optimally computed integration orders. Nabors and White [1] presented a general three-dimensional capacitance extraction algorithm, FASTCAP. The multipole algorithm developed by Greengard [29] and an iterative matrix solver was used to reduce computation time.

2.3 Partial Element Equivalent Circuit Method

In this three-dimensional technique all conductors in a system are broken down into rectangular cells. The equivalent electrical circuit is obtained by computing the partial capacitances and inductances among these partial conductors, resulting in a mesh of circuit elements. Ruehli [30] developed the method to analyze three-dimensional multiconductor systems which could be described in terms of rectangular conductors or portions of a conductor. Self and mutual inductances between rectangular cells, or partial elements, were computed using the basic definition of inductance applied to small parts of a conductor loop, Fig. 2.2. The current flow in any two cells was assumed to be parallel or orthogonal; in the latter case the mutual inductance is zero. Another fundamental assumption was that current density should be constant over the cross section of any cell. The partial mutual inductance between the i^{th} and the j^{th}segments is given by

$$L_{ij} = \sum_{k=1}^{K} \sum_{m=1}^{M} S_{km} L_{p_{km}} \tag{2.8}$$

where K and M are numbers of elements on the i^{th} and the j^{th} segments, respectively, S_{km} represents the sign associated with the particular partial inductance and it depends on the direction of current flow in the segment, and

$$L_{p_{km}} = \frac{\mu}{4\pi} \frac{1}{a_k a_m} \int_{v_m} \int_{v_k} \frac{\mid dl_k . dl_m \mid}{\mid r_k - r_m \mid} dv_k dv_m \tag{2.9}$$

which can be evaluated using the filament approximations given by Grover [10].

The concept of partial capacitance, based on the three-dimensional boundary element method, was employed by Ruehli and Brennan in the calculation of capac-

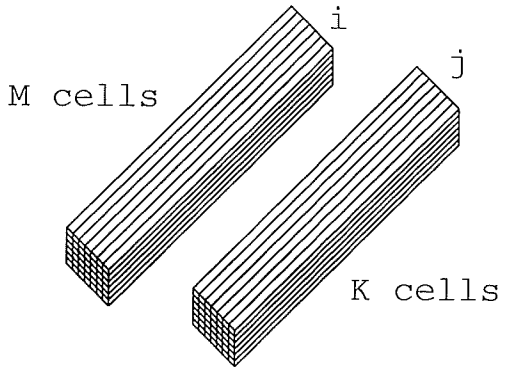

Figure 2.2: *Volume meshing for the inductance calculation using the PEEC method*

itance of three-dimensional structures [31]. As a result, the earlier formulation for inductance calculations was generalized to include both resistance and capacitance matrices [5]. This extended analysis technique is called the partial element equivalent circuit (PEEC) method. The capacitance matrix is calculated using surface integral equation formulation and the inductance and resistance matrices are obtained using integral equation formulation. By using this method, it is possible to determine the resistive, inductive and capacitive parameters of an interconnection system, with the restriction on the geometry arises from the Green's function approach to the capacitance calculation. This restriction stipulates that surfaces of conductors must conform with the Cartesian coordinates and thus it can be approximated by rectangular cells. In addition, all dielectric-dielectric interfaces and ground planes are assumed to be planar, parallel, and infinite in extent.

The frequency-dependent resistance and inductance of an L-shaped conductor were also investigated [32]. Additionally, a good agreement was obtained between measurement and responses from a PEEC solution for conductive loops - located on a dielectric substrate - for pulses with fast rise times [33]. The inductance of

a ground plane and connectors in high-performance computer hardware were analyzed [9]. Furthermore, Wu *et al.* [34] used the PEEC method to obtain the resistance and inductance of three-dimensional multiconductor interconnection structures. Kamon [8] used the multipole expansion technique, to minimize the computational cost of obtaining the inductance and resistance, of multiconductor structures.

2.4 Finite Element Method (FEM)

The potential distribution throughout the region of interest is calculated by the discretization of the region into a mesh. The mesh generation is a very complicated process and for open-region problems it is necessary to truncate the mesh at a finite distance. The meshing of the whole domain results in a very large number of unknowns and the solution of the problem is very costly and requires huge memory storage. The main advantage of this method is its capability of handling nonhomogeneous media; since each element may have its own material properties.

2.4.1 Capacitance Calculations

The FEM seeks the solution to Laplace's equation through the minimization of the function

$$F = \frac{1}{2}\int_v (\epsilon \bigtriangledown \phi . \bigtriangledown \phi) dv \tag{2.10}$$

or

$$F = \frac{1}{2}\int_v \mathbf{D}.\mathbf{E} dv \tag{2.11}$$

where $\mathbf{E} = -\nabla\phi$, $\mathbf{D} = \epsilon\mathbf{E}$ and v represents the whole space. F is equal to the electrostatic energy of the system.

Field energies may then be computed for each set of potential conditions and the capacitance is determined from

$$\mathbf{F} = \frac{1}{2}\mathbf{V}^2 C \tag{2.12}$$

where $\mathbf{V}$ is the set of enforced potentials and C is the capacitance. For a multiconductor system with one volt applied to the i^{th} conductor and all the other conductors in the system grounded, the capacitance is given by

$$C_{ij} = \int_v D_i . E_j dv \tag{2.13}$$

2.4.2 Inductance Calculations

The inductance matrix is computed from the field obtained by setting a unit current flow in one conductor and leaving all other conductors open [35]. Let H_p be the particular solution of Ampere's law

$$\nabla \times \mathbf{H}_{pi} = \mathbf{J_i} \tag{2.14}$$

where the current density $\mathbf{J}_i$ satisfies

$$\int_v J_i dv = \delta_{ij} \tag{2.15}$$

$\delta_{ij} = 1$ if i=j and $\delta_{ij} = 0$ otherwise.

The total magnetic field satisfies

$$H_i = H_{pi} + \nabla\psi_i \tag{2.16}$$

The particular solution $\mathbf{H}_p$ is computed locally by assigning tangential values of $\mathbf{H}_p$ to satisfy Ampere's law. The homogeneous solution ψ_i satisfies the Poisson equation

$$\nabla.\mu \nabla \psi_i = - \nabla .\mu \mathbf{H}_{pi} \tag{2.17}$$

where μ is the permeability of the materials.

The inductance matrix of the system of conductors is given by

$$\mathbf{L}_{ij} = \int_v \mathbf{B}_i.\mathbf{H}_j dv \tag{2.18}$$

where $\mathbf{B}_i = \mu \mathbf{H}_i$ is the magnetic flux density.

The finite element method has been applied to extract the capacitance and inductance matrices for two and three-dimensional systems. Olson [36] applied the finite element method program FIERCE to very general two-dimensional systems and obtained capacitance, inductance and resistance matrices. Cottrel and Buturla [37] explored the line-to-line coupling capacitance and crossover capacitance using a three-dimensional simulator. They also studied the effects of the parasitic coupling capacitance in the noise margin of logic and memory circuits. Additionally, Nayak *et al.* [38] used a two-dimensional FEM simulator to study signal propagations along coupled, lossy, thin-film microstrip lines. In this work, Poisson's equation was solved using a sinusoidal steady-state analysis to produce a frequency-dependent admittance matrix. Two and three-dimensional FEM for the quasi-TEM analysis of arbitrary interconnection structures was presented by Chou *et al.* [35]. They obtained the capacitance and inductance matrices of multiple coupled lines and lines with three-dimensional discontinuities.

2.5 Finite Difference Method (FDM)

For the finite-difference method, the potential distribution throughout the region must be determined in order to obtain the charge distribution on the conductors. The FDM starts by surrounding the conductors with artificial boundaries. The artificial boundaries are chosen to be sufficiently far away from the conductors to allow a zero Dirichlet condition as an acceptable approximation. Then, the domain of interest is discretized into a grid to approximate Laplace's equation. Next, the derivatives in Laplace's equation are replaced by divided differences, relating approximations to the potential at adjacent grid points. For a regular Cartesian grid, the potential at each point, $\psi(x_i, y_i, z_i)$, can be used along with its six neighboring points to write six approximate directional derivatives of the potential [39],

$$\begin{aligned}
\frac{\partial \psi}{\partial x_{i+}} &\equiv \frac{\psi(x_i + h, y_i, z_i) - \psi(x_i, y_i, z_i)}{h}; \\
\frac{\partial \psi}{\partial x_{i-}} &\equiv \frac{\psi(x_i - h, y_i, z_i) - \psi(x_i, y_i, z_i)}{h} \\
\frac{\partial \psi}{\partial y_{i+}} &\equiv \frac{\psi(x_i, y_i + h, z_i) - \psi(x_i, y_i, z_i)}{h}; \\
\frac{\partial \psi}{\partial y_{i-}} &\equiv \frac{\psi(x_i, y_i - h, z_i) - \psi(x_i, y_i, z_i)}{h} \\
\frac{\partial \psi}{\partial z_{i+}} &\equiv \frac{\psi(x_i, y_i, z_i + h) - \psi(x_i, y_i, z_i)}{h}; \\
\frac{\partial \psi}{\partial z_{i-}} &\equiv \frac{\psi(x_i, y_i, z_i - h) - \psi(x_i, y_i, z_i)}{h}
\end{aligned}$$

These quantities are combined for a cubic volume enclosing the n grid points, giving the linear system

$$\frac{\partial \psi}{\partial x_{i+}} + \frac{\partial \psi}{\partial x_{i-}} + \frac{\partial \psi}{\partial y_{i+}} + \frac{\partial \psi}{\partial y_{i-}} + \frac{\partial \psi}{\partial z_{i+}} + \frac{\partial \psi}{\partial z_{i-}} = 0 \quad i = 1, 2, ...n. \tag{2.19}$$

The finite-difference method has been used by Taylor *et al.* to obtain the capacitance of parallel [40] metalization lines. Fictitious boundaries were introduced to truncate infinite domains and the potential at these boundaries was estimated iteratively for each set of excitation voltages. Zemanian *et al.* [6] used a domain-contraction technique with the FDM to compute the capacitance for VLSI/ULSI interconnections. The semi-infinite domain in the three-dimensions was represented by terminating capacitors. This approach leads to a major reduction in the number of nodal points required. A facility for modeling round edges and corners was also included.

2.6 Methods for Special Geometries

Various methods have also been developed for highly specialized applications such as high voltage power application. Chow *et al.* [41] developed the optimized simulated charge method to obtain the capacitance matrix of conducting bodies and the potential field around them. The method used is based on an optimization of the classical method of images and it can be applied to any arbitrarily shaped conducting body. Chow and Yovanovich [42] showed that the capacitance is a slowly changing function of the conductor shape. They tabulated a shape factor, which is independent of the conductor size, for various conductor shapes. This shape factor

can be used to estimate the capacitance of conductors of arbitrary size and shapes with both convex and concave surfaces. Furthermore, a set of formulas has been developed, based on the shape factor for high voltage power applications [43], to estimate the induced voltage, currents and charges for conducting bodies under uniform and quasi-uniform electric fields . Maruvada and Hytenca [44] described a computer program for the calculation of a single conductor-to-ground capacitance. Its formulation is based on the method of images and the charge simulation method. They have obtained the capacitance for a number of basic electrode configurations used in high voltage power applications. A three-dimensional capacitance extraction algorithm which is suitable for parallel computers was developed by Guerrier and Sangiovanni-Vincentelli [45]. Grover [10] gave a nice collection of simple formulas based on filament approximation which can be used in the self and mutual inductance calculation of simple structures. Goldfarb and Pucel [46] presented a simple model for the inductance calculation of a via hole in a microstrip structure. The model is based on the simple formulas given by Grover [10]. More references can be found in [25].

2.7 Methods for Reducing Cost and Memory Requirements

Various attempts have been made to reduce the memory storage and computational time required for the analysis of multiconductor structures. A geometry

dependent Green's function for a particular structure was used to reduce the size of the matrix system, thus reducing the memory storage required and the cost of solving the system [2, 3, 13, 15, 17]. The filament approximations given by Grover [10] are employed in the inductance extraction, using the partial element equivalent circuit method [30, 32, 33, 9, 34]. Zemanian *et al.* [6] introduced the usage of terminating capacitors to represent the infinite domain; hence, reducing the number of nodal points required for the capacitance extraction using the finite difference method. Cangellaris *et al.* [7] combined the finite element method with the integral equation method to calculate the frequency-dependent inductance and resistance matrices, for three-dimensional structures in high-speed interconnect systems. The IEM method reduces the number of equations required for the solution and, at the same time, the non-linear regions can be represented by the FEM. The computation time required to evaluate the Green's function integral equation is reduced by using the multipole expansion technique [1, 8].

The number of unknowns in a system can also be reduced using entire-domain basis functions for expansion of the unknown surface currents and charges. The entire-domain basis function should incorporate as closely as possible the physical conditions of the actual surface currents and charges. If the basis function used closely resemble the unknowns to be represented, the numerical solution will yield results of increased accuracy using far fewer number of unknowns [47]. However, constructing a complex expansion function can be achieved for limited geometrical configurations, making this method impractical for the EMC analysis.

Bagby *et al.* [48] used the entire domain basis function method of moments to

analyze coupled microstrip transmission lines. They utilized entire-domain basis functions which incorporate appropriate edge conditions for transverse and longitudinal current components. Hejase [49] obtained the current distribution and radiation pattern of a printed wire loop antenna using an entire-domain moment method and a rigorous Fourier series expansion for the current distribution.

2.8 Methods for Solving Large Electromagnetic Problems.

Schwering *et al.* introduced the diakoptic theory for multielement antennas in free space [50] and its modified version [51]. In the diakoptic method, the antenna system is divided into its individual structure elements. Each element is assumed to be excited by the currents which are impressed at its terminal and by the electric fields resulting from the currents and charges on all other elements. Impedance matrices and field-coupling matrices form the complete impedance matrix of the diakopted antenna. Enforcing continuity of the currents and equality of the scalar potentials at all interconnections between the elements yields a system of linear equations for the junction current and input impedance of the antenna. Butler [52] presented iterative method for computing open-port current on a structure and its application on obtaining open-port impedance elements characteristic of the diakoptic structure. V. Amoruso and F. Lattarulo [53] applied the diakoptic theory for the calculation of the capacitance of large structures. Large structures are broken

up into small elements. Charge transfers and potential equalities are enforced at the node of each restored junction. P. Naylor and C. Christopoulos [54] presented a comparison between the time-domain and frequency-domain diakoptic methods for solving field problems by transmission line modeling(TLM).

The spatial decomposition technique of Umashanker [55, 56] is similar to the diakoptic theory of Schwering, in that it takes the complex structure and divide it into small sections. The small sections are assumed to be separated by virtual surfaces across which cancelling of tangential electric and magnetic currents are postulated. The method of moments is sequentially applied to each section and the solutions are then iteratively matched at the boundaries until a convergent solution is obtained. This technique has been applied to large scatterer problems.

Howard [57] used the multilevel moment method for the analysis of large MIC and MMIC structures. The multilevel moment method breaks up the problem into many levels of smaller problems for its solution. Each smaller problem is then solved in isolation using classical method of moment. Generalized basis transformation technique is used to enable the more complicated expansion function of the higher level to be described in terms of pulse basis functions. The basis transformation for arbitrary source distributions can also expand the weighting (or testing) functions, in the same manner as the basis fuctions, resulting in a variational solution.

2.9 Signal Integrity Analysis

Signal integrity analysis on printed circuit boards and cables starts with the calculation of the electrical parameters of the structure. The structure can then be modelled as a multiconductor transmission line to study its overall performance. Crosstalk and ground-noise can be significant functional problems on printed circuit boards. The study of these two aspects, in addition to attenuation and time delay, can be carried out using SPICE [58] lumped-element models and the transmission line modal analysis [59].

Paul [60, 61] presented a transmission line model for the prediction of crosstalk involving twisted-wire pairs. The model is valid for low frequencies which separates the total coupling into inductive and resistive coupling. Yen *et al.* [62] represented the skin-effect behavior of the resistance in time-domain by simulating its physical behavior by a lumped-circuit. This model accounts for the frequency effect by including additional inductances and parallel resistances that have a total value equal to the dc resistance. Poltz *et al.* [63, 64] developed a computer-aided design algorithm for the analysis of printed circuit boards with particular emphasis on high-speed transmission line propagation and crosstalk effects. Khan and Costache [65] modeled crosstalk on and radiation from printed circuit boards using the finite element method and the transmission line analysis. Dinh *et al.* [66, 67] analyzed the skin effect in time-domain using the partial element equivalent circuits method in two-dimension to calculate the input impedance. Also Ladd and Costache [68] studied the effect of the additional tracks grounded by vias on reducing crosstalk.

Additional references can be found in [69, 59]

2.10 Conclusion

A review of numerical modelling techniques for multiconductor structures is carried out. Compared with the FEM and FDM, the IEM has much simpler data preparations and requires less computational time and memory storage. Hence, it is possible to use more sophisticated discretization schemes, such as a nonlinear element size, near charge singularities [70]. In addition, open regions are automatically handled in the IEM whereas the FEM and the FDM require truncation of the problem space and other special treatments for the open region problems. The IEM provides the same accuracy as the FEM with fewer elements [71]. For inductance calculations, the PEEC method is the most efficient technique as it combines the versatility of the IEM with the simplicity of circuit analysis.

Chapter 3

The Capacitance of Perfectly Conducting Structures

This chapter presents an efficient two-stage approach for the capacitance calculation. This new approach, based on the Integral Equation Method (IEM), calculates the capacitance of three-dimensional ideal conductors in two stages.

For a structure consisting of m arbitrary shaped conductors, the solution proceeds in two stages. In the first stage, each individual conductor is considered separately. The surface of the i^{th} conductor is discretized into small patches. The IEM is then used to solve for the charge distribution on the i^{th} conductor. In the second stage, the multiple interactions (coupling) among the conductors are included by applying the IEM to the whole structure. For each conductor, the charge distribution obtained in the first stage of the solution is used as a discretized entire domain basis function. The order of the interaction matrix is thus reduced to the number of conductors in the structure. This approach results in an accurate capacitance matrix in spite of the possibility of large error in the charge distribution. In general, the order of accuracy for the charge distribution depends on the relative positioning of each conductor with respect to the others. An accurate charge distribution can be obtained using iterative methods. Using the new approach to solve for a system of

conductors, the maximum memory storage required is equal to the memory required for the solution of the largest conductor in the system. The computation cost is not much larger than the total cost of solving for each conductor separately or solving for one conductor of identical system of conductors (*i.e.*, array of connectors).

The statement of the problem is given in the next section. The integral equation method employed in the capacitance calculations for three-dimensional multiconductor system is described in section 3.2. Next, section 3.3 illustrates the proposed approach. Then comparison between the classical IEM and the two-stage method, with respect to the computational cost and memory storage requirements, is included. It shows that the computational time and memory storage are significantly reduced. Finally, section 3.4 demonstrates the results obtained using the new method. They are then compared with those obtained using the IEM and FASTCAP [1].

3.1 Statement of the Problem

Consider a structure consisting of m ideal conductors embedded in a homogeneous dielectric material. The objective is to determine the capacitance matrix of the system $[C_{ij}]$. $[C_{ij}]$ is a symmetric $m \times m$ matrix where the positive diagonal entries C_{ii}, represent the self capacitances and the negative off-diagonal entries, C_{ij}, represent the coupling between conductors i and j, $i, j = 1, 2, ...m$, $j \neq i$.

The ij^{th} element of the capacitance matrix is the free charge on the i^{th} conductor when the potential on the j^{th} conductor is 1V and all other conductors are grounded.

3.2 Analysis

Consider a structure consisting of m ideal conductors embedded in a homogeneous dielectric medium with constant permittivity ϵ. Its capacitance matrix calculation is equivalent to solving for the conductor charges in m potential problems. The potential in the conductors is specified in these problems and it must satisfy Laplace's equation in the region of interest.

3.2.1 The Equivalent Charge Formulations

The exterior Dirichlet problem for the potential ϕ is

$$\nabla^2\phi(r) = 0, \quad r \in V; \tag{3.1}$$

$$\phi(r) = v(r), \quad r \in S_c; \tag{3.2}$$

$$\lim_{r\to\infty} \phi(r) = 0 \tag{3.3}$$

where V is the domain of interest, S_c is the surface of the conductors, v(r) is forcing function on the conductors which has a value of either one or zero.

For the capacitance calculations only the total charge induced on each conductor is required.

By using the equivalent charge formulations, the conductor surfaces are replaced by a surface charge layer σ. The electrostatic potential at any point in the space is then given by [13]

$$\phi = \int_{S_c} \frac{\sigma(r')}{4\pi\epsilon \mid r - r' \mid} dS', \quad r \in S_c \tag{3.4}$$

where S_c is the surface of the conductors and $\sigma(r')$ is the unknown charge density which may be determined by imposing the boundary conditions. The potential of the conductors $v(r)$ in (3.2), is given by

$$v(r) = \int_{S_c} \frac{\sigma(r')}{4\pi\epsilon \mid r - r' \mid} dS', \quad r \in S_c \tag{3.5}$$

This is the Fredholm integral equation of the first kind [72] for the unknown surface charge density σ. The solution of (3.5) for σ gives the matrix entries, by integration over the conductor surfaces.

3.2.2 The Integral Equation Discretization

The integral equation method commences with the discretization of the surface of the conductors into N small patches. The unknown σ is approximated as a linear combination of a set of N linearly independent expansion functions $W_j(r)$ with the weights A_j,

$$\sigma(r) = \sum_{j=1}^{N} A_j W_j(r) \tag{3.6}$$

where W_j are non-zero only on the j^{th} patch,

$$W_j(r) \equiv \begin{cases} 1 & \text{r} \in \text{patch j;} \\ 0 & \text{otherwise.} \end{cases} \tag{3.7}$$

Substituting the expansion (3.6) into (3.5) gives the residuals,

$$R_1(r) \equiv v(r) - \int_{S_c} \sum_{j=1}^{N} \frac{A_j W_j(r')}{4\pi\epsilon \mid r - r' \mid} dS', \quad r \in S_c \tag{3.8}$$

A good approximate solution which can minimize $R_1(r)$ can be obtained using the point matching testing.

3.2.3 Point Matching Testing

The point matching technique produces a linear system for the unknowns A_j's by forcing (3.8) to hold at the centroid of the conductor patches. The weight A_j represents a constant charge density on the j^{th} patch, such that

$$A_j = \frac{q_j}{a_j} \tag{3.9}$$

where q_j and a_j are the charge and area of the j^{th} patch, respectively.

Applying the point matching testing on (3.8) and substituting for A_j from (3.9) result in a system of N linear equations for the patch charges in terms of the conductor potentials

$$v(r_i) = \frac{1}{4\pi\epsilon} \sum_{j=1}^{N} \frac{q_j}{a_j} \int_{a_j} \frac{1}{\mid r - r' \mid} da' \quad r_i \in S_c \tag{3.10}$$

or in a matrix form,

$$\mathbf{Pq} = \mathbf{V} \tag{3.11}$$

where $\mathbf{P}$ is a square matrix of order N, which is the number of patches. Its entries are given by

$$p_{ij} = \frac{1}{4\pi\epsilon a_i} \int_{patch\ j} \frac{1}{\mid r_i - r' \mid} da' \tag{3.12}$$

$\mathbf{q}$ and $\mathbf{V}$ are column vectors (each) of order N. Their entries are, respectively, the unknown charges and the enforced potentials.

The dense linear system of equations (3.11) can be solved for the surface charge distribution from a given set of patch potentials. To compute the j^{th} column of the capacitance matrix, (3.12) must be solved for q_i given a $\mathbf{V}$ vector where $v_k = 1$ if the k^{th} patch belongs to the j^{th} conductor, else $v_k = 0$. The ij^{th} term of the capacitance matrix is computed by summing all the patch charges on the i^{th} conductor, that is

$$C_{ij} = \sum_k q_{i_k} \ , \ k \in i \tag{3.13}$$

Thus, using the integral equation method, an $N \times N$ system of equations (3.12) must be solved to compute the capacitance matrix. The storage and computation time for this system are proportional to N^2 and N^3, respectively. Hence, attempts at using IEM to solve for complicated structures are usually abandoned.

3.3 The Two-Stage Method

In this section, a two-stage solution is developed and used to calculate the capacitance matrix to overcome the limitation of the integral equation method . This limitation is due to the required memory storage and calculation time.

For a structure consisting of m conductors, the solution proceeds in two stages [73, 74]. In the first stage, each individual conductor is considered separately. The surface of the i^{th} conductor is discretized into N_i small patches. Then the IEM is used to solve for the charge distribution, q_{ik}^1, where $k = 1, 2, ..., N_i$; neglecting the effect of all other conductors. In the second stage, the multiple interactions (coupling) among the conductors are included by applying the IEM to the whole structure. The IEM is then applied by considering each conductor as a single patch and using the results of the first stage, q_{ik}^1 as a discretized entire domain basis function for its respective surface on the i^{th} conductor. Thus, the order of the interaction matrix is reduced to $m \times m$ instead of $(\sum_{i=1}^{m} N_i) \times (\sum_{i=1}^{m} N_i)$. It is assumed that the shape of the charge distribution on each conductor is identical to that of an identical but isolated element.

To illustrate the method, consider a structure consisting of two identical ideal conducting plates, *i.e.* $m = 2$. The dimensions of the plates are (10×10 m) located at $Z = 0$ and $Z = 1\ m$, respectively. The IEM combined with the method of moments is used to solve for the charge distribution on the two plates as one structure (classical IEM solution). The result for the charge distribution on the top plate is shown in Fig. 3.1, and the corresponding charge distribution for an identical isolated plate is

shown in Fig. 3.2 (first stage solution).

In general, the charge distribution and the total charge stored on each conductor depend on the following factors:

1) the geometrical (shape) factor of each conductor and

2) the relative positioning of each conductor with respect to the others.

The result in Fig. 3.2 shows clearly the effect of the first factor on the charge distribution. One can also see from Figs. 3.1 and 3.2 the effect of the second factor on the magnitude of the total charge stored on each conductor; and its distribution. Thus it is clear that the shape of the charge distribution is not strongly dependent on the presence of the second conductor. However the total charge stored on each conductor depends on the presence of the second conductor. Thus an unknown weighting factor, α_i, is used as a first order approximation of the effect of the second factor on the total charge stored on the i^{th} conductor. This assumption is valid only when the separation of the conductors is larger than the cross section. However, by enforcing the boundary conditions and using the charge distribution obtained in the first stage, the accuracy of the capacitance matrix is insured. This charge distribution is considered as entire domain basis function.

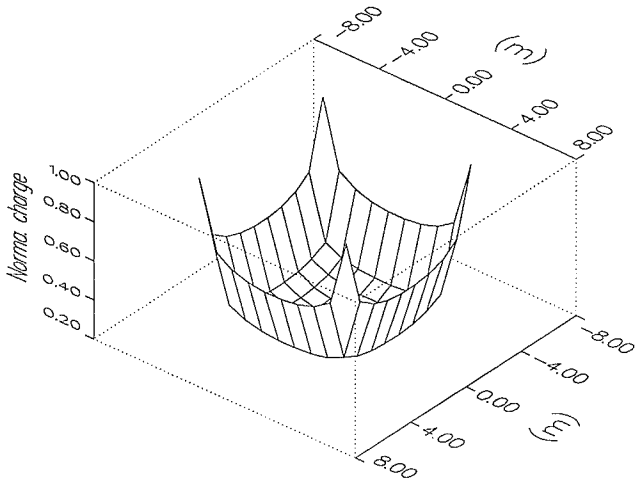

Figure 3.1: *Normalized charge distribution on the upper plate of dimensions* 10 $\times$ 10 *m positioned on the Z=1 plane at unity potential and separated by 1 m from another identical plate positioned at Z=0 plane at zero potential.*

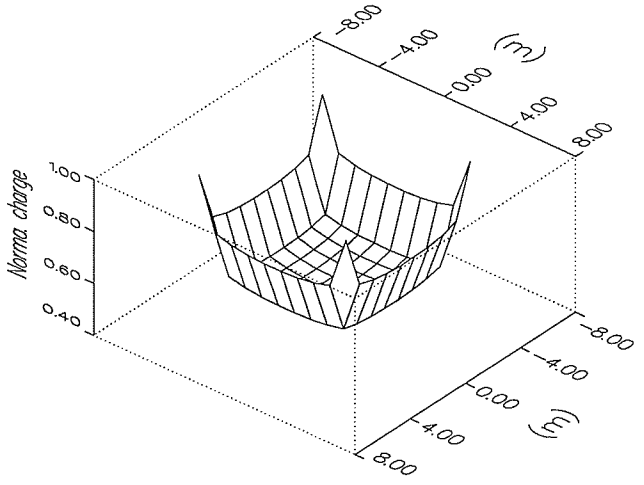

Figure 3.2: *Normalized charge distribution on one plate of dimensions* 10 $\times$ 10 *m positioned on the Z=0 plane at unity potential.*

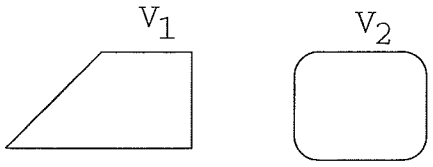

Figure 3.3: *A structure consisting of two conductors*

Consider a structure consisting of two conductors embedded in a homogeneous dielectric materials.Fig. 3.3, the potential at any point on the surface of the conductors is then given by

$$\begin{aligned} V_1 &= [\alpha_1 F(1,1) + \alpha_2 F(1,2)] \\ V_2 &= [\alpha_1 F(2,1) + \alpha_2 F(2,2)] \end{aligned} \tag{3.14}$$

where, for I, II=1,2,

$$F(I,II) = \frac{1}{N_I} \sum_{i=1,\, i \in cond.\, I}^{N_I} \sum_{j=1,\, j \in cond.\, II}^{N_{II}} q_j^1 p_{ij} \tag{3.15}$$

and p_{ij} is given by (3.12).

Equation (3.14), for m conductors, can be written in matrix form as

$$\mathbf{A}\alpha = \mathbf{V} \tag{3.16}$$

where $\mathbf{A}$ is a square matrix of order m, and α and $\mathbf{V}$ is column matrix of order m.

The resulting linear system of equations (3.16) can thus be solved, typically by some form of Gaussian elimination, to compute α. For a two conductor system, the capacitances C_{11} and C_{21} are given by

$$C_{11} = \alpha_1 \sum_{k}^{N_1} q_k \tag{3.17}$$

$$C_{21} = \alpha_2 \sum_{k}^{N_m} q_k \tag{3.18}$$

C_{12} and C_{22} can be obtained by interchanging the value of V_1 and V_2 and solving the linear system of equations (3.16).

To compute the j^{th} column of the capacitance matrix, equation (3.16) must be solved for α_i given a $\mathbf{V}$ vector, where

$$V_i = \begin{cases} 1 & \text{i=j} \\ 0 & \text{otherwise.} \end{cases} \tag{3.19}$$

Then the ij^{th} term of the capacitance matrix is computed with the multiplication of α_i by the Q_i which results from the first stage solution.

The two-stage method gives very good results for the capacitance matrix; however, it does not calculate accurately the charge distribution on each conductor. The main goal of this work is the reduction of the computational cost and memory storage required by the IEM; for the calculation of the capacitance matrix which is in great demand by industry. An accurate charge distribution, due to an enforced potential, can be obtained using an iterative method based on the following equation:

$$f_k = p_{kk} q_k + \sum_{j=1,\, j\neq k}^{N} p_{kj} q_j \tag{3.20}$$

or

$$q'_k = (f_k - \sum_{j=1,\, j\neq k}^{N} p_{kj} q_j)/p_{kk} \tag{3.21}$$

f_k is the potential at the k^{th} patch due to charges on all the patches. The iteration is applied using equation (3.21) and the tolerance (tol) to terminate the iteration, where

$$|(q_k')^2 - (q_k)^2)| < tol, \tag{3.22}$$

Assuming all the patches have comparable geometry, the main contribution to f_k comes from the patches near the k^{th} patch. Since the speed of convergence depends strongly on the initial assumption of the charge distribution, a good guess of the initial values of the charges near the k^{th} patch would substantially speed up convergence. The best initial values of the charges for the iterative method is the charge distribution obtained using the two-stage method, since the coupling of all the charges on a conductor is included in the first stage of the solution for each conductor. In addition, the second stage of the two-stage method accounts for the total coupling amongst the conductors.

The iterative method is tested for various geometries, using the results of the two-stage method as the initial value for the charges. It usually converges after a number of iterations, which is much less than the number of unknowns. The charge distribution obtained by the iterative method could also be used to obtain the capacitance matrix, by summing the charges on each conductor in the system. For the iterative method, there is no additional memory storage requirement and the computation time required for obtaining the desired accuracy is roughly of the order nN^2, where n is the number of iterations.

3.4 Computational Time and Memory Storage Requirements

In order to use the two-stage method to compute an $m \times m$ capacitance matrix, the first stage solution is repeated m times; where m is the number of blocks. Then the second stage is applied to the whole structure. Assuming N patches on each block, the computational cost is proportional to:

$$2mN^2 + mN^3 + m^2N^2 + (m)^3 + (m)^2 \tag{3.23}$$

The cost of using IEM as applied to the whole structure (classical IEM) is proportional to

$$m^2N^2 + m^3N^3 + m^2N^2 \approx m^3N^3 \tag{3.24}$$

Thus, the two-stage method gives a minimal computational time saving of order m^2.

The memory storage required by the two-stage method is proportional to the maximum memory requirement by the classical IEM in solving for a single block of the structure *i.e.* maximum of N^2. On the other hand, the memory storage required by the classical IEM is proportional to $(mN)^2$. Thus, the memory requirement of the two-stage method is much less than the memory requirement of the classical IEM.

3.5 Results and Comparison

Tables 3.1 and 3.2 are included to present a comparison of the computational time and memory storage requirements of the two-stage method, with that of the classical IEM and FASTCAP algorithm which is based on the classical IEM and the multipole expansion [1]. All the computations have been performed on a SPARC10/41 workstation. Table 3.1 presents the computational time and memory storage required to solve for the capacitance matrix of various geometries that are presented in terms of the number of conductors and total number of patches in the geometry using the classical IEM and the two-stage method. In Table 3.2, the computational time and memory storage of FASTCAP and the two-stage method are presented. As shown in these tables, the total computational time and memory storage depend mostly on the requirements of the first stage solution. It is also clear, from the tables, that the two-stage method represents a considerable saving in memory and cost in comparison to the classical IEM and to FASTCAP algorithm. Furthermore, additional savings in computational time can be achieved, in the solution for a system of identical conductors, by solving for only one conductor in the system. As an example, consider the classical IEM in solving for a system consisting of six identical conductors; each discretized to 400 patches. These patches requires a maximum storage of $2.85Mb$ and a computational time $2.21m$. However the computational time of a non-identical system of conductors, each discretized to 400 patches, is $6.46m$. In addition, the maximum memory storage required is also $2.85Mb$.

Geometry		IEM		Two-stage	
# of conductors	# of patches	time [m]	memory [MB]	time [m]	memory [MB]
1	100	0.025	0.248		
2	200	0.1	0.588	0.065	0.451
5	500	1.83	2.544	0.188	0.598
1	400	0.85	1.84		
2	800	7.36	5.96	1.86	2.16
4	1600	63.7	20.6	4.14	2.48
6	2400	310	45.8	6.76	2.85

Table 3.1: *Comparison between the two-stage method and the IEM.*

Geometry		FASTCAP		Two-stage	
# of conductors	# of patches	time [m]	memory [MB]	time [m]	memory [MB]
1	265	0.025	2.412		
4	1060	0.246	7.80	0.132	3.21
1	486	0.07	3.35		
2	972	0.31	4.83	0.167	4.05
9	4374	3.64	34.28	1.45	4.26
1	816	0.26	6.137		
6	4896	4.16	28.45	2.10	7.62
9	7344	9.66	76.90	4.01	7.91

Table 3.2: *Comparison between the two-stage method and FASTCAP.*

Figure 3.4 shows the total capacitance of two identical transmission lines as a function of the edge-to-edge separation, D, between the lines. The length of each line is 15 cm and the cross section of each conductor is 20 by 10 mm. The capacitance of the transmission line obtained using the two-stage solution is compared with the classical IEM method results. As shown in the figure, for separations greater than $20mm$, identical results are obtained using the two-stage solution and classical IEM method, however, the accuracy of the two-stage solution decreases by reducing the separation between the conductors. In general, when the separation between the conductors is smaller than the cross sectional dimension a, the classical IEM method should be used for the extraction of capacitance matrix of the two conductors.

Table 3.3 presents a comparison of the capacitance matrix for a 2×2 array of right angle pins, obtained using the two-stage method and FASTCAP. The pins are discretized to 1147 patches each. It can be seen from the table that the two-stage method is accurate in comparison with FASTCAP.

Table 3.4 presents a comparison of the capacitance matrix for a 3×2 array of pins, obtained using the two-stage method and FASTCAP. Each pin has the dimensions of ($x = 0.508$, $y = 0.508$, $z = 17.78mm$) and the spacings between the pins are ($dx = 2.254$, $dy = 2.254mm$); where dx and dy are respectively the spacings in the X and Y-directions. The pins are discretized to 498 patches each. It can be seen from the table that the two-stage method gives very accurate results in comparison to FASTCAP.

To show the accuracy and convergence of the iterative method, it is used to solve for the charge distribution of two parallel plates and two co-planar plates. The size

of each plate is 10×10 meters and it has been discretized to 400 patches. The separation between the plates is 1 meters. For the two parallel plates, the charge distributions corresponding to the number of iteration $N_i = 0, 5, 20$ and 35 are shown in Fig. 3.5. It is clear from the results that the solution converges after a number of iterations that is much less than the number of unknowns in the structure. For the co-planar plates, the charge distributions for $N_i = 0, 5, 15$ and 20 are shown in Fig. 3.6. It can be seen that the solution converges faster than the solution for the parallel plates because of the coupling level between the plates. Hence, from these two extreme cases, it is clear that the iterative method converges to the correct solution after a small number of iterations.

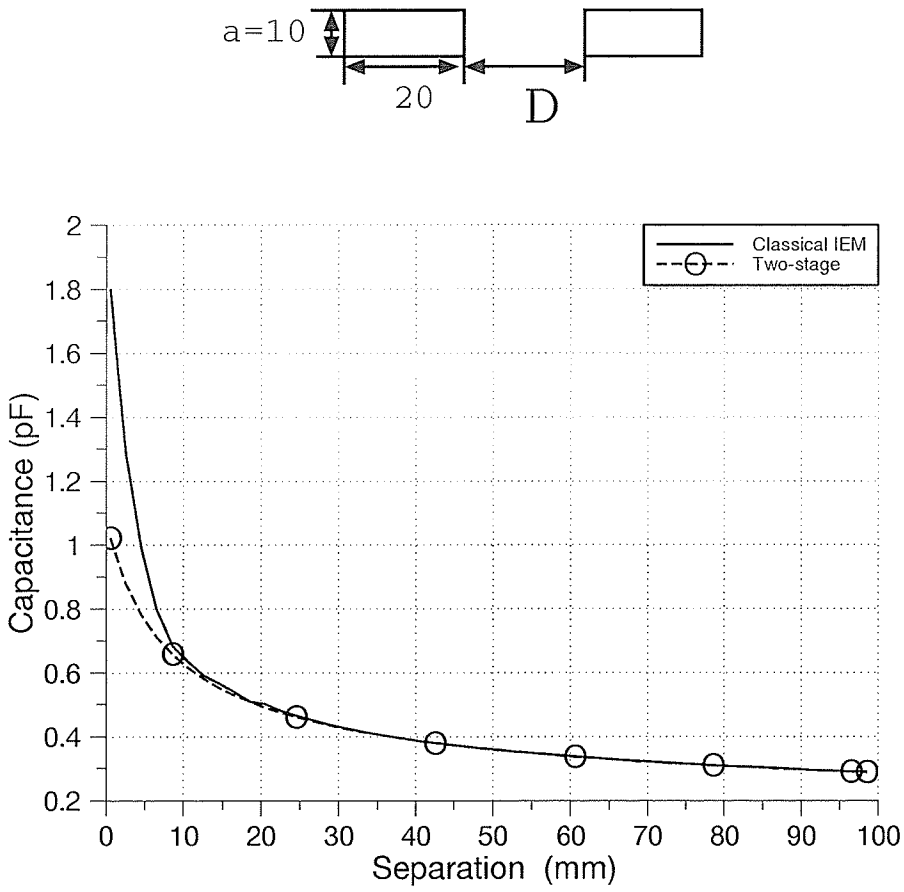

Figure 3.4: *The capacitance of two transmission lines as a function of distance between the lines obtained using IEM and the two-stage method. The length of the line is 15cm*

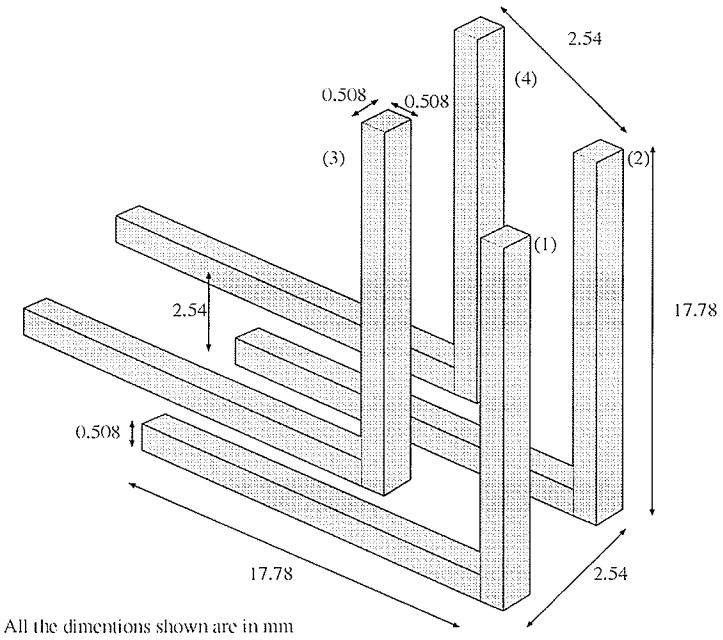

i		1	2	3	4
1	FASTCAP	164.0	-52.32	-55.62	-21.66
	Two-stage	163.26	-52.07	-55.34	-21.52
2	FASTCAP	-52.32	163.7	-21.64	-55.44
	Two-stage	-52.07	163.26	-21.52	-55.34
3	FASTCAP	-55.62	-21.64	184.4	-61.69
	Two-stage	-55.34	-21.52	183.17	-61.19
4	FASTCAP	-21.66	-55.44	-61.69	184.2
	Two-stage	-21.52	-55.34	-61.19	183.17

Table 3.3: *Comparison between the capacitance matrix of a system of 4 pins, as shown above, obtained using the two-stage method and FASTCAP. The unit of the capacitances is pF.*

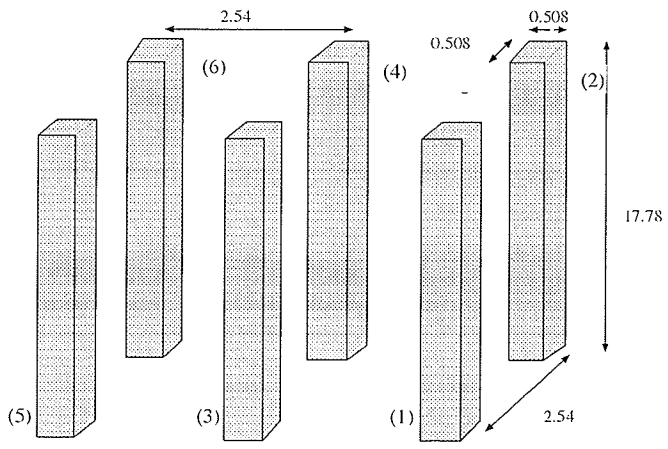

All the dimensions are in mm

Table 3.4: *Comparison between the capacitance matrix of a system of 6 conductors, shown above, obtained using the two-stage method and FASTCAP. The unit is fF.*

i		1	2	3	4	5	6
1	FASTCAP	296	-75.77	-16.35	-80.95	-27.16	-9.263
	Two-stage	294.44	-76.53	-15.74	-81.51	-26.60	-8.675
2	FASTCAP	-75.77	323.6	-76.24	-27.12	-60.94	-26.97
	Two-stage	-76.53	321.27	-76.53	-26.60	-61.26	-26.60
3	FASTCAP	-16.35	-76.24	296.4	-9.238	-26.98	-81.18
	Two-stage	-15.79	-76.53	294.4	-8.67	-26.6	-81.51
4	FASTCAP	-80.95	-27.12	-9.238	296.1	-75.86	-16.44
	Two-stage	-81.51	-26.60	-8.675	294.44	-76.530	-15.79
5	FASTCAP	-27.16	-60.94	-26.98	-75.86	323.5	-75.98
	Two-stage	-26.60	-61.26	-26.60	-76.53	321.28	-76.53
6	FASTCAP	-9.263	-26.97	-81.18	-16.44	-75.98	296.3
	Two-stage	-8.675	-26.6	-81.51	-15.79	-76.53	294.44

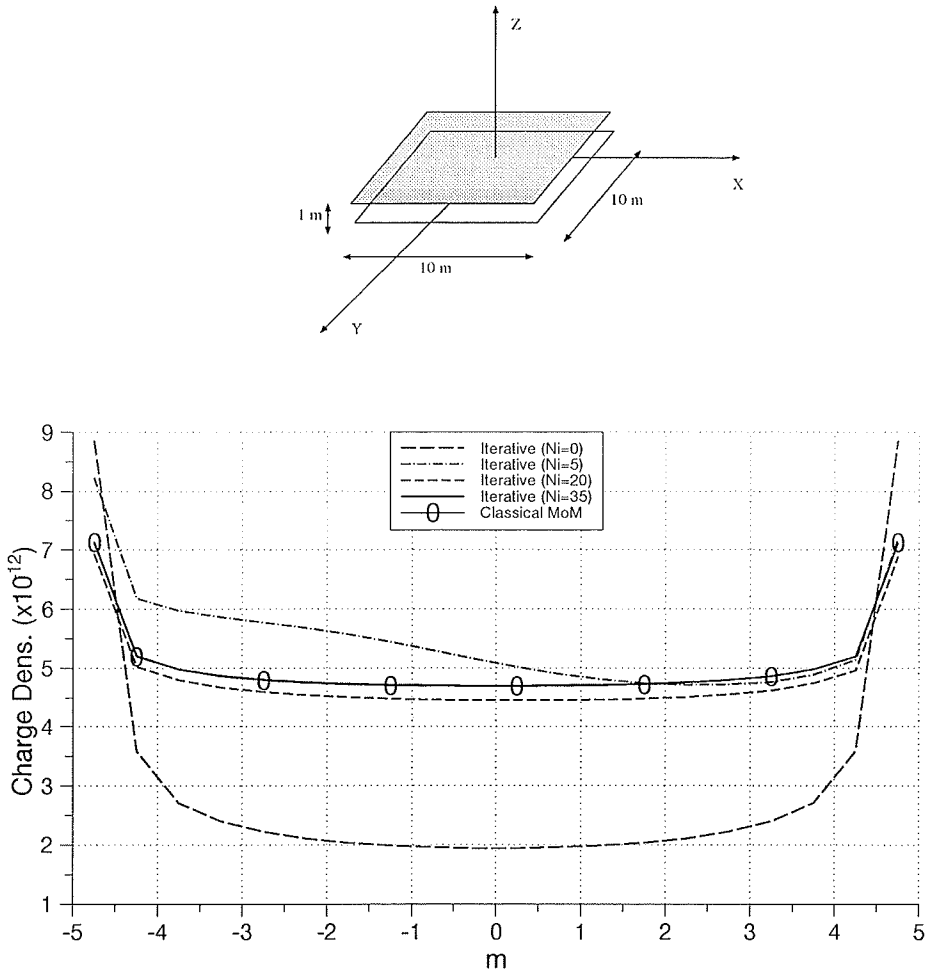

Figure 3.5: *Cross section of the charge distribution on the upper plate of the geometry shown above obtained using the iterative method and the classical IEM.*

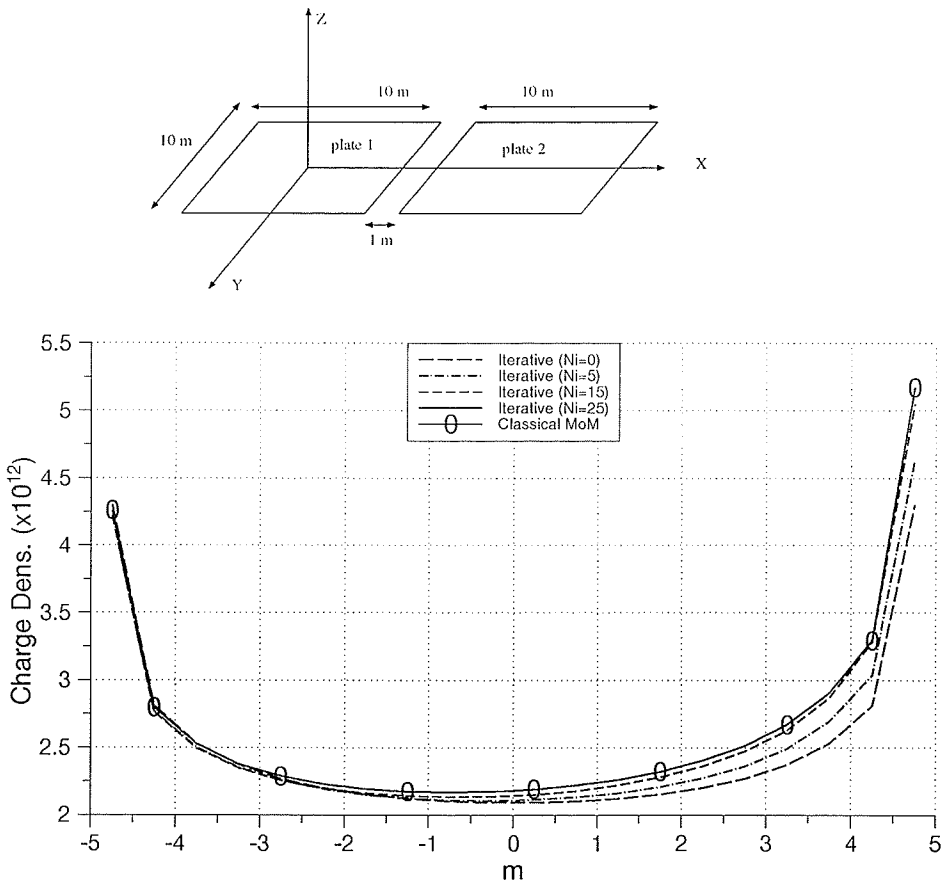

Figure 3.6: *Cross section of the charge distribution on plate one of the geometry shown above obtained using the iterative method and the classical IEM.*

3.6 Numerical Considerations

The use of the integral equation method for the capacitance calculation requires the discretization of conductor surfaces into small patches, formulation of the potential coefficient matrix, and solution of the matrix system. This section will discuss each of the three steps in the development of an efficient algorithm.

3.6.1 The Surface Discretization

The integral equation method for the calculation of the capacitance matrix requires the discretization of the surface of the conductors into small patches. Planar surfaces are usually discretized to planar patches with quadrilateral or triangular shapes. On the other hand, curved surfaces could be discretized into planar or curved patches. However a large number of planar patches are required to accurately simulate curved surfaces which results in very costly solutions. Though curved patches accurately represent the curved surfaces, with much fewer elements, a special transformation is required to evaluate the integral in (3.12) over curved surfaces [22]. Generally, the accuracy of the results, the computational time and the memory storage requirements depend on the number of patches used to discretize the surface of the conductor. Hence, the best discretization is the one that minimizes the number of patches that are required to produce accurate results.

The general rules for surface discretization are:

- The aspect ratio (the ratio of the longest to the shortest side) of each patch should generally not exceed five.
- The patches should be as close to a square or be as equilateral as possible.
- Curved surfaces should, when possible, be discretized using curved patches.
- The patch layout should depict the charge density on the surfaces, *i.e.* denser mesh near the edges and the corners.
- For a structure consisting of multiple conductors, more dense meshing is required on the surfaces that are near to other conductors.

The above five rules produce the most efficient surface discretization algorithm.

3.6.2 Evaluation of the Integrals

The potential coefficients matrix (3.9) is filled by evaluating the integral given by (3.12). The complexity of this integration depends on the shape of the patch.

1) Square Patches [13]

The potential at the center of a square patch of area a_i, due to a unit charge density over its own surface, is given by

$$p_{ii} = \frac{\sqrt{a_i}}{2\pi\epsilon} ln(1+\sqrt{2}) \tag{3.25}$$

The potential at the center of the i^{th} patch, due to a unit charge density over the j^{th}, patch is given by

$$p_{ij} = \frac{a_i}{4\pi\epsilon R_{ij}} \tag{3.26}$$

where $R_{ij} = \sqrt{(x_i - x_j)^2 + (y_i - y_j)^2 + (z_i - z_j)^2}$.

The maximum error in this approximation is about 3.8% for the adjacent elements.

2)Rectangular Patches [75]

The potential at any point due to a unit charge density over a rectangular patch can be evaluated using the following closed form integral.

Let the integral equation (3.12) be represented by

$$P(u, v, w) = \frac{1}{4\pi\epsilon a_i} \int \frac{1}{R} du dv$$

where $R = \sqrt{u^2 + v^2 + w^2}$.

$P(u, v, w)$ is then given by

$$P(u, v, w) = \frac{1}{4\pi\epsilon a_i} \{u[log(v + r) - 1] + vlog(u + R) - wtan^{-1}(\frac{uv}{wR} + wtan^{-1}(\frac{u}{w})$$

3) Numerical Integration

The potential at any point r, due to a unit charge density on a patch of arbitrary shape, can be evaluated using Gaussian quadrature formula and geometrical transformation of the region of integration. The integration over curved patches can be facilitated with the use of the geometrical transformation associated with the boundary element method. However, the use of Green's function results in a singular integral equation when the source and observation points coincide. Special treatment is needed for the handling of this singularity. M. Lean and A. Wexler presented an efficient algorithm for handling the singularity of Green's function [22]. Generally, numerical integration is more costly than closed form analytical integration, since filling the matrix is of order n^2 operation, where n is the total number of patches. An efficient algorithm requires the capability of selecting the method for the integral evaluation according to the cost. The cost of filling the matrix could be minimized by:

- Using the square patch approximation when possible.
- Using the analytical closed form solution for the integral.
- Allowing the number of Gaussian points to be chosen to be proportional to the inverse distance, between the observation and source points, when the Gaussian quadrature integration is used.
- Using the multipole approximation to the potential, presented by Rokhlin [76],

to speed up the filling of the matrix.

Solving The Matrix Equation

The dominant cost in the solution for the capacitance matrix comes from solving the matrix equation. Factorization of the matrix by Gaussian elimination is proportional to n^3 operations. However, the computational cost of solving the matrix can be reduced using an iterative based matrix solver. Saad *et al* [77] and [78] described a simple minimum residuals algorithm (GMRES) for the solution of a linear system of equations. This reduces the computational time to roughly of order mn^2, where m is the number of conductors.

Chapter 4

The Capacitance and Conductance Matrices

The two-stage method presented in chapter 3 applies only to structures with conductors in region filled with a homogeneous material. This chapter describes the extension of the method for the extraction of the capacitance matrix for three-dimensional structures with dielectric layers. The dielectric materials being considered are perfect dielectric and lossy dielectric. In this chapter, the capacitance matrix will be generally referred to as the complex capacitance matrix. The presence of the lossy dielectric will result in a capacitance matrix being represented by the real part of the complex capacitance matrix and a conductance matrix being represented by the imaginary part.

The proposed method minimizes the computational cost and memory requirements of the solution of three-dimensional multiconductor structures. It calculates the complex capacitance in two stages, based on the Integral Equation Method (IEM). In the first stage, the structure is divided into blocks. Each block consists of a single conductor and all the dielectric-dielectric interfaces. The IEM method is then used to solve separately for the charge distribution on each block, neglecting the effect of all other blocks in the structure. In the second stage, the multiple interactions (coupling) among the conductors are included with the application of the IEM to the whole structure [79]. The charge distribution, obtained in the first

stage, is considered as a discretized entire domain basis function for the respective conductor. Thus the order of the interaction matrix is reduced to the number of conductors in the structure.

4.1 Statement of the Problem

Consider a structure consisting of m conductors embedded in a piece wise homogeneous material with complex permittivities. The objective is then to determine the complex capacitance matrix of the system. The complex capacitance matrix of such a structure is an $m \times m$ symmetric matrix $\hat{\mathbf{C}}$. The real part of the complex matrix, $\mathrm{Re}(\hat{\mathbf{C}})$, is the capacitance matrix of the system; the imaginary part, $\mathrm{Im}(\hat{\mathbf{C}})$, represents the conductance matrix of the system, or the dielectric losses. More specifically, the i^{th} row of $\hat{\mathbf{C}}$ has a positive entry, $\hat{C}_{ii}$, which represents the self complex capacitance; and negative off-diagonal entries, $\hat{C}_{ij}$, which represents coupling between conductor i and j, where $j = 1, 2, ...m$, $j \neq i$. The ij^{th} element of the capacitance matrix is the free charge on the i^{th} conductor when the potential on the j^{th} conductor is $1v$ and all other conductors are grounded.

4.2 Analysis

Consider the complex capacitance matrix problem stated in the previous section. The capacitance matrix can be obtained by raising one conductor to unit potential, grounding the rest and calculating the free charges on each conductor. The free

charges in one of the m conductors is the integral of the charge per unit area over the entire surface of the conductor. With conductor j at 1V and the rest grounded, $\hat{C}_{ij}$ is the equivalent to the free charge on the conductor i, $i = 1, 2, ..., m$. Repeating the procedure m times gives the m column of $\hat{C}_{ij}$. Thus, the complex capacitance matrix calculation for m conductors is equivalent to solving for the conductor charges in m potential problems. In these problems, the conductor potentials are specified and the potential must satisfy Laplace's equation in the regions of interest.

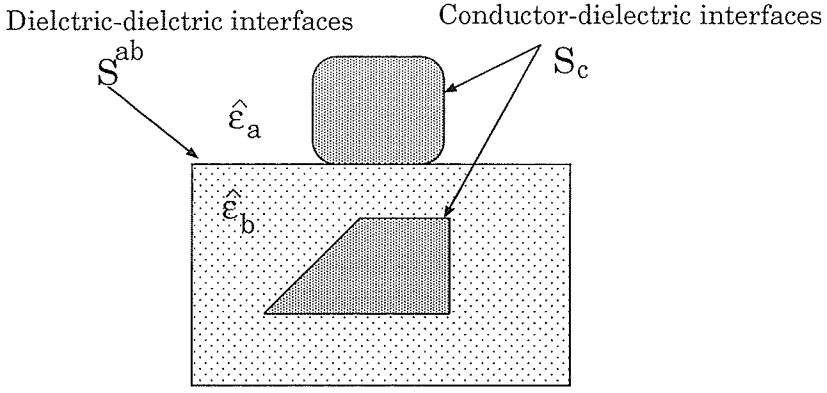

Figure 4.1: *A structure consisting of two conductors*

4.2.1 The Equivalent Charge Formulations

The exterior Dirichlet formulation for the potential ϕ is

$$\nabla^2\phi(r) = 0, \quad r \in V; \tag{4.1}$$

$$\phi(r) = v(r), \quad r \in S_c; \tag{4.2}$$

$$\lim_{r\to\infty} \phi(r) = 0 \tag{4.3}$$

$$\hat{\epsilon}_b \frac{\partial \phi_b(r)}{\partial n_b} = \hat{\epsilon}_a \frac{\partial \phi_a(r)}{\partial n_b}, \quad r \in S^{ab}, \tag{4.4}$$

where a and b correspond to bordering dielectric, V is the region of interest, S_c is the conductor surfaces, S^{ab} is the interface surface between dielectric a and dielectric b, the direction of the normal $\hat{n}_b$ is into medium b, $\hat{\epsilon}_a = \epsilon_a(1 - jtan\delta_a)$ and $\hat{\epsilon}_b = \epsilon_b\ (1 - jtan\ \delta_b)$ are the permittivities of medium a and b, and $tan\delta$ is the loss tangent.

Using the equivalent charge formulations [14], a total charge density σ_T is assumed on the conductor-dielectric interfaces and the dielectric-dielectric interfaces. On each conductor-dielectric interface, the total charge is the sum of the free charges and the polarization charges. On each dielectric-dielectric interface, the total charge is only the polarization charge. The conductor potentials are fixed using the following integral equation:

$$v(r) = \int_S \frac{\sigma_T(r')}{4\pi\hat{\epsilon} \mid r - r' \mid} dS' \tag{4.5}$$

where S is the union of all the dielectric interfaces, S^{ab}, and the conductor surfaces S_C, and $\sigma_T(r')$ is the unknown charge density.

The normal derivative of the potential at the interface surfaces, S^{ab}, are given by

$$\frac{\partial \phi_b(r)}{\partial n_b} = \frac{1}{2\epsilon_o(r)}\sigma_T(r') - \int_{S'} \sigma_T(r') \frac{cos(r - r', \hat{n}_b)}{4\pi\epsilon_o \mid r - r' \mid^2} dS', \quad r \in S^{ab} \tag{4.6}$$

$$\frac{\partial \phi_a(r)}{\partial n_b} = \frac{1}{2\epsilon_o(r)}\sigma_T(r') - \int_{S'} \sigma_T(r') \frac{cos(r - r', \hat{n}_b)}{4\pi\epsilon_o \mid r - r' \mid^2} dS', \quad r \in S^{ab} \tag{4.7}$$

where ϕ_a and ϕ_b are the limiting free-space potentials in the dielectric regions.

Substituting equations (4.6) and (4.7) in (4.4) yields

$$\frac{\hat{\epsilon}_a + \hat{\epsilon}_b}{2\epsilon_0}\sigma_T(r') - \frac{\hat{\epsilon}_a - \hat{\epsilon}_b}{4\pi\epsilon_0}\int_{S'}\sigma_T(r')\frac{cos(r-r',\hat{n}_b)}{\mid r-r' \mid^2}dS' = 0 \tag{4.8}$$

The simultaneous solution of (4.5) and (4.8) for σ_T gives the complex matrix entries by integration over the conductor surfaces.

4.2.2 The Integral Equation Discretization

The integral equation method starts by discretizing the interfaces into small patches. The conductor-dielectric interfaces are discretized to N_c small patches and the dielectric-dielectric interfaces are discretized to N_d small patches. The unknown, σ_T, is approximated as a linear combination of a set of N, $N = N_c + N_d$, linearly independent expansion functions $W_j(r)$ with the weights A_j,

$$\sigma_T(r) = \sum_{j=1}^{N} A_j W_j(r) \tag{4.9}$$

where W_j are non-zero only on the j^{th} patch,

$$W_j(r) \equiv \begin{cases} 1 & \text{r} \in \text{patch j;} \\ 0 & \text{otherwise.} \end{cases} \tag{4.10}$$

Substituting the expansion (4.10) into (4.5) and (4.8) gives two residuals,

$$R_1(r) \equiv v(r) - \int_S \sum_{j=1}^{N} \frac{A_j W_j(r')}{4\pi\hat{\epsilon} \mid r-r' \mid} dS', \quad r \in S_c \tag{4.11}$$

$$R_2(r) \equiv \frac{\hat{\epsilon}_a + \hat{\epsilon}_b}{2\epsilon_0} \sum_{j=1}^{N} A_i W_j(r') - \frac{\hat{\epsilon}_a - \hat{\epsilon}_b}{4\pi\epsilon_0} \int_{S'} \sum_{j=1}^{N} A_j W_j(r') \frac{cos(r - r', \hat{n}_b)}{\mid r - r' \mid^2} dS', \quad (4.12)$$
$$r \in S^{ab}$$

Both residuals are zero when (4.9) satisfies (4.5) and (4.6) exactly. A good approximate solution can be obtained depending on the testing method used.

4.2.3 Point Matching Testing

Point matching produces a linear system for the unknown A_j's by forcing (4.11) and (4.13) to hold at the centroid of the conductor and dielectric-interface patches, respectively. The weight A_j represents a constant charge density on the j^{th} patch.

$$A_j = \frac{q_j}{a_j} \quad (4.13)$$

where q_j and a_j are, respectively, the charge and area of the j^{th} patch.

The application of the point matching testing on (4.11) and (4.13) and substitution for A_j from (4.13) result in

$$v(r_i) = \frac{1}{4\pi a_j \epsilon_o} \sum_{j=1}^{N} \frac{q_j}{a_j} \int_{a_j} \frac{1}{\mid r - r' \mid} da_j \quad r_i \in S_c \quad (4.14)$$

$$0 = q_i \frac{(\hat{\epsilon}_a + \hat{\epsilon}_b)}{2a_i\epsilon_o(\hat{\epsilon}_a - \hat{\epsilon}_b)} - \sum_{j=1}^{N} \frac{q_j}{a_j} \frac{1}{4\pi a_j \epsilon_o} \int_{a_j} \frac{cos(r - r', \hat{n}_b)}{\mid r - r' \mid^2} da_j, \quad ri \in S^{ab} \quad (4.15)$$

The linear system of equations given by (4.14) and (4.15) can be represented in matrix form

$$\begin{bmatrix} \mathbf{P} \\ \mathbf{E} \end{bmatrix} [\mathbf{q}] = \begin{bmatrix} \mathbf{v} \\ \mathbf{0} \end{bmatrix} \quad (4.16)$$

where V is a vector of length N_c, $\mathbf{P}$ is an $N_c \times N$ coefficients matrix of the potential and is given by

$$P_{ij} = \frac{1}{4\pi a_j \epsilon_0} \int_{a_j} \frac{1}{\mid r - r' \mid} da_j, \tag{4.17}$$

and $\mathbf{E}$ is an N_dxN matrix of the normal electric field coefficients

$$E_{ij} = \frac{1}{4\pi a_j \epsilon_o} \int_{a_j} \frac{cos(r - r', \hat{n}_b)}{\mid r - r' \mid^2} da_j \quad i \neq j, \tag{4.18}$$
$$E_{ii} = \frac{(\hat{\epsilon}_b + \hat{\epsilon}_a)}{2a_i \epsilon_o (\hat{\epsilon}_b - \hat{\epsilon}_a)}, \qquad i = j,$$

The unknown vector $\mathbf{q}$ is the vector of N patch charges that can be solved for using a standard matrix solver.

By raising conductor j to 1V and grounding the rest, *i.e.* $v_j = 1$ and $v_i = 0$, with $i \neq j$, and solving (4.16) for the unknown charges, a column of the complex capacitance matrix can be obtained [26]

$$\hat{C}_{ij} = \sum_{k=1}^{N_i} q_k \tag{4.19}$$

The elements of the conductance matrix are given by

$$[G_{ij}] = Re[jw\hat{C}_{ij}] = -Im[w\hat{C}_{ij}] \tag{4.20}$$

and the elements of the capacitance matrix are given by

$$[C_{ij}] = Re[\hat{C}_{ij}] \tag{4.21}$$

4.2.4 Galerkin Testing

Point matching is adequate for problems without dielectric; however it produces large error for geometries with large permittivity changes. The Galerkin testing

yields more accurate results at a higher computational cost [80]. Thus it is sufficient to use the higher accuracy Galerkin method for testing (4.13), while still using the computationally efficient point matching for testing (4.11).

The application of the Galerkin method to (4.13) forms inner products between $R_2(r)$ and the N_d expansion function W_i. This corresponds to patches on the dielectric interfaces such that

$$0 = \frac{(\hat{\epsilon}_a + \hat{\epsilon}_b)}{2\epsilon_o} \int_S W_i(r) \sum_{j=1}^{N} A_j W_j(r) dS$$
$$-(\hat{\epsilon}_a - \hat{\epsilon}_b) \int_S W_i(r) \int_{S'} \sum_{j=1}^{N} A_j W_j(r') \frac{cos(r - r', \hat{n}_b)}{4\pi a_j \epsilon_o \mid r - r' \mid^2} dS' dS, \quad ri \in S^{ab} \tag{4.22}$$

The expansion weight, W_i, can be written in terms of the total charge on each patch since the weight is non-zero only on the i^{th} patch. Equation (4.22) then becomes

$$0 = \frac{(\hat{\epsilon}_a + \hat{\epsilon}_b)}{2\epsilon_o} \frac{q_i}{a_i} \int_{S_i} dS_i$$
$$-(\hat{\epsilon}_a - \hat{\epsilon}_b) \sum_{j=1}^{N} \frac{q_j}{a_j} \int_{S_i} \int_{S_j} \frac{cos(r - r', \hat{n}_b)}{4\pi\epsilon_o \mid r - r' \mid^2} dS_j dS_i, \quad ri \in S^{ab} \tag{4.23}$$

The integral in the first term of (4.23) over the surface of the i^{th} patch is equivalent to its area. The equation then becomes

$$0 = q_i \frac{(\hat{\epsilon}_a + \hat{\epsilon}_b)}{2\epsilon_o(\hat{\epsilon}_a - \hat{\epsilon}_b)}$$
$$-\sum_{j=1}^{N} \frac{q_j}{a_j} \int_{S_i} \int_{S_j} \frac{cos(r - r', \hat{n}_b)}{4\pi\epsilon_o \mid r - r' \mid^2} dS_j dS_i, \quad ri \in S^{ab} \tag{4.24}$$

The linear system of equations given by (4.14) and (4.24) can be represented in matrix form similar to (4.16) and the solution proceeds in the same manner as the point matching testing.

By using the integral equation method, an $N \times N$ system of equations (4.16) must be solved to compute the complex capacitance matrix. This requires storage

and computation time for this system to be proportional to N^2 complex numbers and N^3, respectively. Hence, attempts at using IEM to solve complicated structures are usually abandoned. However, this limitation can be removed, by using the two-stage solution presented in the next section.

4.3 The Two-Stage Method

To overcome limitations of the classical integral equation method (IEM) as a result of the required memory storage and calculation time, a two-stage solution is used to calculate the complex capacitance matrix. For a structure consisting of m conductors, as shown in Fig. 4.2(a), where $m = 2$, the solution proceeds in two stages. In the first stage, each individual conductor is considered separately. The surface of the i^{th} conductor is discretized into N_i small patches. In addition, all the dielectric-dielectric interfaces are discretized into a total of N_d patches. An example of the discretization is shown in Fig. 4.2 (b) and (c). The formulation presented in section 4.2 is then used to solve for the charge distribution on the i^{th} conductor and the entire dielectric-dielectric interface. Notice that the effect of all other conductors in the structure has been neglected in this stage. However, in the second stage, the multiple interaction (coupling) among the conductors is included by applying the IEM to the whole structure. Then the method of moment is applied by considering each conductor as a single patch and using the results of the first stage, as a discretized entire domain basis function, for its respective surface of the i^{th} conductor. The boundary conditions are enforced on each conductor.

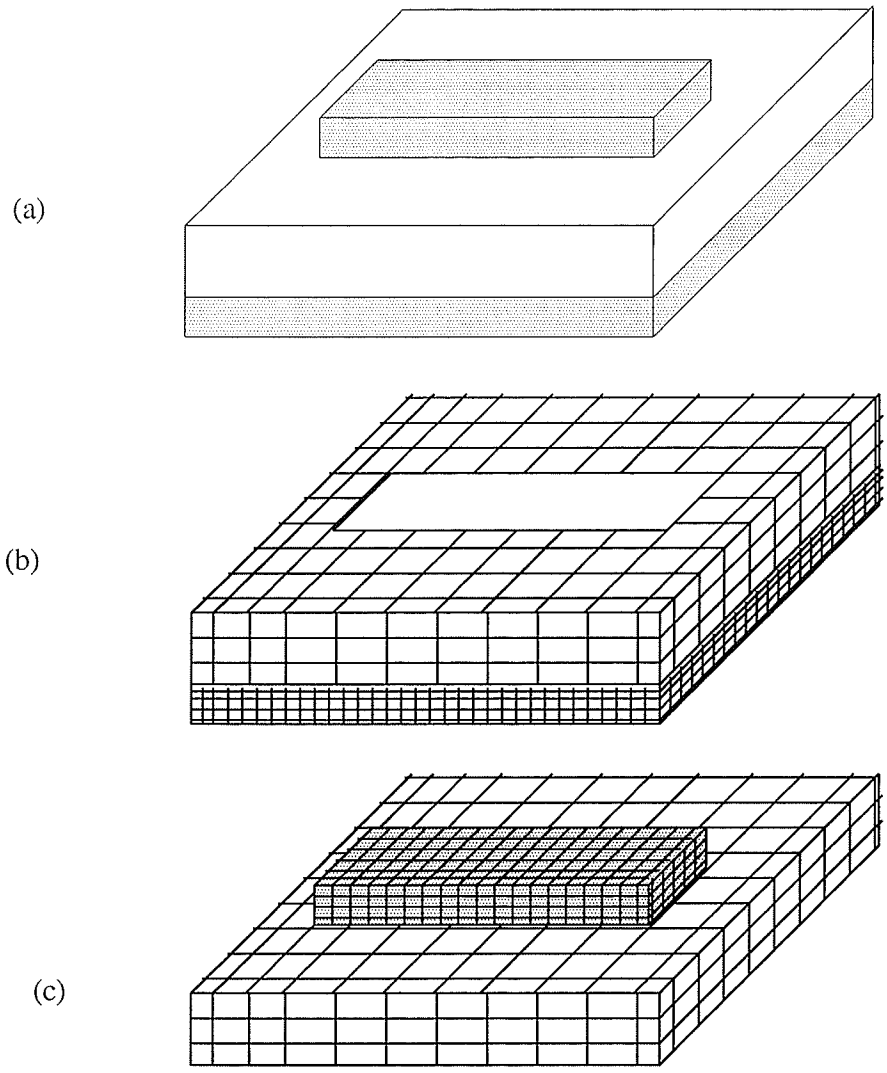

Figure 4.2: *(a) An example of two conductor. (b) and(c) Discretization for the first stage solution.*

In general, the charge distribution and the total charge stored on each conductor depend on the following factors:

a) the geometrical (shape) factor of each conductor,

b) the geometrical factor and the electrical permittivities of the dielectric material in the structure, and

c) the relative positioning of each conductor with respect to the others.

The effects of factors a) and b) are accounted for in the first stage of the solution. The third factor is accounted for in the second stage of the solution. As a first order approximation, the change in the charge distribution due to the coupling of other conductors can be considered as an unknown weighting factor α_i. This assumption is valid only when the separation between the conductors is larger than the conductors cross section. However, enforcing the boundary conditions and using the charge distributions obtained in the first stage, as an entire domain basis functions, ensure the accuracy of the complex capacitance matrix.

Thus the potential at any point on the surface of the conductors, for the system shown in Fig. 4.2 is then given by

$$\begin{aligned} V_1 &= [\alpha_1 F(1,1) + \alpha_2 F(1,2)] \\ V_2 &= [\alpha_1 F(2,1) + \alpha_2 F(2,2)] \end{aligned} \tag{4.25}$$

where V_i is the potential enforced on the i^{th} conductor, and for I, II=1,2

$$\begin{aligned} F(I,I) &= f(I,I) + f(I,d) \\ F(I,II) &= f(I,II) + f(I,d) + f(I,II) * f(II,d) \end{aligned} \tag{4.26}$$

d refers to all the dielectric-dielectric interfaces, and

$$f(I,II) = \frac{1}{N_I} \sum_{i=1,\, i \in cond.\ I}^{N_I} \sum_{j=1,\, j \in cond.\ II}^{N_{II}} q_j p_{ij} \tag{4.27}$$

$$f(I,d) = \frac{1}{N_I} \sum_{i=1,\, i \in cond.\ I}^{N_I} \sum_{j=1,\, j \in S^{ab}}^{N_d} q_j p_{ij} \tag{4.28}$$

p_{ij} is given by (4.17).

Equation (4.25) can be written in matrix form as

$$\mathbf{AB} = \mathbf{V} \tag{4.29}$$

where $\mathbf{A}$ is a square matrix of order 2, $\mathbf{B} = [\alpha_1 \alpha_2]^T$, and $\mathbf{V}$ are column matrices of order 2.

Notice that the value of the diagonal elements A_{ii} are known; A_{ii} is equal to the impressed potential on the i^{th} conductor. Thus in using the impressed potential value for the diagonal elements a reduction in the computation cost is produced.

The resulting linear system of equations (4.29) can be solved for α_1 and α_2. Then the capacitances C_{11} and C_{21} are given by

$$\hat{C}_{11} = \alpha_1 \sum_{k=1}^{N_1} q_k \tag{4.30}$$

$$\hat{C}_{21} = \alpha_2 \sum_{k=1}^{N_m} q_k \tag{4.31}$$

$\hat{C}_{12}$ and $\hat{C}_{22}$ can be obtained by interchanging the value of V_1 and V_2 and solving the linear system of equations (4.29).

A system of m linear equations, similar to (4.1), is obtained for a system of m conductors. To compute the j^{th} column of the complex capacitance matrix,

equation (4.29) must be solved for α_i given a vector $\mathbf{V}$ where $V_i = 1, i = j$ and $V_i = 0$ otherwise. Then the ij^{th} term of the capacitance matrix is computed by multiplying α_i by the sum of the charges resulting from the first stage solution.

Note that for a system consisting of m conductors embedded on a homogeneous material, equation (4.26) is transforms to

$$F(I, I) = f(I, I), \qquad F(I, II) = f(I, II) \tag{4.32}$$

The solution proceeds as described above for the general case.

While the two-stage method gives accurate complex capacitance matrix, it does not accurately calculate the charge distribution on each conductor. The main goal of this work is the reduction of the computational cost and memory storage required by the IEM; for the calculation of the complex capacitance matrix. This calculation is in great demand by industry.

An accurate charge distribution, as a result of an enforced potential, can be obtained using an iterative method. With this method the speed of convergence depends strongly on the initial estimate of the charge distribution. A good estimate of the initial value of the charges would speed up convergence substantially. The best initial values of the charges for the iterative method, is the charge distribution obtained using the two-stage method since the coupling of all the charges on a conductor is included in the first stage of the solution for each conductor. The effect of the dielectric on the charge distribution of each conductor is also included in the first stage. In addition, the second stage of the two-stage method accounts for the total coupling among the conductors.

4.4 Computational Time and Memory Storage

In order to use the two-stage method to compute an $m \times m$ capacitance matrix, the first stage solution must be repeated m times. Note, that for practical cases, the number of patches on the conductor-dielectric interfaces are usually much larger than the number of patches on the dielectric-dielectric interfaces. Assuming equal number of patches on each conductor, the cost of computing the entries and solving each matrix is proportional to

$$2m(N_i + N_d)^2 + m(N_i + N_d)^3. \tag{4.33}$$

While the cost of the second stage solution is proportional to

$$(mN_i)^2 + m^3 + m^2 \tag{4.34}$$

Then the total computational cost for an equal number of patches on each conductor, is proportional to

$$2m(N_i + N_d)^2 + m(N_i + N_d)^3 + (mN_i)^2 + m^3 + m^2 \tag{4.35}$$

The dominant term in (4.35) is $m(N_i+N_d)^3$ since, for practical cases, the number of conductors in the system is much less than the number of patches used to discretize a single conductor.

The computational cost of using the classical IEM, as applied to the whole structure, is proportional to the cost of computing the entries of the matrix, the LU decomposition and the solution of the decomposed matrix m times; that is

$$(mN_i + N_D)^2 + m(mN_i + N_D)^3 + m(mN_i + N_D)^2 \tag{4.36}$$

The memory storage required by the two-stage method is proportional to the maximum memory required by the classical IEM in solving for a single conductor in the structure and the dielectric interfaces; *i.e.* a maximum of $(N_i+N_d)^2$. The number of patches on the conductor-dielectric interfaces are usually much larger than the number of patches on the dielectric-dielectric interfaces. On the other hand, the memory storage required by the classical IEM is proportional to $(\sum_{i=1}^{m} N_i)^2$. Thus, the memory requirement of the two-stage method, is much less than that of the classical IEM.

4.5 Results and Comparison

A general code was developed using the formulation of the two-stage method. This algorithm was tested for various geometries in comparison with the classical IEM.

Table 4.1 presents a comparison of the capacitance and conductance matrices obtained using the two-stage method and the classical IEM. The structure is shown in Fig. 4.3. It consists of two traces and a finite ground plane. The dielectric permittivity is $\hat{\epsilon}_r = 3(1 - jtan\delta)$, $tan\delta = 0.001$ and the structure was discretized to 2524 small patches. The large number of patches results from the need to satisfy the criteria of numerical convergence by using patches with an aspect ratio less than 5. In addition, the conductor surfaces that are common to the dielectric material require a large number of elements to accurately calculate the charge distribution using the IEM. The computational time and the memory required by the IEM are

$365m$ and 98 MB, respectively. However, the computational time and the memory requirement of the two-stage method are respectively $90.4m$ and $16MB$. For such a structure, reducing the spacing between the traces or increasing the dielectric permittivity causes increase in the errors of the two-stage method. Table 4.2 presents a comparison of the capacitance matrix for a microstrip structure. The dimensions of the strip are $(1.5, 0.05, 0.02)mm$; the ground plane has dimensions of $(2, 2, 0.02)mm$ and the dielectric thickness is $0.09mm$. Table 4.3 presents a comparison of the capacitance matrix for a 2x2 array of connectors, shown in Fig. 4.4, obtained using the two-stage method and the classical IEM.

It can be seen from the tables that the results obtained using the new method are accurate in comparison with those obtained using the classical IEM.

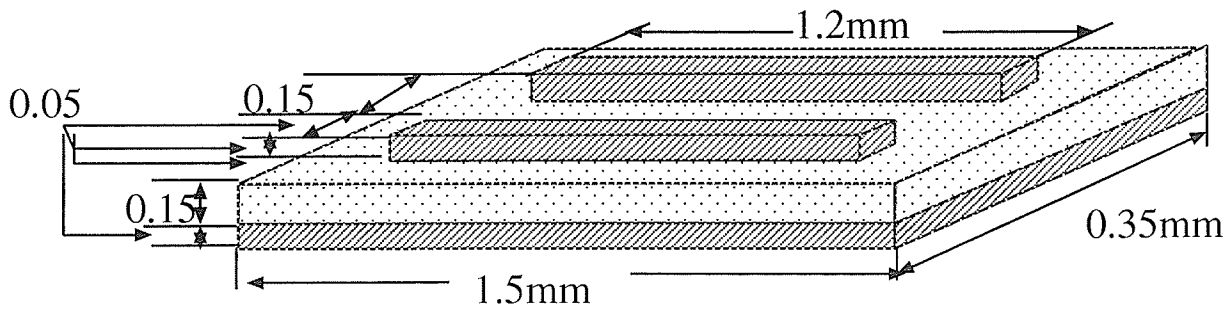

Figure 4.3: *Two traces over a dielectric with* $\hat{\epsilon}_r = 3(1 - tan\delta)$, $tan\delta = 0.001$.

i		1	2	3		1	2	3
C_1	IEM.	51.72	-12.24	-33.34	G_1	1.25	-0.37	-0.78
	Two-stage	49.79	-11.33	-31.75		1.2	-0.36	-0.76
C_2	IEM.	-12.24	51.72	-33.34	G_2	-0.37	1.25	0.78
	Two-stage	-11.33	49.79	-31.75		-0.36	1.2	-0.76
C_g	IEM.	-33.47	-33.47	102.75	G_g	-0.78	-0.78	1.85
	Two-stage	-31.76	-31.76	96.72		-0.76	-0.76	1.2

Table 4.1: *Comparison between the capacitance and conductance matrices of the system shown in Fig. 4.2. The unit of the capacitances is fF and the conductance is mS.*

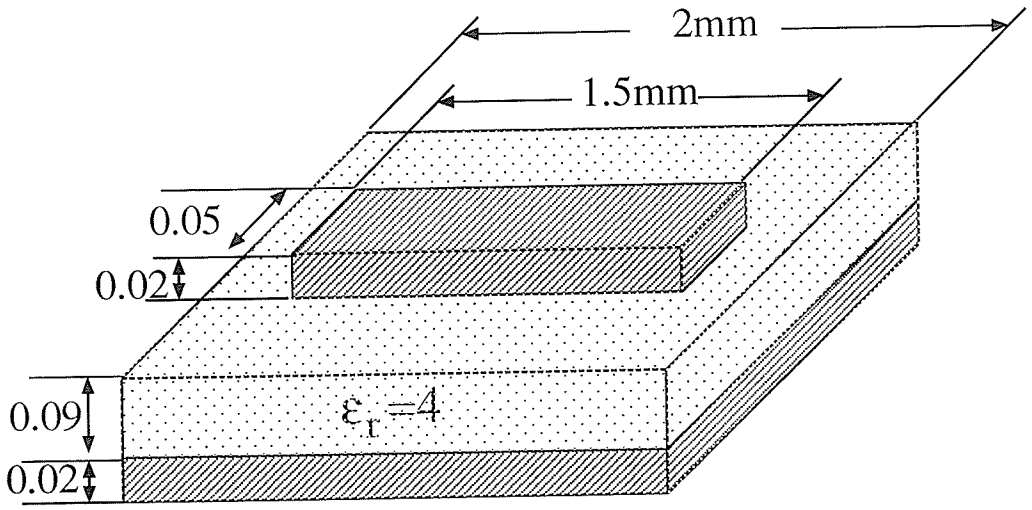

		l	g
l	IEM.	173.5	169.1
	Two-stage	170.3	168.5
g	IEM.	169.1	275.4
	Two-stage	168.5	271.1

Table 4.2: *Comparison between the capacitance matrix of a microstrip structure. The units of the capacitances are fF.*

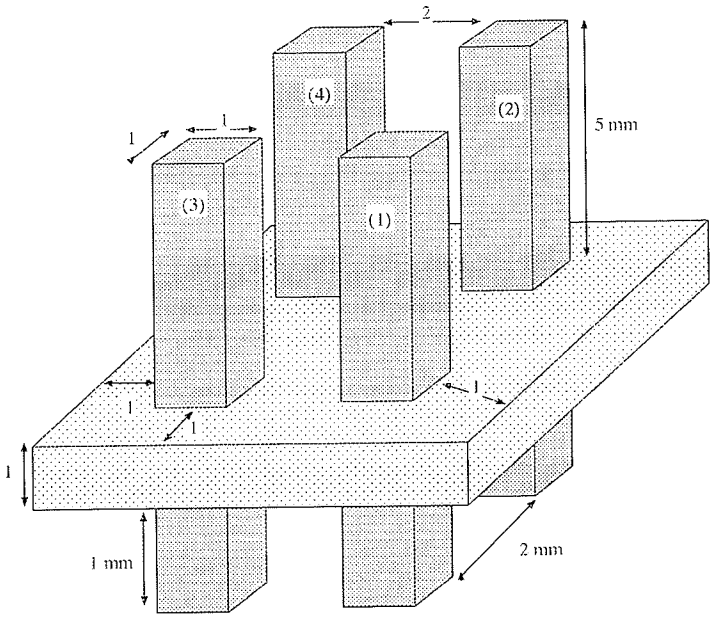

Figure 4.4: *A system of four pin connectors*

i		1	2	3	4
1	IEM.	325.1	-100.5	-100.5	-30.9
	Two-stage	320.8	-99.7	-99.7	-30.6
2	IEM.	-100.5	325.1	-30.88	-100.5
	Two-stage	-99.7	320.8	-30.6	-99.7
3	IEM.	-100.5	-30.88	325.1	-100.5
	Two-stage	-99.7	-30.6	320.8	-99.7
4	IEM.	-30.9	-100.5	-100.5	325.1
	Two-stage	-30.6	-99.7	-99.7	320.8

Table 4.3: *Comparison between the capacitance matrix of a system of 4 connectors, as shown in Fig. 4.3. The units of the capacitances are fF.*

Chapter 5

Frequency Dependent Inductance and Resistance Matrices

In this chapter, an efficient two-step approach is used to calculate the inductance and resistance matrices for three-dimensional multiconductor structures. In the first step, the partial element equivalent circuit method is used to calculate the self inductance and resistance of each conductor. Each conductor is considered separately in isolation of all other conductors in the structure. The conductor is divided into straight sections and each section is discretized into thin filaments. These filaments are then assembled into the desired equivalent impedance matrix using network theory. Mesh analysis is then used to solve for the complex frequency-dependent impedance of the conductor. In the second step, The mutual inductances among the conductors are estimated by using the filaments approximation. The two step approach gives accurate self impedance. However, the accuracy of the approximation of the mutual inductance depends on the separation between the conductors and the conductor cross sectional dimensions relative to the skin depth.

In the next section the PEEC approach is described. It is based on the integral equation formulation and network theory. The proposed two-step solution is presented in section 5.2. Results and comparison are given in section 5.3. Finally, a

discussion of the generalization of the algorithm is given is section 5.4

5.1 Integral Equation Formulations

Maxwell's equations for the sinusoidal steady state case are

$$\bigtriangledown \times \mathbf{E} = -jw\mu\mathbf{H} \tag{5.1}$$

$$\bigtriangledown \times \mathbf{H} = jw\epsilon\mathbf{E} + \mathbf{J} \tag{5.2}$$

$$\bigtriangledown.(\epsilon\mathbf{E}) = \rho \tag{5.3}$$

$$\bigtriangledown.(\mu\mathbf{H}) = 0 \tag{5.4}$$

The following formulation assumes quasi-static conditions which imply that the size of the structure is small compared to the minimum wavelength of interest and retardation effects can be neglected. The displacement current ($jw\epsilon\mathbf{E}$) is negligible compared to the conduction currents ($\mathbf{J}$) since the conductivity is very high. This assumption implies that the current in the conductor has zero divergence,

$$\bigtriangledown.J = 0 \tag{5.5}$$

To allow for ideal current sources, equation (5.5) becomes

$$\bigtriangledown.J = \begin{cases} I_s(r) & \text{r} \in \text{the feed point;} \\ 0 & \text{otherwise.} \end{cases} \tag{5.6}$$

The formulation of the magnetic quasi-static problem for the calculation of the inductance is independent of the dielectric properties of the surrounding material. Therefore, the electric field $\mathbf{E}$ inside the conductor is given by

$$\mathbf{E} = -jw\mathbf{A} - \bigtriangledown\phi \tag{5.7}$$

where ϕ is the electric potential and w is the angular frequency.

Using Ohm's law and neglecting the displacement currents, equation (5.7) becomes

$$\frac{\mathbf{J}}{\sigma} = -jw\mathbf{A} - \bigtriangledown\phi \tag{5.8}$$

In the quasi-static limit, the magnetic vector potential $\mathbf{A}$ is given by

$$\mathbf{A} = \frac{\mu}{4\pi}\int_{v'}\frac{\mathbf{J}(r')}{\mid r - r' \mid}dv' \tag{5.9}$$

where v' is the volume of all conductors.

Substituting (5.9) into (5.8) yields the following integral equation

$$\frac{\mathbf{J}(r)}{\sigma} + \frac{jw\mu}{4\pi}\int_{v'}\frac{\mathbf{J}(r')}{\mid r - r' \mid}dv' = -\bigtriangledown\phi(r) \tag{5.10}$$

Using equation (5.10) and the current conservation, given by equation (5.6), the conductor current density ($\mathbf{J}$) and the scalar potential (ϕ) can be computed.

Charge accumulation on the surface of the conductor is assumed to be negligible. This implies that the component of the current that is normal to the surface of the conductor is zero at the surface. Thus the conductor can be divided into very thin filaments where the current is assumed to flow along the length of the filaments. The structure can then be represented by a planar graph where the nodes in the

graph are associated with connection points between filaments and the branches. The branches represent the filaments into which each conductor is discretized. A sample circuit for a single conductor is shown in Fig. 5.1(a) with its circuit model in Fig. 5.1(b). This circuit model is obtained after the model of 5.1(a) was discretized into filaments.

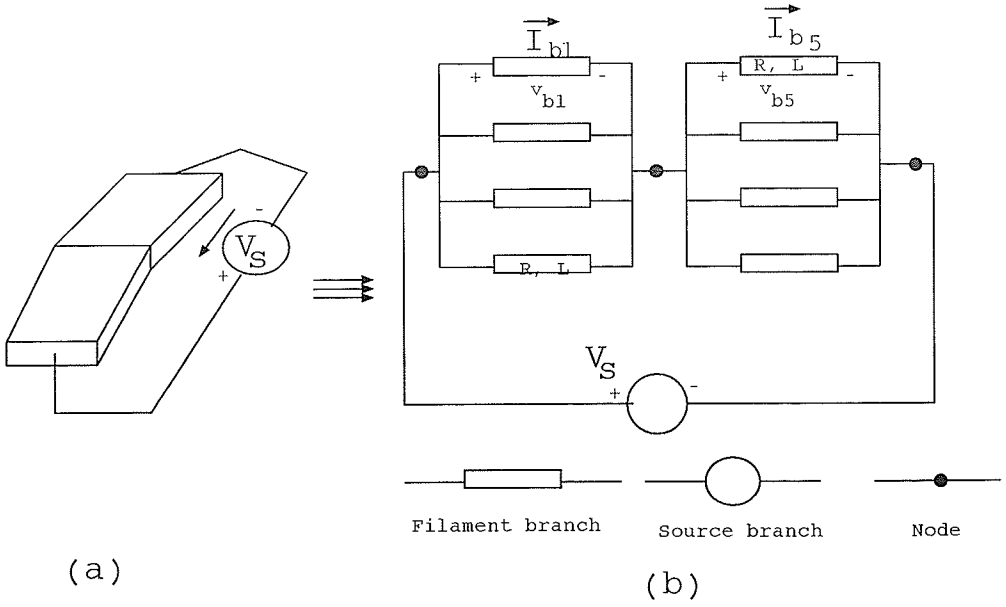

Figure 5.1: *(a) A two-straight sectioned conductor, (b) circuit model*

By defining a weighting function, the unknown current distribution can be approximated by

$$\mathbf{J}(r) \approx \sum_{i=1}^{n} \mathbf{I}_i \mathbf{W}_i(r) \mathbf{l}_i \tag{5.11}$$

where I_i is the current inside filament i, l_i is a unit vector along the length of the filament and

$$\mathbf{W}_i(r) \equiv \begin{cases} \frac{1}{a_i} & \text{r} \in \text{ patch i;} \\ 0 & \text{otherwise.} \end{cases} \tag{5.12}$$

where a_i is the cross sectional area of the i^{th} filament.

By following the method of moment formulations a system of equations can be obtained by taking the inner product of the weighting function, equation (5.12), with the integral equation, given by equation (5.10),

$$(\frac{\mathbf{l}_i}{\sigma a_i})I_i + jw\sum(\frac{\mu}{4\pi a_i a_j}\int_{v_i}\int_{v_j'}\frac{\mathbf{l}_i.\mathbf{l}_j}{\mid r-r'\mid}dvdv')I_j = \frac{1}{a_i}\int_{a_i}(\phi_A - \phi_B)dA \qquad (5.13)$$

where l_i is vector representing the length of filament i, a_i is the cross section, ϕ_A and ϕ_B are the potential on the filament end faces and V_i and V_j are the volumes of filaments i and j, respectively.

Equation (5.13) can also be written in matrix form

$$(\mathbf{R} + jw\mathbf{L})I_b = \mathbf{P} \qquad (5.14)$$

where $\mathbf{I}_b$ is a vector of b filament currents, $\mathbf{P}$ is a column vector of filament voltages $P_i = \phi_{A_i} - \phi_{B_i}$, $\mathbf{R}$ is a diagonal matrix of order b which consists of the dc resistance of each filament,

$$\mathbf{R}_{ii} = \frac{l_i}{\sigma a_i} \qquad (5.15)$$

$\mathbf{L}$ is a dense symmetric matrix of order b,

$$\mathbf{L}_{ij} = \frac{\mu}{4\pi a_i a_j}\int_{v_i}\int_{v_j'}\frac{\mathbf{l}_i.\mathbf{l}_j}{\mid r-r'\mid}dvdv' \qquad (5.16)$$

Equation (5.14) can also be written as

$$\mathbf{Z}\mathbf{I}_b = \mathbf{V}_b \qquad (5.17)$$

where $\mathbf{Z} = \mathbf{R} + jw\mathbf{L}$ is a branch impedance matrix of order b and $\mathbf{V}_b = \phi_A - \phi_B$ is the vector of branch voltages. The method that is used to obtain the circuit as described above is called the Partial Element Equivalent Circuit (PEEC) [7].

5.1.1 Nodal Analysis Formulation

According to Kirchhoff's current law (KCL) and voltage law (KVL), the nodal voltages and currents can be related to that of the branches by

$$\mathbf{A}\mathbf{I}_\mathrm{b} = \mathbf{I}_\mathrm{s} \quad \textit{and} \quad \mathbf{A}^T\mathbf{V}_\mathrm{n} = \mathbf{V}_\mathrm{b} \tag{5.18}$$

Here, $\mathbf{A}$ is the incidence matrix of the circuits and $\mathbf{I}_s$ is a mostly zero vector of source currents at the node locations. Column i in $\mathbf{A}$ has two nonzero entries; minus one in the row corresponding to the node from which the filament i's current leaves and plus one in the row corresponding to the node into which the filament i's current enters. The superscript T denotes the matrix transpose. Combining equations (5.17) and (5.18) yields

$$\mathbf{A}\mathbf{Z}^{-1}\mathbf{A}\mathbf{V}_\mathrm{n} = \mathbf{I}_\mathrm{s} \tag{5.19}$$

Thus column i of the reduced impedance matrix $\mathbf{Z}_r$ can now be computed by setting the source current equal to unity (unit current through conductor i) and then solving equation (5.19) for the node voltages ($\mathbf{V}_n$). The difference of appropriate node potentials gives the voltages across each of the conductors. Thus forming equation (5.19) requires a memory storage of order b^2. The inversion of the $\mathbf{Z}$ matrix costs a CPU time of order b^3 where b is the number of current filaments into which the system of conductors is discretized. In addition, solving (5.19) requires a computational time of order n^3 (n is the number of nodes). The computational cost can be reduced by using the mesh analysis formulation which doesn't require the inversion of the $\mathbf{Z}$ matrix.

5.1.2 Mesh Analysis Formulation

The need for the inversion of the impedance matrix, (**Z**) in equation (5.19) can be avoided by reformulating the equation using a mesh analysis approach. In a network, a mesh is defined as any loop of branches in the graph which does not enclose any other branches [81]. The unknowns are the currents flowing around any mesh in the network, Fig. 5.2 shows an example of one conductor.

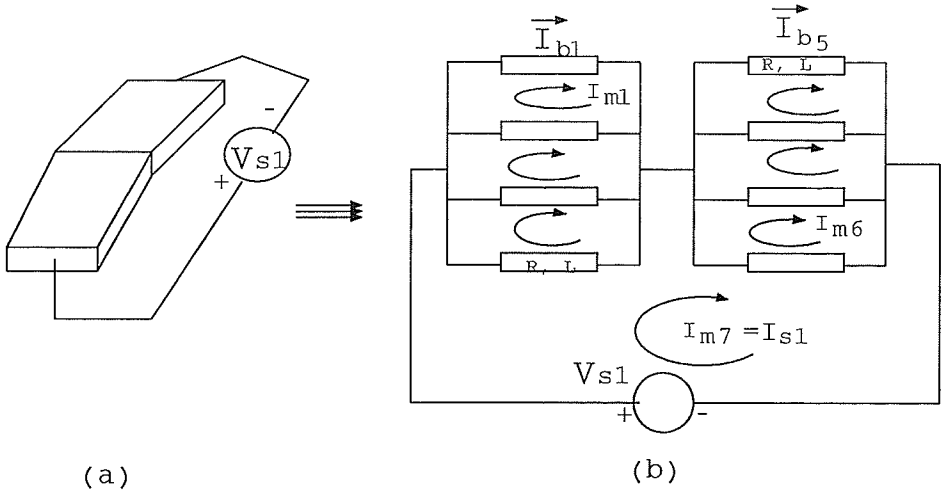

Figure 5.2: (a) *A two-straight sectioned conductor, (b) circuit model*

According to the Kirchhoff's voltage law, the sum of branch voltages around each mesh in the network must be zero, *i.e.*,

$$\mathbf{M}\mathbf{V}_b - \mathbf{V}_s = 0 \tag{5.20}$$

where $\mathbf{V}_s$ is the mostly zero vector of source branch voltages, $\mathbf{V_b}$ is the vector across each branch except the source branch and $\mathbf{M}$ is a matrix of order $m \times b$.

Note: $m = b - n + c$, b is the number of filament branches, n is the number of conductor sections and c is the number of conductors.

The $\mathbf{M}$ matrix has the property that most of its columns $(m - c)$ have no more than two nonzero entries, a plus one and minus one.

The current around each loop satisfies Kirchhoff's current law:

$$\mathbf{M}^T\mathbf{I}_m - \mathbf{I}_b = 0 \tag{5.21}$$

where T denotes the matrix transpose and $\mathbf{I}_m$ is the vector of the mesh currents.

The relationship between branch currents and voltages is given by

$$\mathbf{Z}\mathbf{I}_b = \mathbf{V}_b \tag{5.22}$$

However a combination of equation (5.20) with (5.21) and (5.22) results in

$$\mathbf{M}\mathbf{Z}\mathbf{M}^T\mathbf{I}_m = \mathbf{V}_s \tag{5.23}$$

Thus to compute the i^{th} column of the reduced admittance matrix ($\mathbf{Y}_r = \mathbf{Z}_r^{-1}$), equation (5.23) is solved in terms of a $\mathbf{V}_s$ whose only nonzero entries correspond to v_{si}. The entries of $\mathbf{I}_m$ associated with the source branches can then be extracted.

The solution of the system of equations (5.23) requires a memory storage of order m^2 and a computational time of order m^3 . For a complex structure, m could be more than ten thousand, which presents a limitation to the applicability of the method. In the next section, an approach is proposed to overcome this limitation.

5.2 The Two-Step Solution

To overcome the limitation of the Partial Element Equivalent Circuits (PEEC) method, a two step solution is used to calculate the inductance and resistance matrices [82]. In general, the inductance and resistance matrices of the conductors depend on:

a) the path of the current in the conductor,

b) the geometrical (shape) factor of each conductor, and

c) the spacing and the positioning of each conductor with respect to the others.

The first step of the solution takes into account factors a) and b) while the second step of the solution gives approximation to the effect of the third factor.

For a structure consisting of N conductors, each individual conductor is considered separately in the first step of the solution. Each conductor is divided into sections which are then individually discretized into very thin filaments. The PEEC method is then used to solve for the inductance and resistance (the Z impedance) of each conductor while neglecting the effect of all other conductors. However in the second step, the mutual inductances among the conductors are approximated using the filaments approximation [30].

To illustrate this approach, consider a structure consisting of two conductors (N=2) shown in Fig. 5.3. In the first step of the solution, each conductor is considered separately. The first conductor is discretized into N_I thin filaments and then represented by a circuit model as shown in Fig. 5.4.

The inductance (L_{11}) and the resistance (R_{11}) of the conductor are solved for

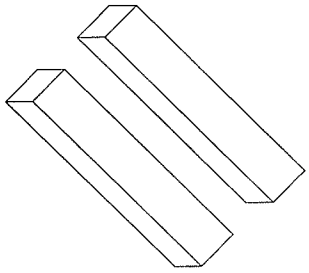

Figure 5.3: *Example of two conductors*

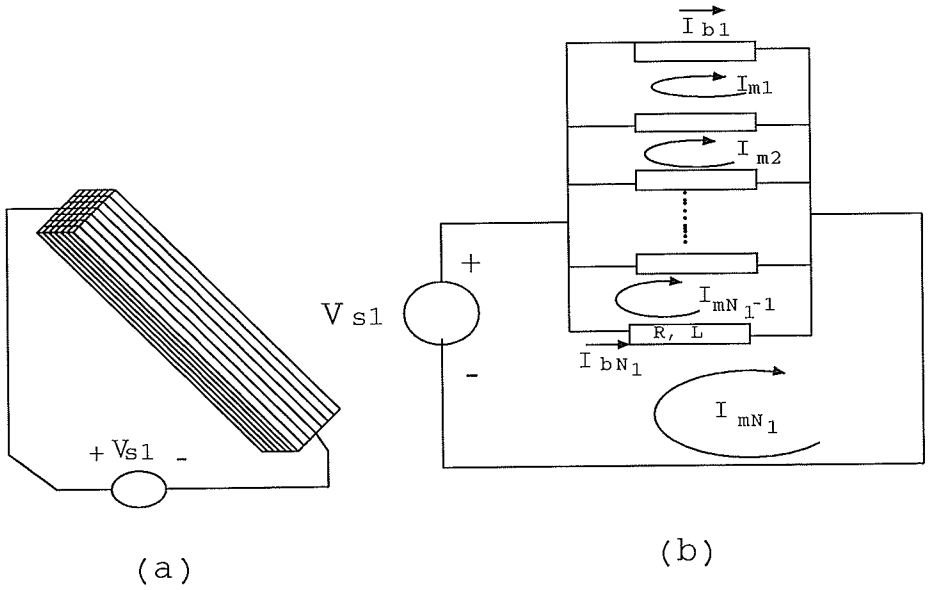

Figure 5.4: *One conductor discretized to filaments, (b) modelled as a circuit*

using the PEEC method and the mesh analysis approach. This process is then repeated for the second conductor. In the second step of the solution, the mutual inductance is obtained using the filaments approximation . The impedance matrix (**Z**) for this structure is then given by

$$[\mathbf{Z}] = \begin{bmatrix} R_{11} + jwL_{11} & jwL_{12} \\ jwL_{21} & R_{22} + jwL_{22} \end{bmatrix} \tag{5.24}$$

The diagonal elements of the (**Z**) matrix are obtained from the first step of the solution. The off-diagonal elements ($L_{12} = L_{21}$) can be estimated using the filament approximation [30]. In this approximation, the mutual inductance between the two conductors is given by,

$$L_{nm} = L_{mn} = \frac{1}{N_n N_m} \sum_{i=1}^{N_n} \sum_{j=1}^{N_m} L_{fij} \tag{5.25}$$

where N_n and N_m are the number of filaments corresponding to conductor n and m, respectively, the subscript f denotes the filament approximation and L_{fij} is the mutual inductance between the i and j filaments; which is given by

$$L_{fij} = L_{fji} = \frac{\mu}{4\pi} \int_i \int_j \frac{d\mathbf{l}_i . d\mathbf{l}_j}{\mid r - r' \mid} \tag{5.26}$$

The accuracy of evaluating L_{nm} for fixed N_n and N_m depends on the relative position of the conductors. The number of filaments used in the first step of the solution can be used again to obtain L_{nm}. However the accuracy and computation time can be improved by choosing the number of filaments to be an inverse function

of the distance between the conductors. This results in a considerable reduction in the computation time, since only a small number of conductors can be physically close to each other in a multiconductor structure. An algorithm can be developed for the selection of an appropriate number of filaments for each geometry. In addition, more accurate mutuel inductance between two conductors that have small separation compares to their cross-section can be obtained by solving for the two conductor together in the first step of the solution.

5.3 Results and Comparison

To check the validity of the present approach, a transmission line formed by two copper conductors is considered. The conductors are of rectangular cross section 2 by $2mm$ and separated by $2mm$. For comparison with available two-dimensional analysis results [5], the length of the conductors was chosen to be 100 meters and the results scaled appropriately. Each conductor is then divided into 100 thin filaments. The total inductancd, $[L = L_{11}+L_{22}-2L_{12}]$, inductance and resistance, $R = R_1+R_2$ variations with the frequency obtained using the classical PEEC method and the two-step method are shown in Fig. 5.5. The errors in the inductance and resistance values obtained by using the two-step method are less than 5% and 1%, respectively, in comparison with those obtained using the classical PEEC method.

At high frequencies, the dc resistance representation in the formulation is not valid since the resistance increases with the square root of the frequency [6]. However this aspect can be incorporated in the algorithm, as described in section 5.4.2, to

further improve the accuracy of the method.

Figure 5.6 shows the total inductance of two identical transmission lines as a function of the edge-to-edge separation, D, between the lines. The length of the line is 1 inch and the cross section of each conductor is 15 by 5 mils. Each conductor is divided into 30 thin filaments and the frequency of operation is 50 MHz. The total inductance of the transmission lines is obtained using the classical PEEC method and the two-step solution. The numerical results are compared with the following approximate closed form equation [83],

$$\frac{L}{l} = 0.01 ln \left[\frac{\pi(D)}{w+t} + 1 \right] \ (\mu H/in) \tag{5.27}$$

where l, w and t are the length, width, and thickness of each conductor, respectively. As shown in the figure, results obtained using the two-step solution compare well with those obtained using the classical PEEC method. On the orher hand, the closed form equation gives about 15% error.

Table 5.1 presents a comparison of the inductance matrix for a 3x2 array of right angle pin connectors, obtained using the two-step method and the classical PEEC method. The frequency of operation is 1 MHz. The pins are discretized to 200 filaments each. The memory storage requirements and the computational time using the classical PEEC are $51Mb$ and 272 m, respectively. On the other hand, the storage memory required by the two-step method is $1.8Mb$ and the computational time is $3.5m$. All computations have been done using SPARC10/41 workstation.

Table 5.2 compares the inductance matrix of a microstrip structure obtained using the two-step method and the classical PEEC method. This structure con-

sists of three identical traces above a ground plane. In addition, the frequency of operation is $1MHz$ and the traces are discretized to 210 filaments each with the ground plane being discretized to 660 filaments. The memory storage requirements $58Mb$ and the computational time $311m$ using the classical PEEC are much larger than the memory storage $14.5Mb$ and the computational time $41.5m$ required by the two-step method. It can be seen from the tables that the two-step method gives very accurate results in comparison to the classical PEEC method.

Fig. 5.7 shows the inductance of two identical parallel conductors as a function of the conductors length, l, for two different conductor separations (D). As shown in the figure, the results obtained using the new approach are in good agreement with those obtained using the classical PEEC method.

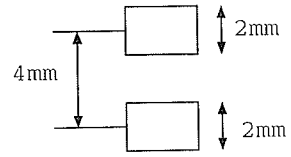

Transmission line of 100 m length

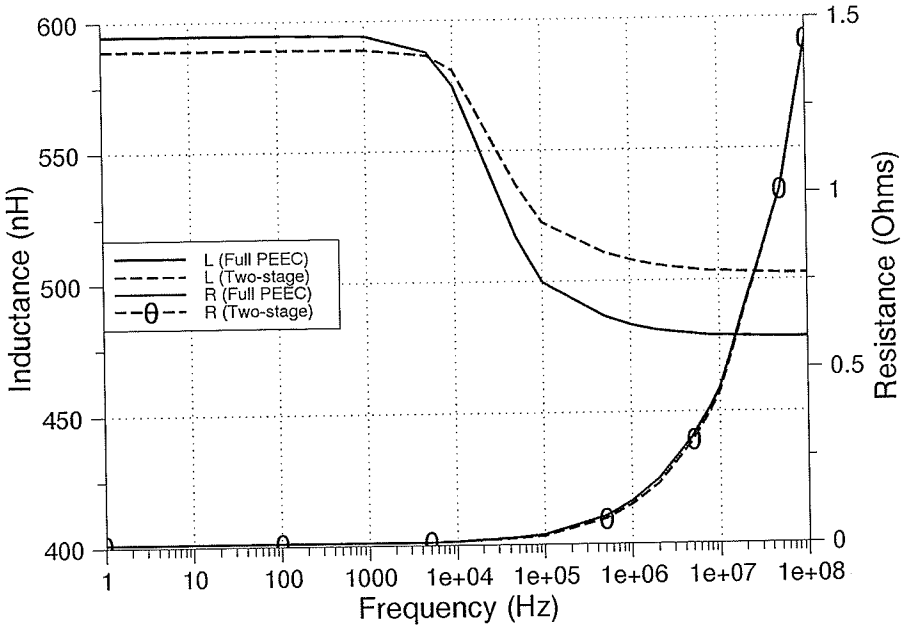

Figure 5.5: *Resistance and inductance of transmission line*

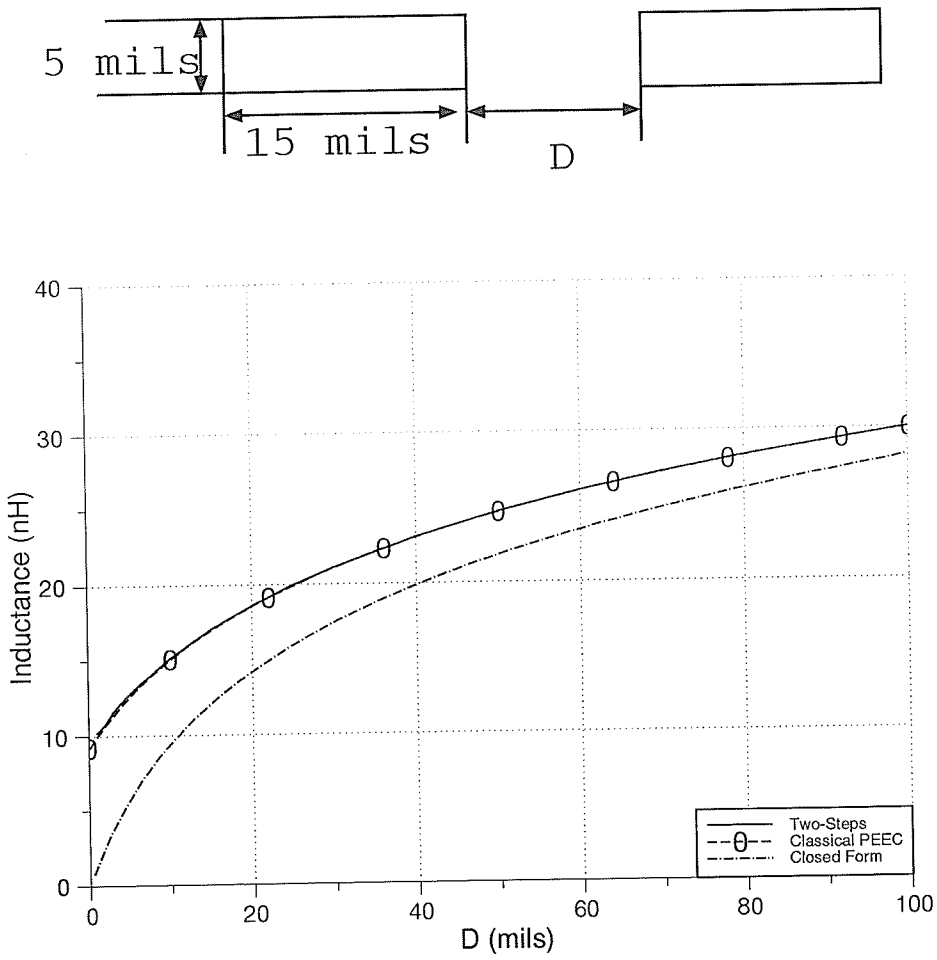

Figure 5.6: *Inductance of two parallel conductors as a function of conductors separation.*

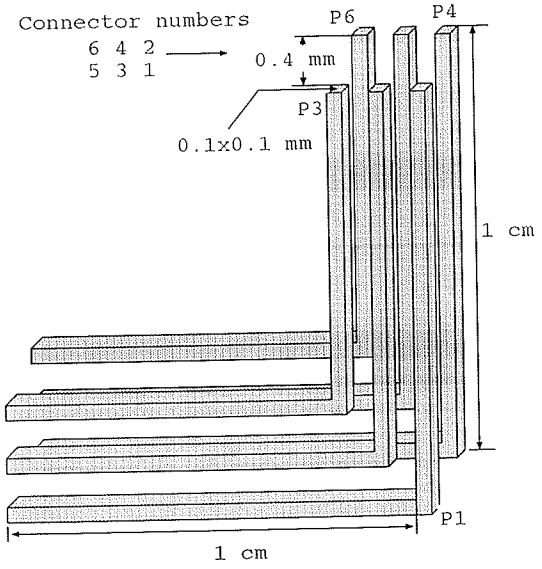

i		1	2	3	4	5	6
p1	PEEC	20.56	10.61	7.71	11.02	9.34	7.34
	Two-step	20.54	10.60	7.70	11.0	9.34	7.34
p2	PEEC	10.60	19.33	9.82	9.32	10.29	8.64
	Two-step	10.60	19.34	9.83	9.34	10.29	8.65
p3	PEEC	7.71	9.83	18.0	7.34	8.64	9.4
	Two-step	7.71	9.84	18.01	7.34	8.65	9.45
p4	PEEC	11.0	9.34	7.34	20.54	10.60	7.70
	Two-step	11.01	9.34	7.34	2.056	10.61	7.71
p5	PEEC	9.34	10.28	8.64	10.60	19.33	9.83
	Two-step	9.34	10.29	8.65	10.61	19.34	9.83
p6	PEEC	7.34	8.64	9.45	7.70	9.83	18.0
	Two-step	7.34	8.65	9.5	7.71	9.83	18.01

Table 5.1: *Comparison between the inductance matrix of a system of 6 connectors, as shown, obtained using the two-step approach and the classical PEEC method. The unit of the inductances is nH.*

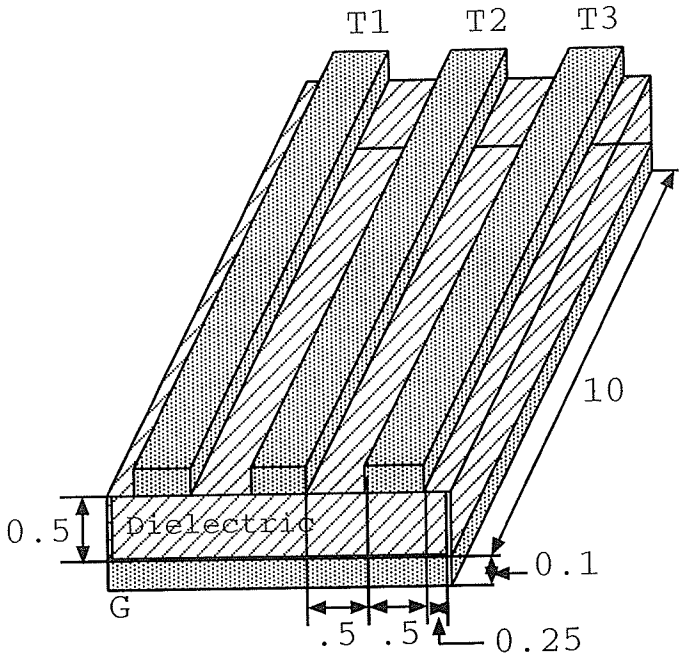

i		T1	T2	T3	G
T1	PEEC	7.76	4.18	3.54	3.94
	Two-step	8.06	4.23	3.69	3.89
T2	PEEC	4.18	7.91	4.18	4.20
	Two-step	4.23	8.21	4.23	4.34
T3	PEEC	3.54	4.18	7.76	3.94
	Two-step	3.69	4.23	8.06	3.89
G	PEEC	3.94	3.20	3.94	4.79
	Two-step	3.89	4.34	3.89	4.80

Table 5.2: *Comparison between the inductance matrix of a microstrip structure, as shown above, obtained using the two-step approach and the classical PEEC method. The dimensions are mm and the units of the inductances are nH.*

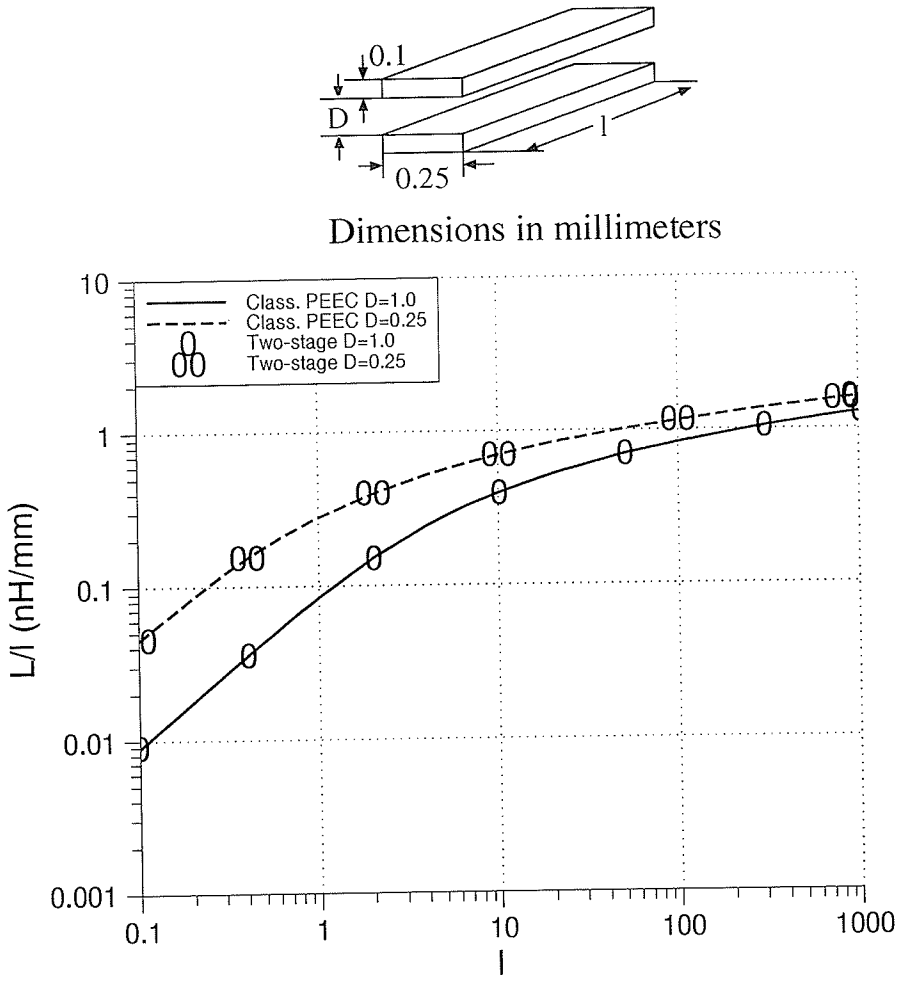

Figure 5.7: *The inductance of two parallel conductors as a function of the conductors length.*

5.4 Generalization of the Algorithm

In this section the effect of a ground plane and the calculation of the partial resistance, considering the skin effect, are presented.

5.4.1 Inclusion of Ground Plane

A ground plane can be accounted for by one of two approaches which depend on the relative size of the ground plane with respect to the conductors in the structure.

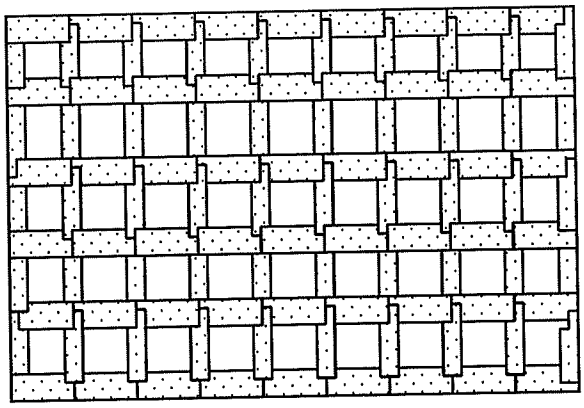

Figure 5.8: *Discretization of a finite ground plane in a width scale of 0.5:1*

1)Finite Ground Plane:

The filament approach described previously in this chapter can be applied to a finite ground plane. This ground plane is discretized to small filaments as shown in Fig. 5.8. The path of the current in the plane can be specified according to the connection of the sources to the conductors. A planar graph can then be constructed to represent the ground plane and the conductors in the structure.

2)Infinite Ground Plane:

Consider a structure consisting of two conductors over an infinite ground plane, as shown in Fig. 5.9a. The pretence of the ground plane can be modelled using image theory. The ground plane can be replaced by two image conductors under the ground plane as shown in Fig. 5.9b. The end of each conductor is connected to its image and both are treated as one unit. The inductance matrix can then be obtained for the equivalent structure.

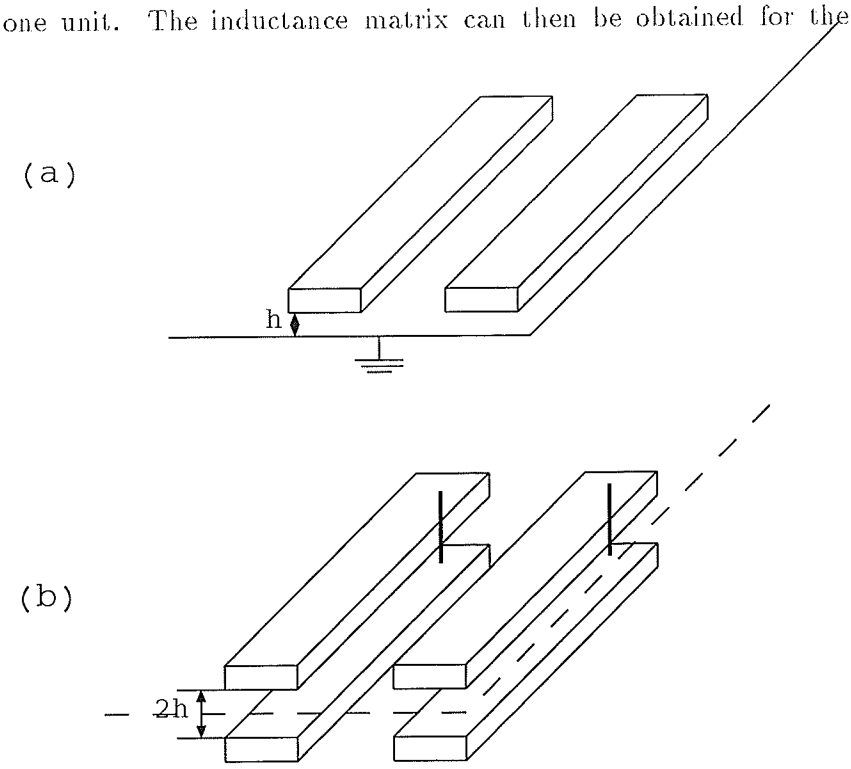

Figure 5.9: *Two traces over infinite ground plane. (a) Original structure, (b) equivalent structure by image theory.*

5.4.2 Evaluation of the Partial Resistance

The partial resistance for a straight segments can be calculated using the following equation:

$$R_i = \frac{l_i}{\sigma a_{ieff}} \tag{5.28}$$

where, l_i and a_{ieff} are the length and the effective area of the i^{th} filament and σ is the conductivity. At low frequencies, the effective area is equivalent to the cross section area of the filament. However, at high frequencies, the current is crowded into the portion near the surface of the conductor, the so-called skin effect. Thus the effective area of the conductor decreases such that the resistance increases dramatically. The effective area can be calculated by assuming the current density decays exponentially along the radial direction of the cross section [84]. By neglecting the nonuniformity of the current along the periphery of the conductor's surface, the so called proximity effect [85], the effective area is then approximated by

$$a_{eff} = \frac{|\int\int J(r)da\,|^2}{\int\int |\,J(r)\,|^2\,da} \approx \frac{|\int\int e^{-(1+j)\epsilon(s)}da\,|^2}{\int\int e^{-2\epsilon(s)}da} \tag{5.29}$$

NOTE: $\epsilon(s)$ is the radial distance measured from the surface and normalized to the skin depth δ, that is

$$\epsilon(s) = \frac{d(s)}{\delta}, \quad \delta = \frac{1}{\sqrt{\pi\mu\sigma f}} \tag{5.30}$$

When the filament's cross section is smaller than the skin depth, the effective area is the cross section of the filament. For rectangular filaments, let T be the length of the shortest side of the filament, the distance function $d(s) = T/2 - s$ and incremental area $da = 2[2s + (W - T + 2s)]ds$. The effective area is then given by [34]

$$a_{eff} = 2(W+T)\delta \frac{|\,1 - \frac{1-\alpha}{1+\alpha}e^{-\gamma\epsilon} - \frac{2\alpha}{1+\alpha}\frac{1-e^{-\gamma\epsilon}}{\gamma\epsilon}\,|^2}{1 - \frac{1-\alpha}{1+\alpha}e^{-2\epsilon} - \frac{\alpha}{1+\alpha}\frac{1-e^{-2\epsilon}}{\epsilon}} \tag{5.31}$$

or

$$a_{eff} = WT[1 - \epsilon^2(3 - \epsilon_2)/18] \quad \text{if} \quad \epsilon << 1, \tag{5.32}$$

where

$$\gamma = 1 + j \quad \alpha = \frac{T}{W} \quad \text{and} \quad \epsilon = \frac{T}{2\delta} \tag{5.33}$$

For a filament with circular cross section, the distance function $d(s) = \rho - s$ and the incremental area $da = 2\pi s ds$. Hence the effective area is given by

$$a_{eff} = 2\pi\rho\delta \frac{|\, 1 - \frac{1-e^{-\gamma\epsilon}}{\gamma\epsilon} \,|}{1 - \frac{1-e^{-2\epsilon}}{2\epsilon}} \tag{5.34}$$

or

$$a_{eff} = \pi\rho^2(1 - \epsilon^2)/9) \quad \text{if} \epsilon << 1, \tag{5.35}$$

where $\gamma = 1 + j$ and $\epsilon = \rho/\delta$.

5.5 Volume Element Discretization

The partial element equivalent circuit method requires the conductors to be meshed into small volume elements. Generally, these conductors should be discretized into straight sections or segments to facilitate the use of the filaments approximation. Evaluation of the partial inductance for arbitrarily shaped filaments requires the integration of sixfold integrals. Therefore the discretization of the conductors into nonstraight filaments is not recommended, although it is theoretically valid. Curved conductors can be discretized into straight segments as shown in Fig. 5.10. Each straight segment is then meshed into thin volume elements. Conductors having curved cross-sections can be discretized using a staircase meshing. An efficient meshing should take into account the frequency of operation and the proximity of another conductor in the structure.

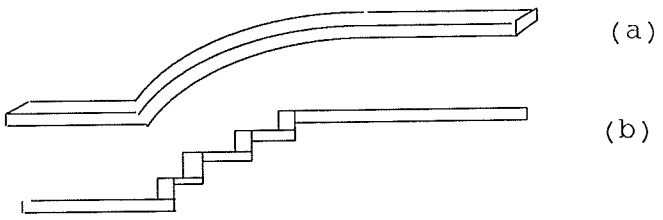

Figure 5.10: *(a)Conductor with curved segment. (b) Discretized straight segments*

5.5.1 Meshing For Low Frequencies

At low frequencies, the conductors' cross sections are generally smaller than the skin depth (δ). Thus the current flows along the conductors through each cross section. The segments of the conductor could be meshed into filaments by taking into account only the proximity of the other conductors. In addition, the effect of the proximity of other conductors can be taken into account by meshing the nearest side of each conductor, with respect to the other, into more dense volume elements, Fig. 5.11.

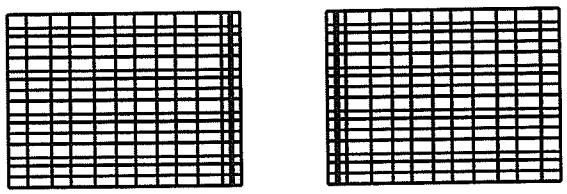

Figure 5.11: *Low frequency meshing that accounts for the proximity effect.*

5.5.2 Meshing For High Frequencies

At high frequencies, the conductors cross sections are generally smaller than the skin depth (δ); with the current flowing along the surface of the conductors. The skin effect reduces the effective area of the cross section of the conductors. This causes a huge increase in the resistance and the reduction of the internal inductance of each conductor. Two schemes of discretization can be used:

1) Using significantly more dense filaments near the surface of the conductors (as shown in Fig. 5.12a). This is preferable at medium to high frequencies.

2) When the conductors cross sections are much larger than δ, the discretization can be done using very thin elements surrounding the conductors [86]; as shown in Fig. 5.12b.

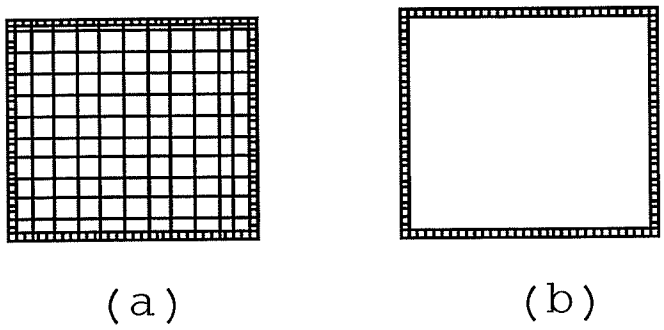

Figure 5.12: (a) *Medium to high frequency meshing.* (b) *High frequency meshing*

Chapter 6

Application

In this chapter the electrical parameters are employed in the calculation of crosstalk, ground-noise and radiated emissions from traces on printed circuit boards (PCBs). The inclusion of these aspects are very important in the analysis and design of electromagnetically compatible products.

The electromagnetic fields are hybrid, in general, and have field components in the transverse and longitudinal directions. However, a quasi-static analysis can be applied since, for the present frequencies of interest to the electromagnetic compatibility analysis, the cross sectional dimensions of the PCBs are electrically small in general [65]. Under the quasi-static conditions, the longitudinal components of the field can be neglected. Therefore coupled lines system on PCB can be modelled as multiconductor transmission lines. The quasi-static analysis can be applied to obtain the electrical parameters of the structure. Then voltage and differential mode current distributions on the transmission lines can be calculated by modal analysis or lumped-element approximations. The time-domain response of the system can be obtained from the frequency-domain response using Fourier transformation. The radiated emissions can be calculated using the current distributions, obtained in the crosstalk analysis, and a simple radiation model.

In the next section, the solution to the multiconductor transmission lines in the frequency-domain is reviewed. Lumped-element approximation is discussed in section 6.2. Frequency-domain to time-domain transformation is given in section 6.3. Crosstalk and ground-noise analysis are given in section 6.4 and 6.5, respectively. The radiated

emissions from traces on PCBs are calculated using a simple radiation model. Results are given in section 6.6. and are compare with other numerical techniques.

6.1 Frequency-Domain Transmission Line Analysis

Consider a circuit consisting of $(n+1)$ transmission lines, as shown in Fig 6.1, and a source that has a sinusoidal variation with time. Assuming the line is in steady state, the multi-transmission line (MTL) equations are given by [59]

$$\begin{aligned} \frac{\partial}{\partial z}\mathbf{V}(z,t) &= -\mathbf{R}\mathbf{I}(z,t) - \mathbf{L}\frac{\partial}{\partial t}\mathbf{I}(z,t) \\ \frac{\partial}{\partial z}\mathbf{I}(z,t) &= -\mathbf{G}\mathbf{V}(z,t) - \mathbf{C}\frac{\partial}{\partial t}\mathbf{V}(z,t) \end{aligned} \tag{6.1}$$

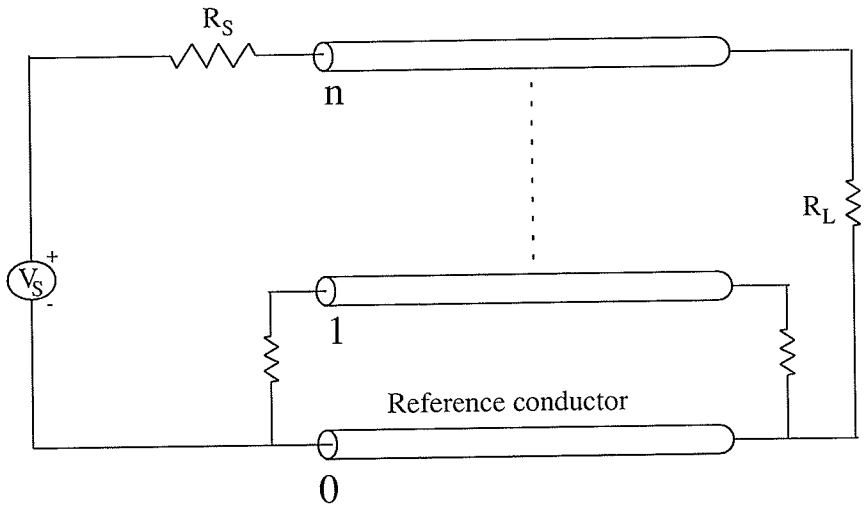

Figure 6.1: (a) *A circuit of multiconductor transmission lines*

The time variation is assumed to be e^{jwt}. Assuming that the per-unit parameter matrices, **R**, **L**, **G** and **C** are independent of time, t, and that the circuit has a linear termination network, then the derivation with respect to time can be replaced by jw;

such that:

$$\frac{\partial}{\partial z}\mathbf{V}(z) = -\mathbf{Z}\mathbf{I}(z)$$
$$\frac{\partial}{\partial z}\mathbf{I}(z) = -\mathbf{Y}\mathbf{V}(z) \tag{6.2}$$

where

$$\mathrm{Z} = \mathbf{R} + jw\mathbf{L}\,, \quad \mathrm{Y} = \mathbf{G} + jw\mathbf{C} \tag{6.3}$$

The linear termination network allows the employment of a simple terminal constraint equation. This constraint equation contains the lumped voltage and current source excitations and the load impedances.

The coupled first order differential equation, (6.2), can be placed in a form of uncoupled second order ordinary differential equation by differentiating both equation with respect to the line position, z, in the form

$$\frac{\partial^2}{\partial z^2}\mathbf{V}(z) = \mathbf{Z}\mathbf{Y}\mathbf{V}(z)$$
$$\frac{\partial^2}{\partial z^2}\mathbf{I}(z) = \mathbf{Y}\mathbf{Z}\mathbf{I}(z) \tag{6.4}$$

The differentiation is performed by assuming that the per-unit parameter matrices, **R**, **L**, **G** and **C** are independent of z.

Each equation of (6.4) is a coupled MTL equation since the parameter matrices are coupled. The MTL equations can be decoupled by using the similarity transformation which diagonalizes the parameter matrices. A change of variables is defined as:

$$\mathbf{V}(z) = \mathbf{T}_v\mathbf{V}_m(z)$$
$$\mathbf{I}(z) = \mathbf{T}_i\mathbf{I}_m(z) \tag{6.5}$$

where $\mathbf{T}_v$ and $\mathbf{T}_i$ are matrices of order nxn. They are said to be a similarity transformations between the actual phaser line voltages and currents, **V** and **I**, and the mode voltage and currents, $\mathbf{V_m}$ and $\mathbf{I_m}$. In order for this to be valid, the transformation matrices must

be nonsingular. The substitution of the similarity transformations into equation (6.4) gives

$$\begin{aligned}\frac{\partial^2}{\partial z^2}\mathbf{V}_m(z) &= \mathbf{T}_v^{-1}\mathbf{Z}\mathbf{Y}\mathbf{T}_i^{-1}\mathbf{V}_m(z) \\ &= \mathbf{T}_v^{-1}\mathbf{Z}\mathbf{T}_i\mathbf{T}_i^{-1}\mathbf{Y}\mathbf{T}_v\mathbf{V}_m(z) \\ &= \mathbf{z}\mathbf{y}\mathbf{V}_m(z)\end{aligned} \tag{6.6}$$

and

$$\begin{aligned}\frac{\partial^2}{\partial z^2}\mathbf{I}_m(z) &= \mathbf{T}_i^{-1}\mathbf{Y}\mathbf{Z}\mathbf{T}_i\mathbf{I}_m(z) \\ &= \mathbf{T}_i^{-1}\mathbf{Y}\mathbf{T}_v\mathbf{T}_v^{-1}\mathbf{Y}\mathbf{T}_i\mathbf{I}_m(z) \\ &= \mathbf{y}\mathbf{z}\mathbf{I}_m(z)\end{aligned} \tag{6.7}$$

Since the parameter matrices are symmetric and the transpose of the product of two matrices is the product of the transposes of the matrices in reverse order, *i.e.*,

$$\begin{aligned}(\mathbf{T}_v^{-1}\mathbf{Z}\mathbf{Y}\mathbf{T}_v)^t &= (\mathbf{T}_v)^t(Y)^t(Z)^t(\mathbf{T}_v^{-1})^t \\ &= (\mathbf{T}_v)^t Y Z(\mathbf{T}_v^{-1})^t = \mathbf{z}\mathbf{y} = \mathbf{y}\mathbf{z}\end{aligned} \tag{6.8}$$

Comparing (6.8) to (6.7) one can observe that

$$\mathbf{T}_i^t = \mathbf{T}_v^{-1} \tag{6.9}$$

Therefore, it is sufficient to diagonalize the product $\mathbf{YZ}$ or the product $\mathbf{ZY}$. Equation (6.7) can be diagonalized as:

$$\frac{\partial^2}{\partial z^2}\mathbf{I}_m(z) = \mathbf{T}_i^{-1}\mathbf{Y}\mathbf{Z}\mathbf{T}_i\mathbf{I}_m(z) = \mathbf{E}^2\mathbf{I}_m(z) \tag{6.10}$$

where

$$\mathbf{E}^2 = \begin{bmatrix} \gamma_1^2 & 0 & \dots & 0 \\ 0 & \gamma_2^2 & \ddots & \vdots \\ \vdots & \ddots & \ddots & 0 \\ 0 & \dots & 0 & \gamma_n^2 \end{bmatrix} \tag{6.11}$$

The elements of the matrix $\mathbf{E}^2$ are the eigenvalues of the matrix $\mathbf{YZ}$. The general solution of these decoupled equations is

$$\mathbf{I}_m(z) = e^{-\mathbf{E}z}\mathbf{I}_m^+ - e^{\mathbf{E}z}\mathbf{I}_m^- \tag{6.12}$$

where the exponential matrix is defined as:

$$e^{\pm Ez} = \begin{bmatrix} e_1^{\pm\gamma_1 z} & 0 & \dots & 0 \\ 0 & e_2^{\pm\gamma_2 z} & \dots & 0 \\ \vdots & \vdots & \vdots & \vdots \\ 0 & \dots & 0 & e^{\pm\gamma_n z} \end{bmatrix} \tag{6.13}$$

and the vector of undetermined constants are

$$\mathbf{I}_m^{\pm} = \begin{bmatrix} \mathbf{I}_{m1}^{\pm} \\ \mathbf{I}_{m2}^{\pm} \\ \vdots \\ \mathbf{I}_{mn}^{\pm} \end{bmatrix} \tag{6.14}$$

The column vector corresponding to the current on the lines can be expressed in terms of the mode current as:

$$\mathbf{I}(z) = \mathbf{T}_i(e^{-\gamma z}\mathbf{I}_m^+ - e^{\gamma z}\mathbf{I}_m^-) \tag{6.15}$$

Equation (6.2) can be written as:

$$\mathbf{V}(z) = -\mathbf{Y}^{-1}\frac{\partial}{\partial z}\mathbf{I}(z) \tag{6.16}$$

Substituting equation (6.12) in (6.16) yields

$$\begin{aligned}\mathbf{V}(z) &= -\mathbf{Y}^{-1}\mathbf{T_i}\mathbf{E}(e^{-\gamma z}\mathbf{I}_m^+ - e^{\gamma z}\mathbf{I}_m^-) \\ &= \mathbf{Z}_c\mathbf{T}_i(e^{-\gamma z}\mathbf{I}_m^+ - e^{\gamma z}\mathbf{I}_m^-)\end{aligned} \tag{6.17}$$

where $\mathbf{Z}_c$ is the characteristic impedance matrix given by

$$\mathbf{Z}_c = \mathbf{Y}^{-1}\mathbf{T}_i\mathbf{E}\mathbf{T}_i^{-1} \tag{6.18}$$

Equations (6.12) and (6.17) give the general solution of the phaser transmission line equation via the similarity transformations.

The general solution involves $2n$ undetermined constants of the n vectors $\mathbf{I}_m^+$ and $\mathbf{I}_m^-$. Therefore, $2n$ additional constraint equations are needed in order to evaluate these unknowns. It should be noted that these additional equations are provided by the terminal conditions at $z = 0$ and $z = l$.

6.1.1 Incorporating the Terminal Conditions

The driving sources and load impedances are contained in the terminal conditions. For a linear circuit network, the relationship between the voltage and current at the terminals is linear. The Thevenin equivalent representation of a port is [59]

$$\begin{aligned}\mathbf{V}(0) &= \mathbf{V}_s - \mathbf{Z}_s\mathbf{I}(0) \\ \mathbf{V}(l) &= \mathbf{V}_l - \mathbf{Z}_l\mathbf{I}(l)\end{aligned} \tag{6.19}$$

where $\mathbf{V}_s$ and $\mathbf{V}_l$ are columns of order n and they contain the effect of the independent voltage and current sources in the termination networks at $z = 0$ and $z = l$, respectively. The nxn matrices $\mathbf{Z}_s$ and $\mathbf{Z}_l$ contain the effect of the impedances and any controlled sources in the termination networks at $z = 0$ and $z = l$, respectively.

Substituting the terminal conditions, (6.19), in (6.12) and (6.17) yields

$$\mathbf{Z}_c\mathbf{T}_i(\mathbf{I}_m^+ + \mathbf{I}_m^-) = \mathbf{V}_s - \mathbf{Z}_s\mathbf{T}_i(\mathbf{I}_m^+ - \mathbf{I}_m^-) \tag{6.20}$$

and

$$\mathbf{Z}_c\mathbf{T}_i(e^{-\gamma l}\mathbf{I}_m^+ + e^{\gamma l}\mathbf{I}_m^-) = \mathbf{V}_l - \mathbf{Z}_l\mathbf{T}_i(e^{-\gamma l}\mathbf{I}_m^+ - e^{\gamma l}\mathbf{I}_m^-) \tag{6.21}$$

Equations (6.20), and (6.21) can be written in a matrix form as

$$\begin{bmatrix} (\mathbf{Z}_c + \mathbf{Z}_s)\mathbf{T}_i & (\mathbf{Z}_c - \mathbf{Z}_s)\mathbf{T}_i \\ (\mathbf{Z}_c - \mathbf{Z}_l)\mathbf{T}_i & (\mathbf{Z}_c + \mathbf{Z}_l)\mathbf{T}_i \end{bmatrix} \begin{bmatrix} \mathbf{I}_m^+ \\ \mathbf{I}_m^- \end{bmatrix} = \begin{bmatrix} \mathbf{V}_s \\ \mathbf{V}_l \end{bmatrix} \tag{6.22}$$

Once the matrix equation is solved for the unknown modal currents, the line voltages and currents can be obtained at any point along the lines by substituting into the phaser transmission line equations.

6.2 Lumped-Element Approximation

Lumped-element approximation can be applied to a structure whose largest dimension is electrically small. The π and the T models of the lumped-circuit structures are shown in Fig 6.2 (a) and (b), respectively [87].

Lumped-circuit analysis programs such as SPICE [58] can be used to analyze the lumped-circuit as an alternative to solving the phaser MTL equations. It also provides a method of calculating the ground-noise and the ground-bounce which can not be calculated using the phaser MTL equations. In addition, nonlinear termination such as transistors and diodes can be readily incorporated into the terminations since lumped-circuit programs include sophisticated model for them.

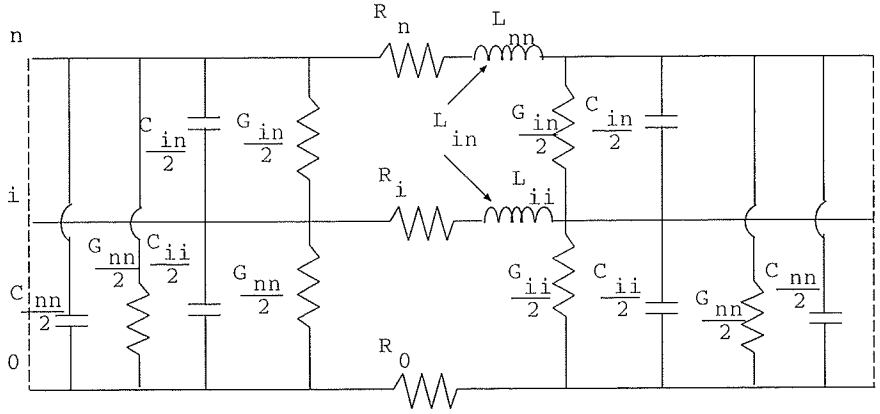

(a)

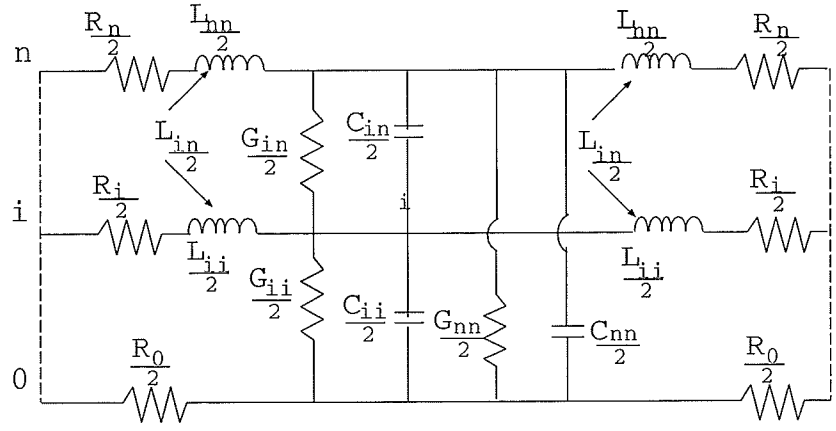

(b)

Figure 6.2: (a) *Lumped Pi model, (b) Lumped T model*

6.3 Frequency-Domain to Time-Domain Transformation

The time-domain (TD) response of a multiconductor transmission line structure can be determined from the frequency-domain (FD) response using FD to TD transformation. Consider the single-output single-input lumped linear system shown in Fig. 6.3

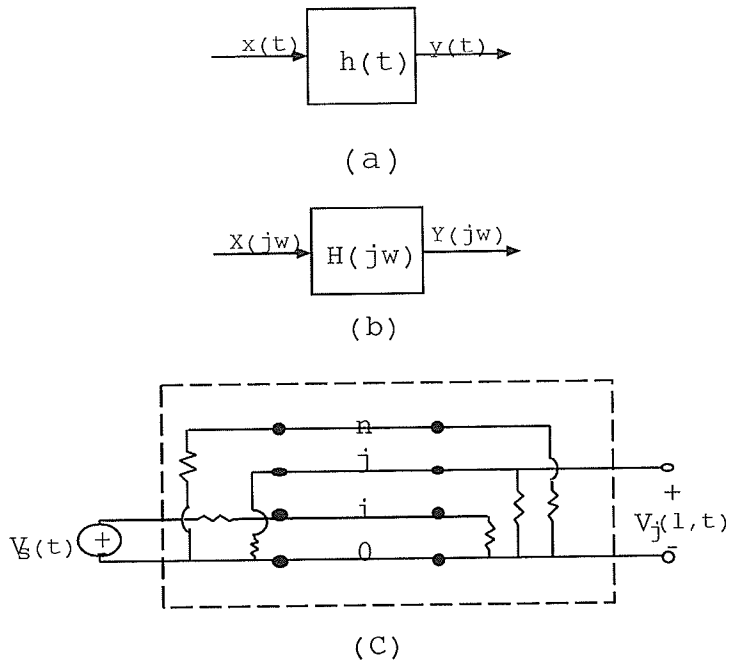

Figure 6.3: (a) *A single-input single-output linear system in time-domain, (b) A single-input single-output linear system in frequency-domain (c) representation of the MTL as a single-input single-output linear system*

The response of the circuit in time-domain can be obtained via the convolution integral

$$y(t) = \int_{-\infty}^{t} h(t-\tau)x(\tau)d\tau \tag{6.23}$$

which is denoted as

$$y(t) = h(t) * x(t) \tag{6.24}$$

where $x(t)$ is the input signal, $y(t)$ is the output signal and the unit-impulse response ($x(t) = \delta(t)$, $y(t) = h(t)$) is denoted by $h(t)$.

The response in the frequency-domain is

$$Y(jw) = H(jw)X(jw) \tag{6.25}$$

where $H(jw)$ is the Fourier Transform of $h(t)$ and is called the transfer function of the system.

The frequency-domain transfer function, $H(jw)$, can be obtained by applying unit-magnitude sinusoids to the input and computing the response using the phaser computational method with the frequency of those sinusoids varying over the desired frequency range. The time-domain impulse response can then be obtained as the inverse Fourier transform of $H(jw)$

$$h(t) = \mathcal{F}^{-1}\{H(jw)\} \tag{6.26}$$

Any time-domain waveform can be decomposed into its sinusoidal components with the Fourier series if it is periodic and the Fourier transform if it is not periodic. For a periodic waveform with a period T, these frequency components appear at discrete frequencies that are multiples of the basic repetition frequency, $w_0 = 2\pi f$. In addition, $x(t)$ can be represented as the sum of these time-domain sinusoidal components with the Fourier series as

$$x(t) = c_0 + \sum_{n=0}^{NH} c_n cos(nw_0 t + \angle c_n) \tag{6.27}$$

The series has been truncated to NH harmonics. As an example, consider a periodic train of trapezoidal pulses, as shown in Fig. 6.4. The pulses have peak magnitude, A, duty cycle, $D = t/\tau$, where τ is the pulse width and equal rise/fall times of τ_r. The coefficients of equation (6.27) are then given by

$$c_0 = AD$$

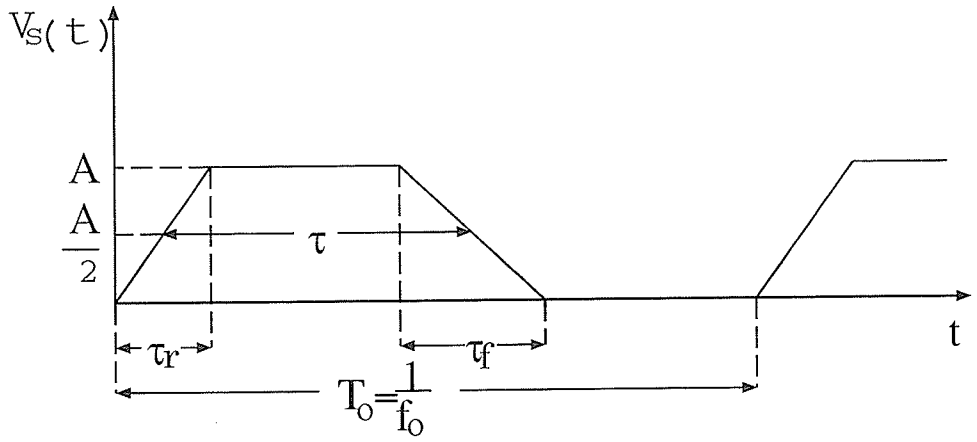

Figure 6.4: *General trapezoidal pulse train*

$$c_n = 2AD\frac{sin(n\pi D)}{n\pi D}\frac{sin(n\pi f_0\tau_r)}{n\pi f_0\tau_r}$$
$$\angle c_n = -n\pi(D + f_0\tau_r) \tag{6.28}$$

The frequency domain transfer function is computed at each of the NH harmonic frequency, then

$$H(jnw_0) = \mid H(jnw_0) \mid \angle H(jnw_0) \tag{6.29}$$

$$y(t) = c_0H(0) + \sum_{n=1}^{NH} c_n \mid H(jnw_0) \mid cos(nw_0t + \angle c_n + \angle H(jnw_0)) \tag{6.30}$$

6.4 Crosstalk Analysis

Crosstalk refers to the unintended electromagnetic coupling between traces on printed circuit boards (PCB) and cables. Crosstalk is a near field coupling problem that arises from the presence of the voltages and currents on the traces. It generally concerns the intrasystem interference performance of the PCB and Cables [69]. Therefore, crosstalk analysis is essential for the design of products that do not interfere with themselves. Crosstalk can also affect the susceptibility of the products to emission from other products.

	C_{i0}	C_{i1}	C_{i2}	L_{i0}	L_{i1}	L_{i2}
0	409.2	-186.8	-65.5	28.06	16.4	13.1
1	-186.8	485.5	-186.8	16.4	29.16	16.4
2	-65.5	-186.8	409.2	13.1	16.4	28.06

Table 6.1: *The general capacitance matrix in fF and the general inductance matrix in nH.*

The objective of crosstalk analysis is to determine the near-end and far-end voltages given the dimension of the structure and the termination characteristics.

Consider a PCB structure consisting of three traces over a dielectric material as shown in Fig. 6.5. The electrical parameters of the structure are obtained using the methods presented in the previous chapters. Table 6.1 gives the general capacitance and inductances matrices, for the traces with a separation $d = 20$ mils. The resistance of the traces is 52.4 $m\Omega$ at 10 MHz frequency

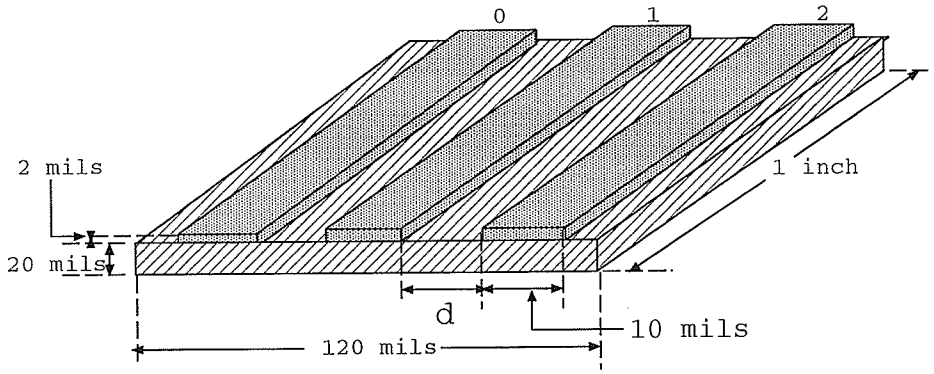

Figure 6.5: *Three traces over a dielectric of permittivity* ϵ_r*=3.7*

For the transmission line analysis, one of the conductors should serve as a return conductor. Therefore, the conductor "0" is taken as the reference conductor and the reduced parameter matrices, $\mathbf{L_r}$ and $\mathbf{C_r}$ are obtained from the general parameter matrices;

using the following equations:

$$L_{rij} = L_{ij} - L_{i0} - L_{0i} + L_{00} \tag{6.31}$$

where $i, j = 1, 2, ..., n$ and $i \neq j$, and

$$C_{rij} = C_{ij} - \frac{(\sum_{k=0}^{n} C_{ik})(\sum_{m=0}^{n} C_{mj})}{(\sum_{k=0}^{n} \sum_{m=0}^{n} C_{km}} \tag{6.32}$$

The three-conductor transmission lines representation of the PCB is shown in Fig. 6.6 along with the spice model in Fig. 6.7. Both models are used for the calculation of the crosstalk in the frequency and time-domain, respectively.

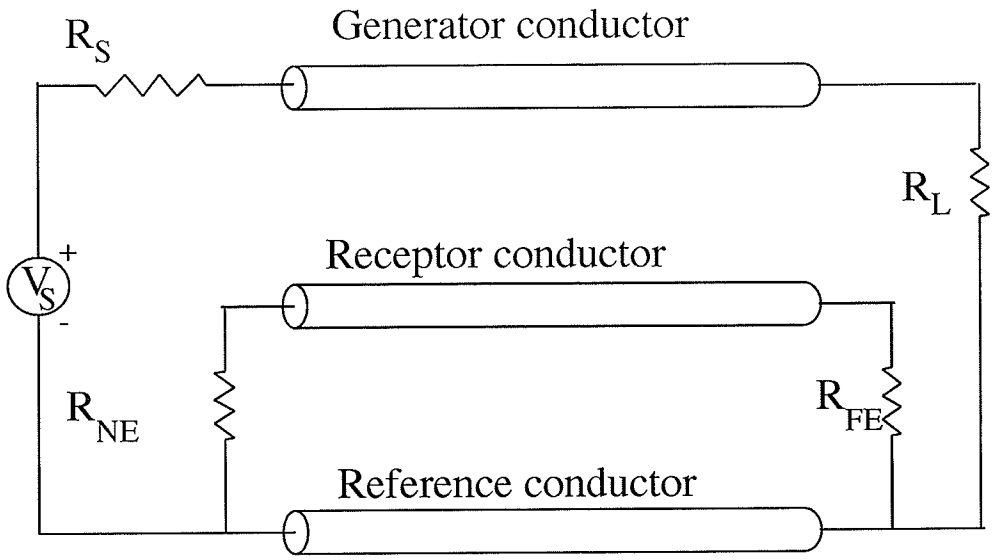

Figure 6.6: *Three-conductor transmission lines model of the PCB*

6.4.1 Frequency-Domain Crosstalk Analysis

For the frequency-domain analysis, the termination resistances are 50Ω each and the source have a sinusoidal signal with peak value of $V_s = 1v$; with frequency variation of $1MHz$ to $1GHz$. Generally the crosstalk is considered as the superposition of three components namely: inductive, capacitive and common impedance coupling. The inductive

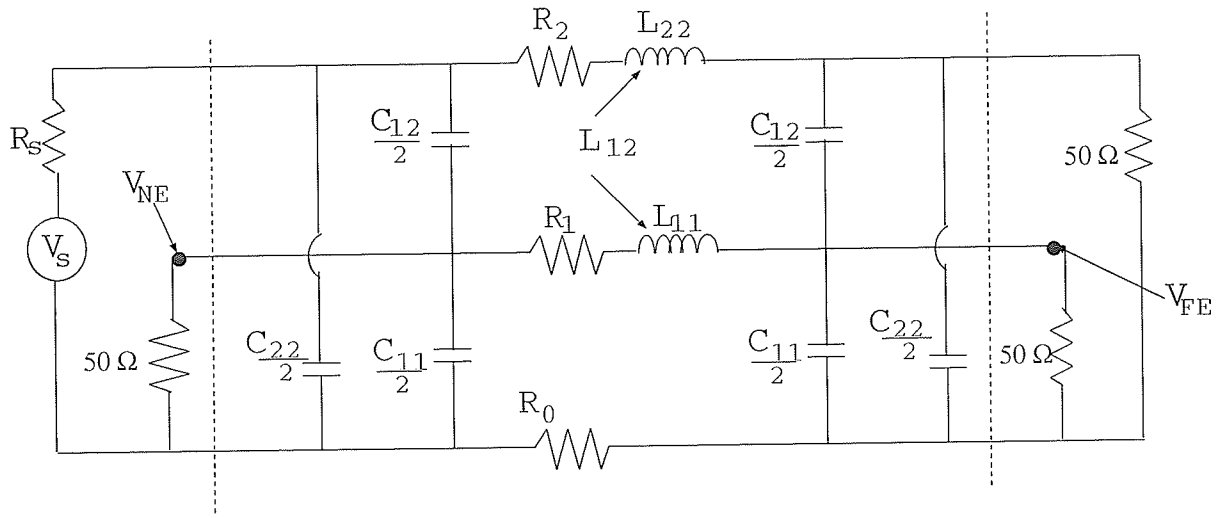

Figure 6.7: *Spice Pi model of the PCB*

coupling is due to mutual inductances among the traces in the structure [69]. The capacitive coupling is due to mutual capacitances among the traces in the structure. However common impedance coupling is due to the resistive losses in the structure which are of significant values at low frequencies. The inductive coupling component dominate the capacitive coupling component for low impedance circuits (high currents and low voltages). The capacitive coupling component dominates the inductive coupling component for high impedance circuits (low currents and high voltages). Since the resistance is increasing with the frequency, the current that flows in the transmission lines is decreasing causing the dominance of the capacitive coupling.

The modal analysis of the transmission line is used to calculate the near-end and far-end crosstalk of the PCB shown in Fig. 6.5 using a computer code written by C. Paul [59]. The results are given in Fig. 6.8 and Fig. 6.9, respectively, and is compared against voltages calculated using HSPICE [11]. The figures show close agreement between HSPICE and the modal analysis in the low frequency range. However, HSPICE predicts higher crosstalk in the higher frequency range since the frequency-domain modal analysis approximates the resistance variation with frequency.

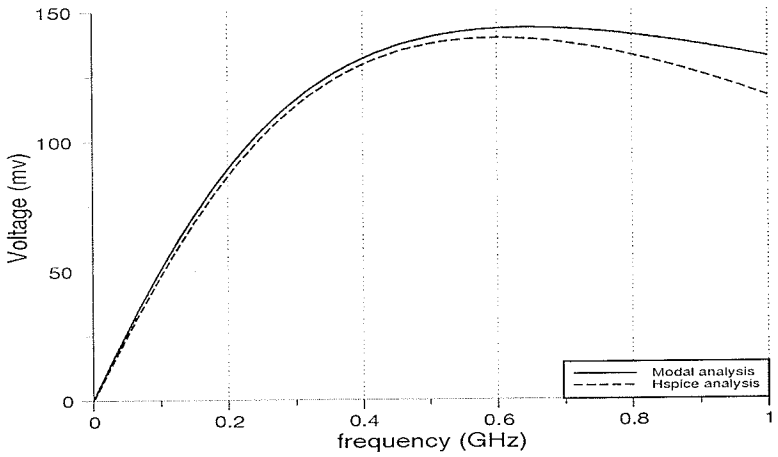

Figure 6.8: *A comparison of the frequency-domain near-end crosstalk voltages, calculated by using HSPICE and the modal analysis method.*

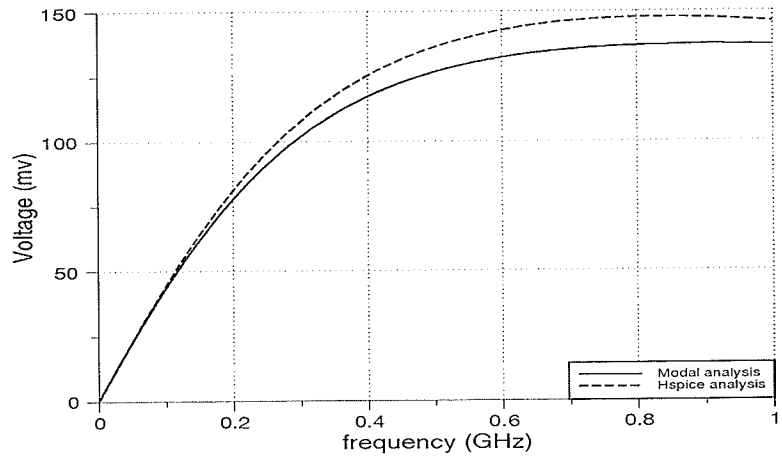

Figure 6.9: *A comparison of the frequency-domain far-end crosstalk voltages, calculated by using HSPICE and the modal analysis method.*

d		C_{i1}	C_{i2}	L_{i1}	L_{i2}
10	1	1.16	-0.58	19.96	13.48
10	2	- 0.58	0.84	13.48	26.96
20	1	0.912	-0.456	24.1	15.46
20	2	-0.456	0.702	15.46	30.9
30	1	0.796	-0.398	26.9	16.8
30	2	-0.398	0.633	16.8	33.36

Table 6.2: *The capacitance matrix in pF and the inductance matrix in nH for a separation d = 10, 20 and 30 mils*

To study the effect of the separation between the traces, the crosstalk voltages are calculated for the PCB with a separation $d = 10, 20$ and 30 mils. The electrical parameter matrices with reference to the conductor "0" are given in table 6.2. Notice that the capacitance values are decreasing with increasing separation. However, the inductances are increasing with separation. It can be seen from the figures, that, the crosstalk voltage is increasing proportionally with separation in the low frequency ranges; a result of increasing the inductance values. However, the crosstalk voltage is decreasing with increasing separation in the high frequency range due to the decreasing of the capacitance values.

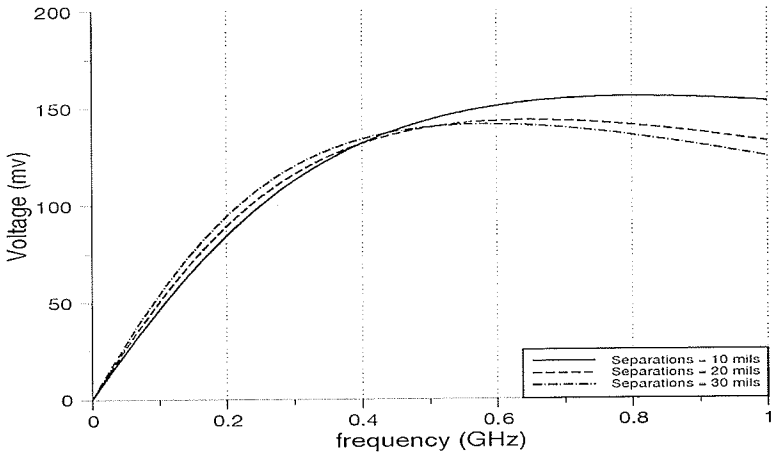

Figure 6.10: *A comparison of the frequency-domain near-end crosstalk voltages, calculated for a separation d=10, 20 and 30 mils*

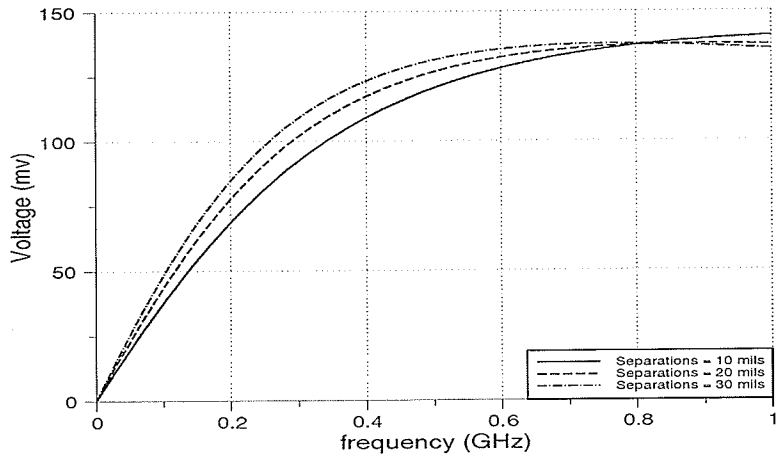

Figure 6.11: *A comparison of the frequency-domain far-end crosstalk voltages, calculated for a separation d=10, 20 and 30 mils*

To demonstrate the capability of the developed codes to handle complex PCBs, the crosstalk analysis is performed for the structure shown in Fig. 6.12. The PCB structure consisting of six traces and two dielectric layers. The width of each trace is $8mils$ and the thickness is $3mils$. The electrical parameters of the structure are obtained using the methods presented in the previous chapters where trace "T0" is considered as the reference conductor. Table 6.3 gives the capacitance, inductance and resistance matrices for the traces calculated at 100 MHz frequency.

HSPICE circuit simulator is used for the crosstalk analysis where a spice sub-circuit model is generated using the electrical parameters in table 6.3. A $1v$ source with 75Ω resistance is connected to trace "T2" and the ends of each trace are connected to 75Ω load resistances. The near-end and far-end crosstalk are given in Figs. 6.13 and 6.14,respectively.

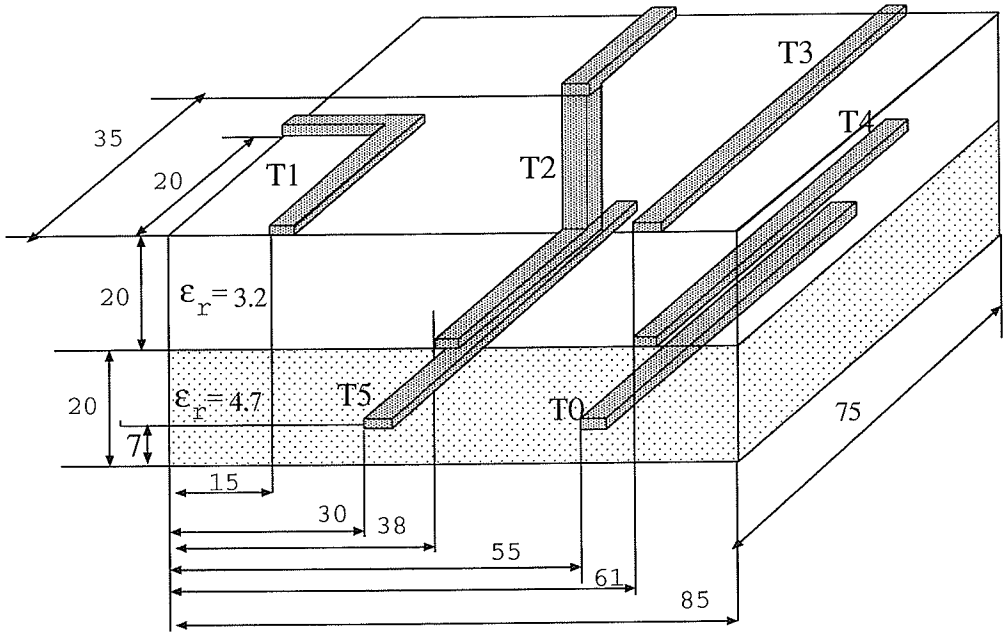

The unit of the dimensions is mil

Figure 6.12: *PCB structure consisting of five traces and ground trace*

i	1	2	3	4	5
C1	45.0	-19.15	-3.64	-3.65	-13.41
C2	-19.15	170.7	-21.2	-30.4	-63.28
C3	-3.64	-21.2	57.55	-24.62	-26.72
C4	-3.65	-30.39	-24.62	141.0	-16.27
C5	-13.41	-63.28	-26.71	-16.28	144.22
L1	1.32	1.08	0.96	1.10	1.03
L2	1.08	2.08	1.28	1.44	1.4
L3	0.96	1.28	1.66	1.38	1.17
L4	1.10	1.44	1.38	1.94	1.35
L5	1.03	1.4	1.17	1.35	1.75
R	28.9	37.0	29.22	29.22	29.23

Table 6.3: *The capacitance matrix in fF, the inductance matrix in nH and the resistance in mΩ*

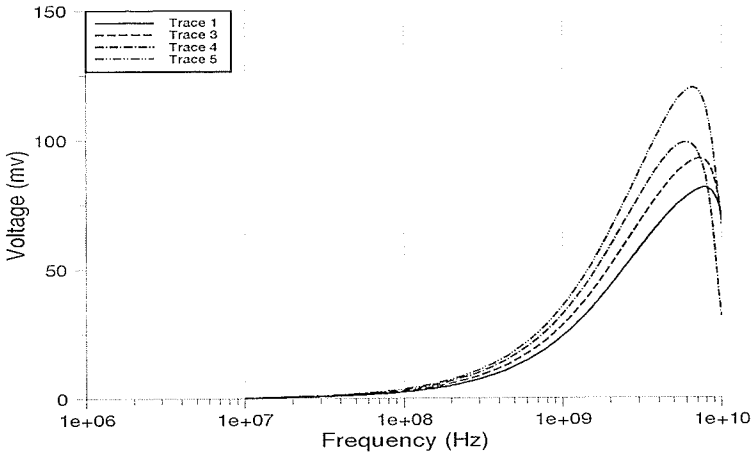

Figure 6.13: *The frequency-domain near-end crosstalk voltages*

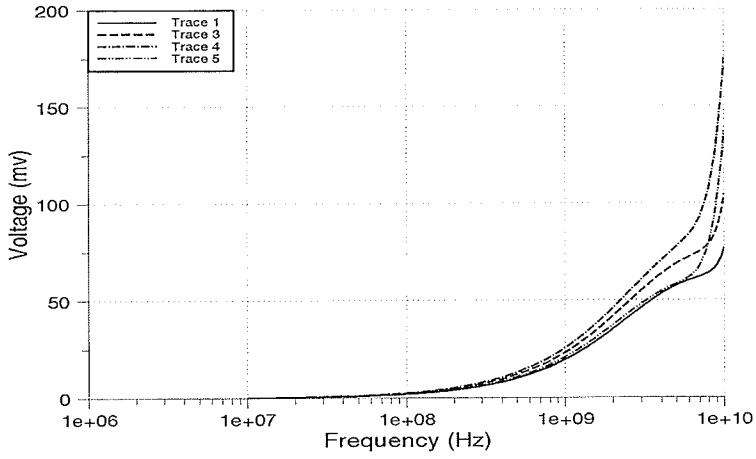

Figure 6.14: *The frequency-domain far-end crosstalk voltages*

6.4.2 Time-Domain Crosstalk Analysis

The time-domain crosstalk is calculated from the frequency-domain crosstalk by using Fourier transforms [65]. The input signal is a trapezoidal pulse train, shown in Fig. 6.15- which has a period of ($1us$), a (50%) duty cycle, a rise/fall time of ($3.25ns$) and a peak voltage of ($5v$). The time-domain near-end and far-end crosstalk voltages of the

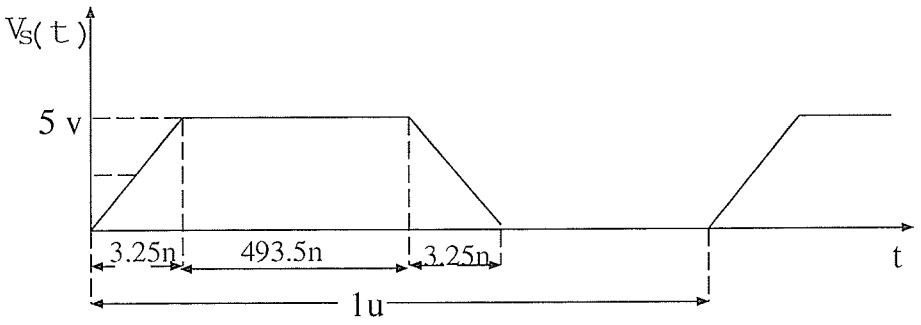

Figure 6.15: *Trapezoidal pulse train*

PCB, shown in Fig 6.5, for a separation d= 20 mils are given in Fig 6.16 and Fig 6.17, respectively. The results are compared with those calculated using HSPICE transient analysis. The time-domain crosstalk voltages are calculated for the PCB with a separation d=10, 20 and 30 mils, using the Fourier transformation. The electrical parameter matrices with reference to conductor "0" are given in table 6.2. The near and far-end time-domain crosstalks are shown in Fig 6.18 and Fig 6.19, respectively. It can be seen that the crosstalk voltages are decreasing by increasing the separation distance between the traces on the PCB.

Effect of pulse rise/fall time in crosstalk

Paul [59] showed that reducing the pulse rise/fall time causes higher time-domain crosstalk voltages for a shorter period of time. The effect of the rise/fall time in the near-end and far-end crosstalk voltages is shown in Fig. 6.20 and 6.21. The time-domain near-end and far-end crosstalk voltages of the PCB, shown in Fig 6.5 with a separation d= 20 mils are obtained using the transmission line modal analysis.

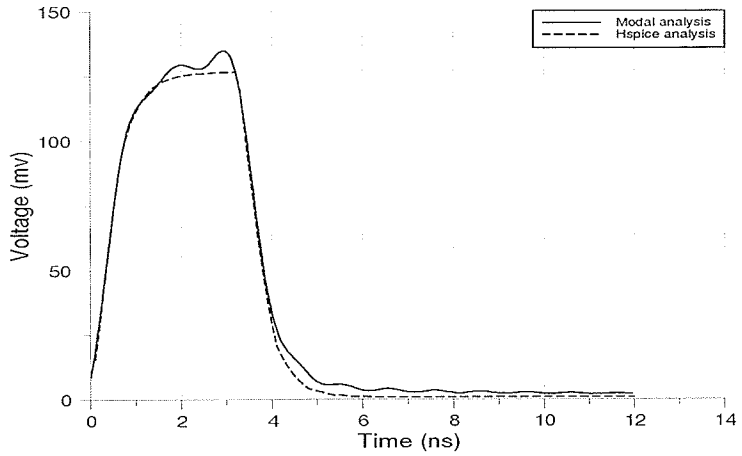

Figure 6.16: *A comparison of the time-domain near-end crosstalk voltages, calculated by using HSPICE and the modal analysis method.*

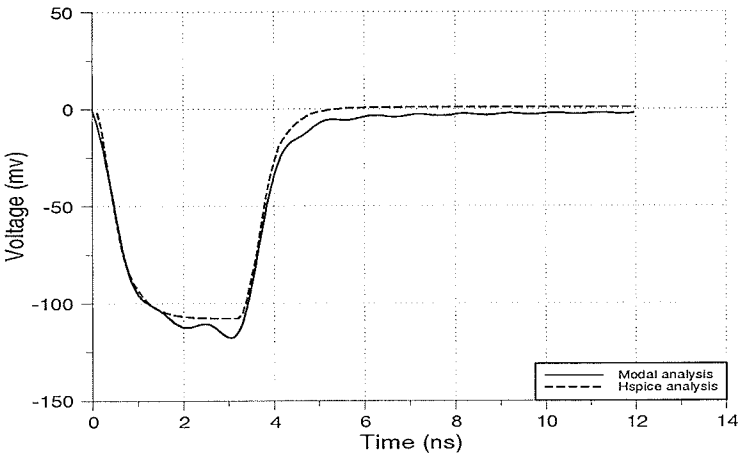

Figure 6.17: *A comparison of the time-domain far-end crosstalk voltages, calculated by using HSPICE and the modal analysis method.*

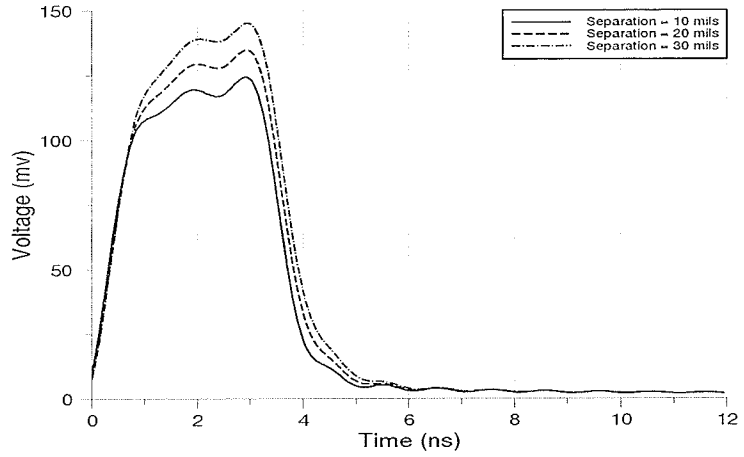

Figure 6.18: *A comparison of the time-domain near-end crosstalk voltages, calculated for a separation d=10, 20 and 30 mils*

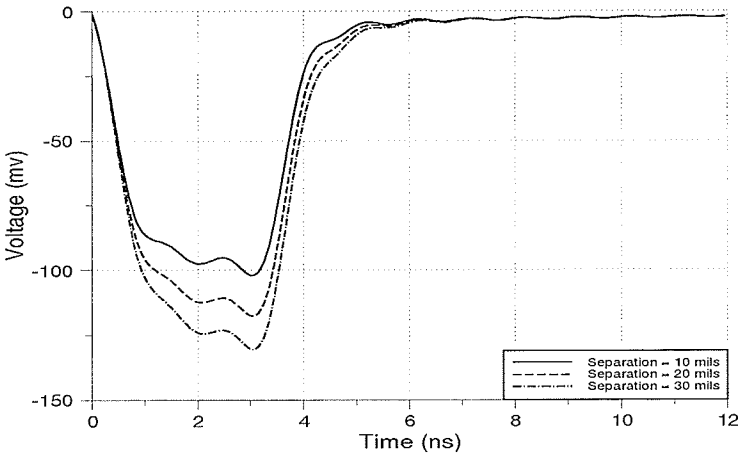

Figure 6.19: *A comparison of the time-domain far-end crosstalk voltages, calculated for a separation d=10, 20 and 30 mils*

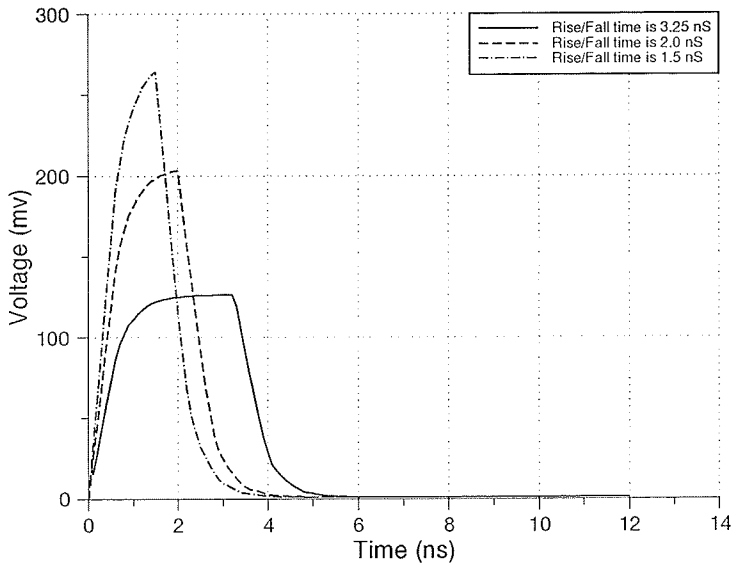

Figure 6.20: *Time-domain near-end crosstalk voltages obtained using trapezoidal pulse train with three different rise/fall times.*

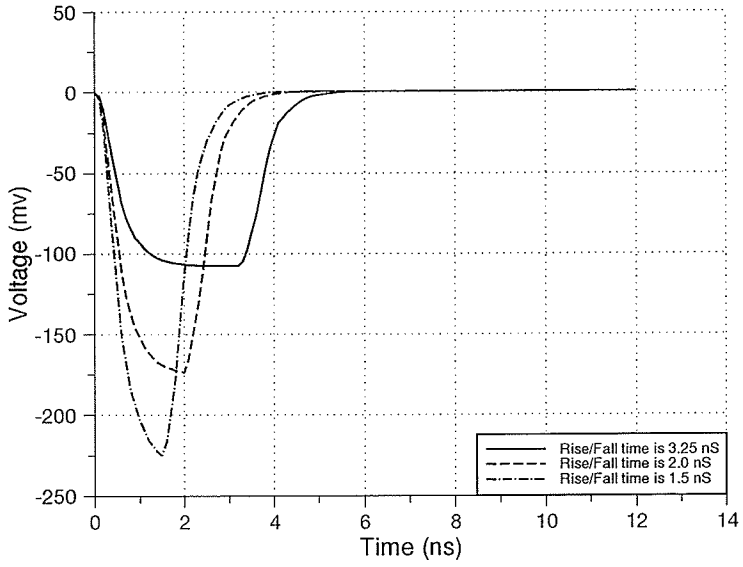

Figure 6.21: *Time-domain far-end crosstalk voltages obtained using trapezoidal pulse train with three different rise/fall times.*

6.5 Ground-Noise Calculations

A printed circuit board consisting of two traces over a dielectric layer, shown in Fig. 6.22, is used to study the ground-noise. The PCB structure can be represented by a two-conductor transmission line where one of the traces is a signal conductor and the other is a return conductor. The electrical parameters of the structure are obtained using the methods presented in the previous chapters. Table 6.4 gives the general capacitance and inductances matrices for the traces with a separation d = 10, 20 and 40 mils. The resistance of each traces is 52.4 $m\Omega$ at 10 MHz frequency.

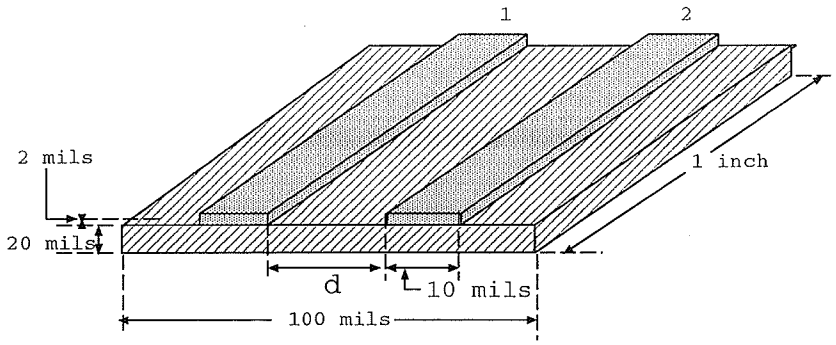

Figure 6.22: *Two traces over a dielectric of permittivity* ϵ_r=*3.7*

A lumped-circuit model for the structure is shown in Fig. 6.23, [88, 89], which can be analyzed using HSPICE. A sinusoidal source with a peak voltage of $1v$, source resistance $R_s = 50\Omega$ and a frequency range of $(1 - 1000MHz)$, is used for the frequency-domain calculations. Furthermore, the time-domain ground-noise is calculated using HSPICE transient analysis. The input signal is a trapezoidal pulse train, shown in Fig. 6.15, with a period of (1 micro Sec), a (50%) duty cycle, a fall/rise time of $(3.25ns)$ and a peak voltage of $(5v)$.

HSPICE is used to calculate the ground-noise V_{GN}, using the lumped-circuit model with load resistances of R_L = 5, 50, 100 and 200 Ω. The frequency-domain results are shown in Fig. 6.24 and the time-domain results are shown in Fig. 6.25. The figures show

d		C_{i1}	C_{i2}	L_{i1}	L_{i2}
10	1	466.14	-293.0	28.5	18.52
10	2	-293.0	466.14	18.52	28.5
20	1	399.35	-216.8	28.5	16.45
20	2	-216.8	399.35	16.45	28.5
40	1	348.75	-154.0	28.5	13.92
40	2	-154.0	348.75	13.92	28.5

Table 6.4: *The capacitance matrix in fF and the inductance matrix in nH for a separation d = 10, 20 and 40 mils*

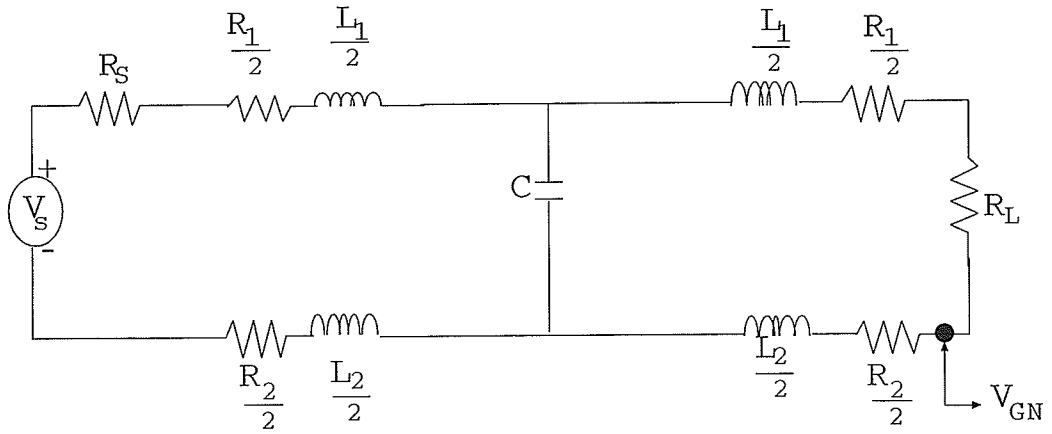

Figure 6.23: *Lumped-circuit ground-noise model for a two-conductor transmission line.*

that the ground-noise is decreasing by increasing the load resistance. This is due to the decreasing of the current that flows in the transmission line.

To study the effect of the separation between the traces, the ground-noise voltage is calculated for the PCB with a separation $d = 10$, 20 and 40 mils. The frequency-domain results are shown in Fig. 6.26 and the time-domain results are shown in Fig. 6.27. It can be seen from the figures that the ground-noise voltage is increasing proportionally with the separation between the traces.

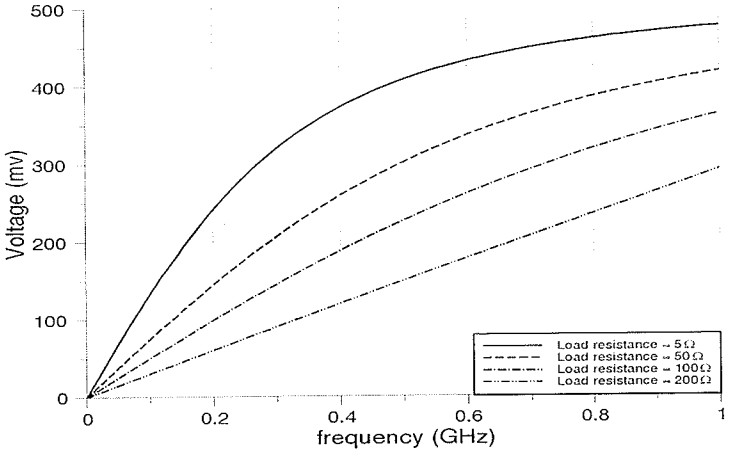

Figure 6.24: *A comparison of the frequency-domain ground-noise voltages, calculated for load resistances of R_L =5, 50, 100 and 200 Ω.*

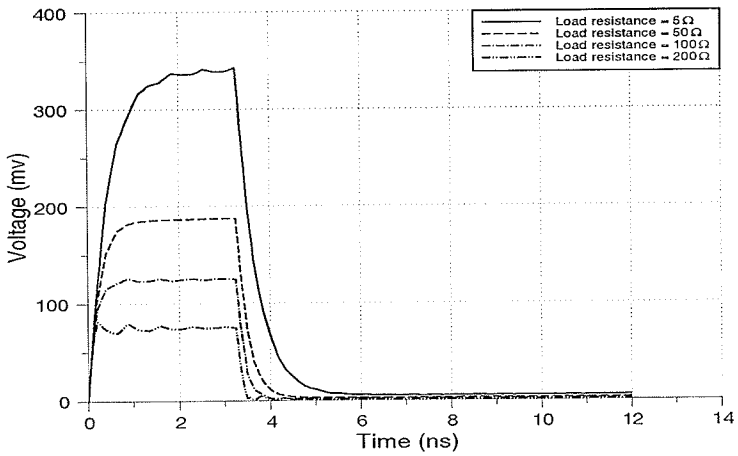

Figure 6.25: *A comparison of the time-domain ground-noise voltages, calculated for load resistances of R_L =5, 50, 100 and 200 Ω.*

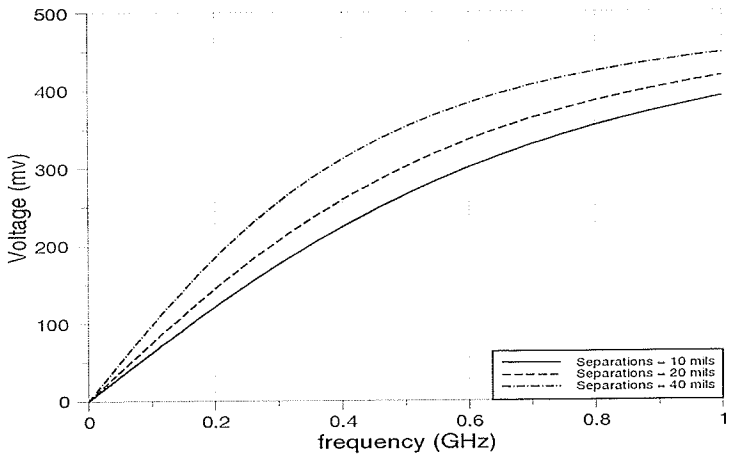

Figure 6.26: *A comparison of the frequency-domain ground-noise voltages, calculated for a separation d=10, 20 and 40 mils.*

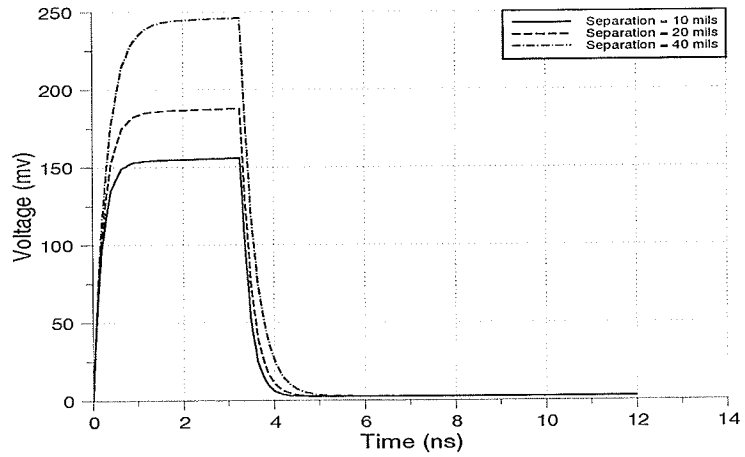

Figure 6.27: *A comparison of the time-domain ground-noise voltages, calculated for a separation d=10, 20 and 40 mils.*

6.6 Radiation Model

An approximate radiation model based on the differential mode current distributions can be used for the calculation of the radiation emissions from traces on PCBs. The differential mode current distributions are obtained using circuit analysis or transmission line modal analysis. These analysis are performed assuming the field structure surrounding the conductors obeys transverse electromagnetic or quasi-TEM structure. The cross sectional dimensions of the structure is also assumed to be electrically small. The quasi-TEM solution is not valid for imperfect lines or for structures with sever inhomogeneity in the surrounding medium. Furthermore, the sum of the currents at any cross section is assumed zero by taking the reference conductor as the return bath for other conductor currents. In reality, the sum of the currents at any cross section might not be zero, as a results of the existence of other currents. Conductors or other metallic structures which are not included in the analysis may cause these additional currents. In addition, asymmetries in the physical terminal excitation, such as offset source position can create non-TEM (common mode) currents. Furthermore, the physical termination such as the wires connecting the loads and the source to the traces also create non-TEM currents. These common mode currents can not be predicted by the transmission line modal analysis. These limitations, in the transmission line analysis, hamper the capability of the method to predict accurately the radiation emission from traces on PCBs. Accurate radiation emission estimation can be obtained using full wave analysis which dose not presuppose the existence of only differential mode currents. However, quasi-TEM analysis can be used to obtain indication about the level of radiation and the radiation patterns for structures with complexity that can not be handled by the full wave analysis.

6.6.1 Formulations

The radiation emission from the traces on PCBs may be calculated by

$$\mathbf{E} = -jw\mu\mathbf{A} - \frac{j}{w\epsilon} \bigtriangledown (\bigtriangledown \cdot \mathbf{A}) \tag{6.33}$$

where the magnetic vector potential is given by

$$\mathbf{A} = \frac{1}{4\pi} \int_v \mathbf{J}(r') \frac{e^{-jkR}}{R} dv', \tag{6.34}$$

and

$$R = \sqrt{(x - x')^2 + (y - y')^2 + (z - z')^2} \tag{6.35}$$

Substituting equation 6.34 into 6.33, gives the following integral equation

$$\mathbf{E} = \frac{-j\eta}{4\pi k} \int_v (k^2 \mathbf{J}(r') + (\mathbf{J}(r') \cdot \bigtriangledown) \bigtriangledown) \frac{e^{-jkR}}{R} dv', \tag{6.36}$$

where

$$k = \sqrt{\mu_0 \epsilon_0}, \quad \eta = \sqrt{\frac{\mu_0}{\epsilon_0}} \tag{6.37}$$

If the current x-directed then

$$\mathbf{J}(r') \cdot \bigtriangledown v' = I(x') \frac{\partial}{\partial x} x' \tag{6.38}$$

After some mathematical manipulation, the following equation can be obtained

$$\mathbf{E} = \frac{-j\eta}{4\pi k} \int_x I(x') \left(\frac{(x - x')}{R} \left(\frac{3}{R^2} + \frac{3jk}{R} - k^2 \right) + \left(k^2 - \frac{jk}{R} - \frac{1}{R_2} \right) x' \right) \frac{e^{-jkR}}{R} dx' \tag{6.39}$$

The three components of the electric field are then given by

$$E_x = \frac{-j\eta}{4\pi k} \int_x I(x') \left(\frac{(x - x')^2}{R^2} \left(\frac{3}{R^2} + \frac{3jk}{R} - k^2 \right) + \left(k^2 - \frac{jk}{R} - \frac{1}{R_2} \right) \right) \frac{e^{-jkR}}{R} dx' \tag{6.40}$$

$$E_y = \frac{-j\eta}{4\pi k}\int_x I(x')\frac{(x-x')(y-y')}{R^2}\left(\frac{3}{R^2}+\frac{3jk}{R}-k^2\right)\frac{e^{-jkR}}{R}dx' \tag{6.41}$$

$$E_z = \frac{-j\eta}{4\pi k}\int_x I(x')\frac{(x-x')(z-z')}{R^2}\left(\frac{3}{R^2}+\frac{3jk}{R}-k^2\right)\frac{e^{-jkR}}{R}dx' \tag{6.42}$$

Similar equations can be obtained for y- and z-directed currents.

The far field radiation pattern can be obtained using the following equation

$$\mathbf{E} = \frac{-jw\mu}{4\pi r}e^{-jkr}\int_s \mathbf{J}_s e^{-jkr'cos\psi}ds' \tag{6.43}$$

where

$$r'cos\psi = \mathbf{r}'\cdot\mathbf{r} \tag{6.44}$$

6.6.2 Results and Comparison

The following example illustrates all steps needed to obtain the radiation emission from traces on PCBs. Consider a PCB structure consisting of two traces over a ground plane, as shown in Fig. 6.28. The electrical parameters of the traces referenced to the ground plane are given in Table. 6.5. A spice sub-circuit model is generated using these electrical parameters where each trace is connected to the ground through a 100Ω resistance. A voltage source with 50Ω internal resistance, magnitude $V = 1v$ and frequency $f = 200MHz$ is connected to trace "T1". The current distribution on the traces are obtained using HSPICE circuit.

A simple radiation model is used for the field calculation [65]. Each trace of the PCB is modeled by x-directed line source with current distribution $I(x')$ obtained by HSPICE simulator, and the termination ends by z-directed line source with a constant current distribution. The ground plane is replaced by an image line source below the ground, Fig. 6.29. Two conductors configuration used for radiation results is shown in Fig. 6.30. Each line source is discretized into small segments and the current distribution is assumed constant over each segment.

The electric field integral equation formulation given above is used to calculate the radiated fields at a distance $r = 1\lambda$. The radiated fields in the y-z plane, $\phi = 90^o$, and the x-z plane, $\phi = 0^o$ are given in Figs. 6.31 and 6.32, respectively, and they are compared with results obtained using the Numerical Electromagnetic Code (NEC). The results obtained using the radiation model for $\phi = 90^0$ pattern cut agree well with those obtained using NEC. However, the the results for $\phi = 0^0$ pattern cut have about 50% error compare to those obtained using NEC as a results of the approximate representation of the z-directed current components in the radiation model.

The radiated fields patterns calculated using the radiation model are given in Figs. 6.32, 6.33 and 6.34 and they agree well with those obtained using NEC.

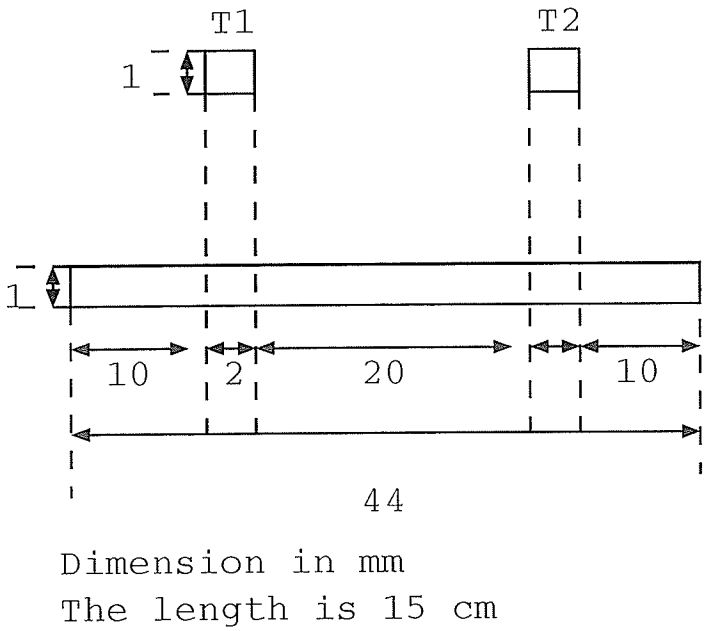

Figure 6.28: *Cross section of microstrip structure consisting of two traces and ground plane*

i	1	2
C1	26.53	-3.37
C2	-3.37	26.53
L1	97.88	12.18
L2	12.18	97.88
R	0.357	0.357

Table 6.5: *The capacitance matrix in pF, the inductance matrix in nH and the resistance in mΩ*

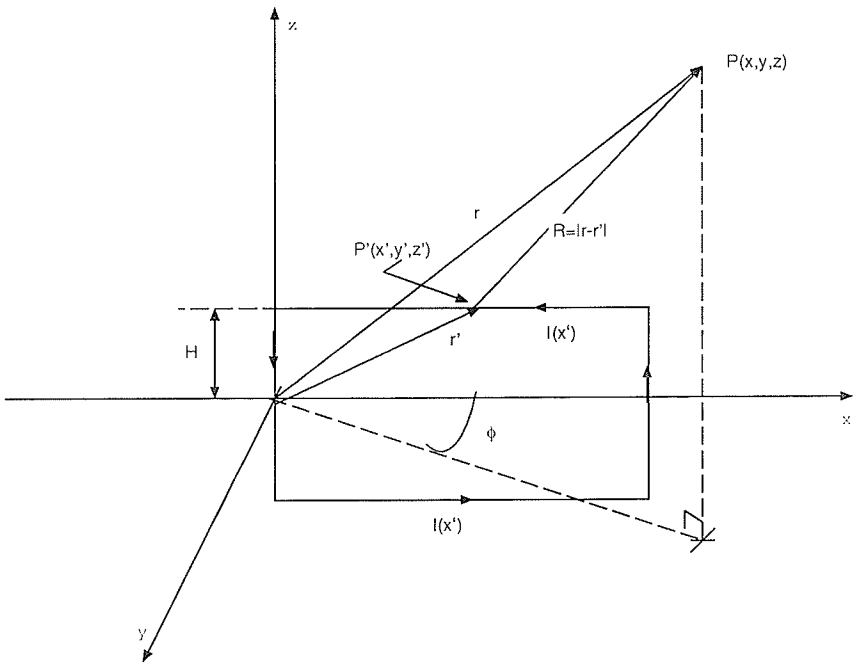

Figure 6.29: *Radiation model*

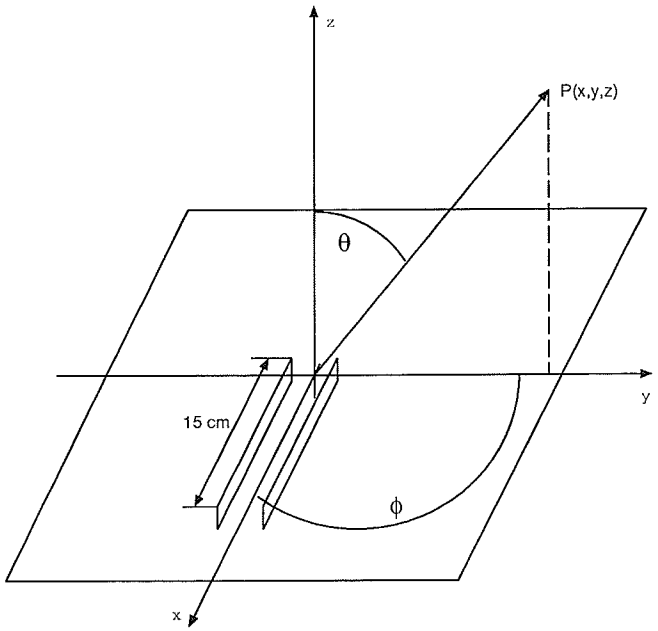

Figure 6.30: *Two conductors configuration used for radiation results*

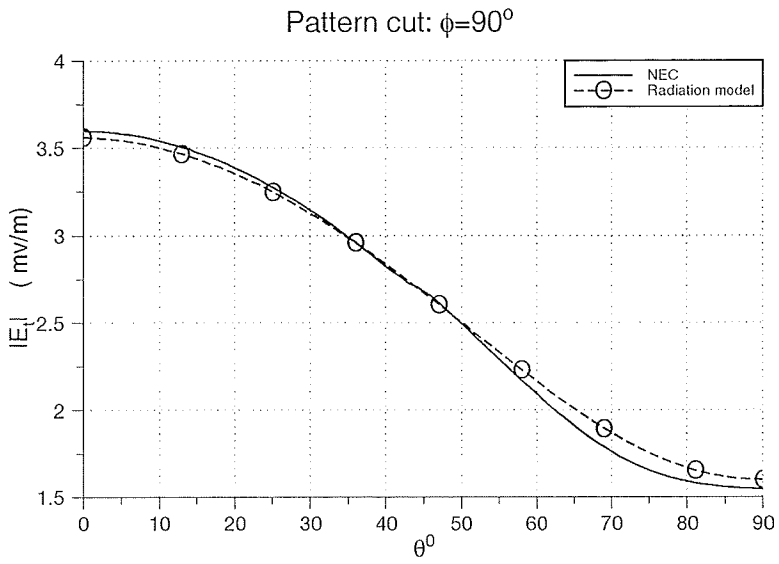

Figure 6.31: *Near-field emissions versus the angle θ with $\phi = 90^o$ and $r = 1\lambda$*

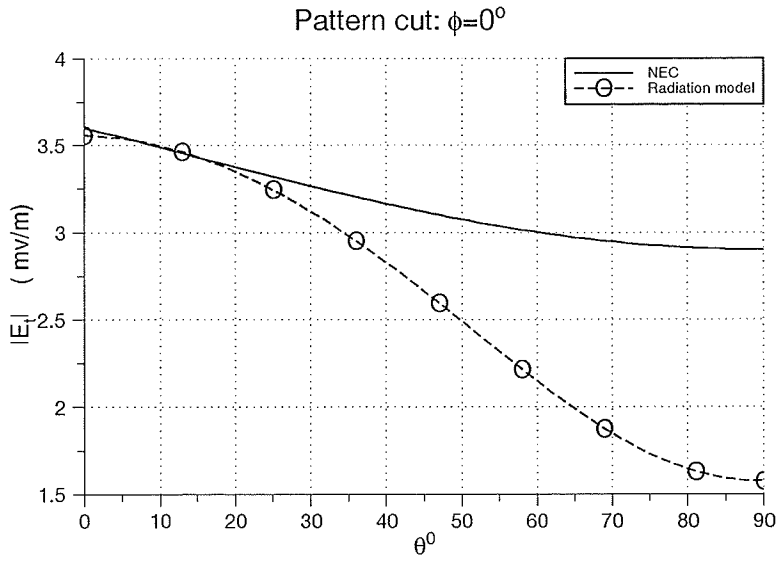

Figure 6.32: *Near-field emissions versus the angle θ with $\phi = 0^o$ and $r = 1\lambda$*

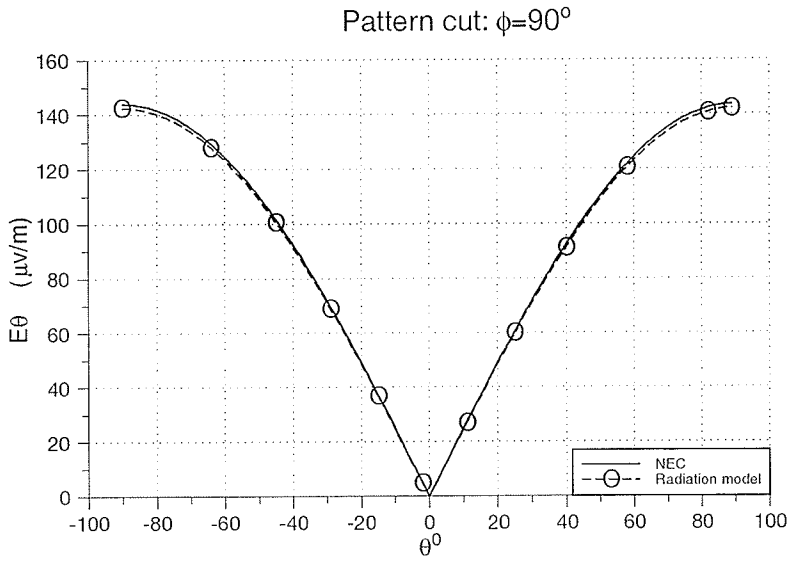

Figure 6.33: *Radiation pattern versus the angle θ with $\phi = 90^o$ and $r = 10\lambda$*

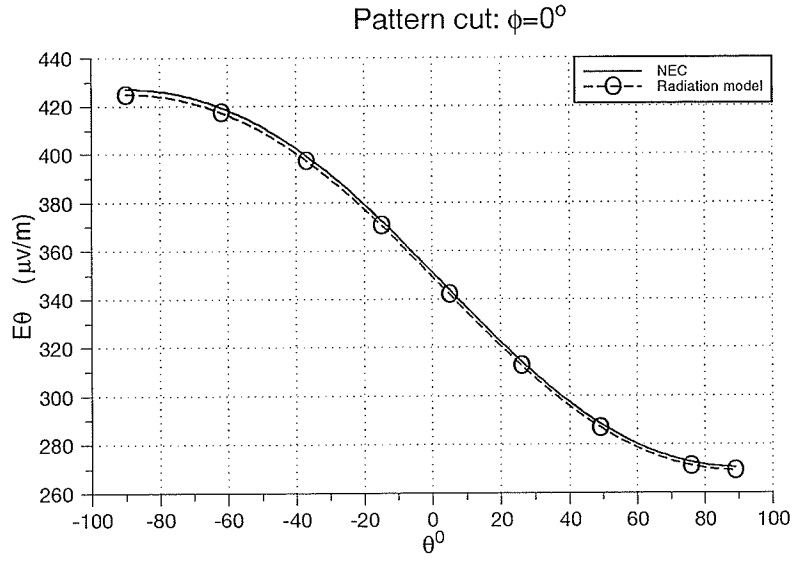

Figure 6.34: *Radiation pattern versus the angle θ with $\phi = 90^o$ and $r = 10\lambda$*

Figure 6.35: *Radiation pattern versus the angle θ with $\phi = 90^o$ and $r = 10\lambda$*

Chapter 7

Conclusion

A review of numerical modelling techniques employed in the electrical parameter extraction for multiconductor structures was carried out. When compared with other methods, the integral equation method was found to be the most suitable one for the capacitance calculation. However, for a complex three-dimensional structure, the IEM becomes impractical because of extremely large computational cost and memory storage requirements.

A new two-stage technique was presented to reduce the cost and memory storage requirement of the IEM for the problem of the capacitance and conductance matrices extraction for multiconductor structures. The numerical results indicate that the proposed method is faster than the classical IEM by a factor of m^2 for a system consists of m conductors. The results also show that the memory requirement by the proposed method is much less than the requirement of the classical integral equation method. Furthermore, the proposed method has proven to be accurate in comparison to the classical IEM and FASTCAP program [1]. In addition, an iterative method is used to further improve the accuracy of the charge distribution. The convergence of the iterative method can be achieved with a smaller number of iterations, by using the results of the proposed method as the initial values of the charges.

For the frequency-dependent inductance and resistance calculations, the partial element equivalent circuit (PEEC) method is the most efficient technique; since it combines the versatility of the IEM with the simplicity of general circuit network theory. However, for a complex three-dimensional structure, the PEEC becomes impractical and the avail-

ability of memory storage presents a limitation to applicability of this method. A two-step technique was used to overcome the limitation of the method. The technique was applied to various structures and it gives accurate results in comparison to those obtained using the classical PEEC method for conductors with separations larger than their cross sectional dimensions. Furthermore, the two-step technique gives a substantial reduction in memory storage requirements and computation cost in comparison to the PEEC method.

The shortcoming of the two stage technique and the two-step method is that the error increases with decrease in separation between the conductors. Furthermore the error also increases with the dielectric permittivity since increasing the dielectric permittivity has similar affect as decreasing the spacing between the conductors. For such cases, where the conductors are close to each other in comparison to their cross sectional dimensions, more accurate results can be obtained by solving for the neighboring conductors together in the first stage of the solution.

The near-end and far-end crosstalk and ground-noise voltages were calculated in the frequency and time-domains for some printed board structures. The electrical parameters of the structures were obtained using the methods presented in the thesis. Crosstalk and ground-noise analysis were carried out using the transmission line and HSPICE circuit simulator. In addition, the radiation emission from traces on a PCB was calculated by modelling the traces as line sources with current distributions obtained from the crosstalk analysis.

Recommendations

Electrical parameters extraction CAD package can be developed based on the two-stage technique for the capacitance and conductance calculations and the two-step approximation for the resistance and inductance calculation. This package should be capable of:

- Selecting the most efficient discretization of the geometry,
- Selecting fast and accurate integration algorithm for the calculation of the matrix

elements, *i.e.* applying multipole expansions, closed form integrals and an adaptive Gaussian point selection algorithm,

- Selecting an efficient method for the solution of the matrix system,
- Generating a proper spice sub-circuit for the geometry of interest.

Future Work

- Combining the two-dimensional analysis with the three-dimensional two-stage solution to achieve more efficient parasitics extraction algorithm,
- Studying the possibility of extracting the inductance and resistance matrices over a range of frequencies, rather than at a single frequency,
- Developing SPICE and radiation model for general boards with or without ground planes.

REFERENCES

[1] K. Nabors and J. White. FASTCAP: A multipole accelerated extraction program. *IEEE Trans. on Computer-Aided Design of Integrated Circuits and Systems*, vol. CAD-10, pp. 1447–1459, Nov. 1991.

[2] Ruey-Beei Wu and L. L. Wu. Exploiting structure periodicity and symmetry in capacitance calculations for three-dimensional multiconductor system. *IEEE Trans. Microwave Theory and Tech.*, vol. MTT-36, pp. 1311–1318, Sept. 1988.

[3] Z. Q. Ning, P. Dewilde, and F. L. Neerhoff. Capacitance coefficients for VLSI multilevel metalization lines. *IEEE Trans. Electron Devices*, vol. ED-34, pp. 644–649, Mar. 1987.

[4] C. D. Taylor, G. N. Elkhouri, and T. E. Wade. On the parasitic capacitances of multilevel skewed metalization lines. *IEEE Trans. Electron Devices*, vol. ED-33, pp. 41–46, Jan. 1986.

[5] A. E. Ruehli. Equivalent circuit models for three-dimensional multiconductor system. *IEEE Trans. Microwave Theory and Tech.*, vol. MTT-22, pp. 216–221, Mar. 1974.

[6] A. H. Zemanian, R. P. Tewarson, C. P. Ju, and J. F. Jen. Three-dimensional capacitance computations for VLSI/ULSI interconnections. *IEEE Trans. on Computer-Aided Design of Integrated Circuits and Systems*, vol. CAD-12, pp. 1319–1326, Dec. 1989.

[7] A. C. Cangellaris, J. L. Prince, and L. P. Vakanas. Frequency-dependent inductance and resistance calculation for three-dimensional structures in high-speed interconnect system. *IEEE Trans. Components, Hybrid, Manuf. Technol.*, vol. 13, pp. 154–159, Mar. 1990.

[8] M. Kamon, M. Tsuk, C. Smithhisler, and J. White. Efficient techniques for inductance extraction of complex 3-D geometries. *in Proc. Int. Conf. Comp. Aided Design*, Nov. 1992.

[9] P. A. Brennan, N. raver, and A. E. Ruehli. Three dimensional inductance computation with partial element equivalent circuits. *IBM J. Res. Develop.*, vol. 23, pp. 661–668, Nov 1979.

[10] F. Grover. *Inductance Calculation: Working formulas and Tables.* Dover, New York, 1962.

[11] Inc. Meta-Software. *HSPICE user's manual.* Campbell, CA, 1992.

[12] L. Maliniak. Signal analysis: a must for the PCB design success. *Electronic design*, vol. 43, pp. 69, Sept. 18 1995.

[13] R.F. Harrington. *Field computation by moment methods.* Macmillan, New York, 1968.

[14] S. M. Rao, T. K. Sarkar, and R. F. Harrington. The electrostatic field of conducting bodies in multiple dielectric media. *IEEE Trans. Microwave Theory Tech.*, vol. MTT-32, pp. 1441–1448, Nov. 1984.

[15] W. T. Weeks. Calculation of coefficients of capacitance of multiconductor transmission lines in the presence of a dielectric interface . *IEEE Trans. Microwave Theory Tech.*, vol. MTT-18, pp. 35–43, Jan. 1970.

[16] R. Crampagne, M. Ahmadpanah, and J. L. Guiraud. A simple method for determining the Green's function for a large class of MIC lines having multilayered dielectric structures. *IEEE Trans. Microwave Theory Tech.*, vol. MTT-26, pp. 82–87, Feb. 1978.

[17] P. D. Patel. Calculation of capacitance coefficients for a system of irregular finite conductor on a dielectric sheet. *IEEE Trans. Microwave Theory Tech.*, vol. MTT-19, pp. 862–869, Mar. 1971.

[18] B. H. McDonald, M. Friedman, and A. Wexler. Variational solution of integral equations. *IEEE Trans. Microwave Theory and Tech.*, vol. MTT-22, pp. 237–248, Mar. 1974.

[19] B. H. McDonald, M. Friedman, and A. Wexler. Correction to 'Variational solution of integral equations'. *IEEE Trans. Microwave Theory and Tech.*, vol. MTT-23, pp. 265–266, Feb. 1975.

[20] G. Jeng and A. Wexler. Self-adjoint variational formulation of problems having non-self adjoint operators. *IEEE Trans. Microwave Theory and Tech.*, vol. MTT-26, pp. 91–94, Feb. 1978.

[21] G. Jeng and A. Wexler. Isoparametric, finite element, variational solution of integral equations for three-dimensional fields. *Int. J. Numer. Math. Eng.*, vol. 11, pp. 1455–1472, 1977.

[22] M. H. Lean and A. Wexler. Accurate numerical integration of singular boundary element kernels over boundaries with curvature. *Int. J. Numer. Meth. Eng.*, vol. 21, pp. 211–228, 1985.

[23] A. Gopinath and P. Silvester. Calculation of inductance of finite-length strips and its variation with frequency. *IEEE Trans. Microwave Theory and Tech.*, vol. MTT-21, pp. 380–386, June 1973.

[24] C. E. Smith and R. Chang. Microstrip transmission line with finite-width dielectric. *IEEE Trans. Microwave Theory Tech.*, vol. MTT-28, pp. 90–94, Feb. 1980.

[25] C. Wei, R. F. Harrington, J. R. Mauts, and T. K. Sarkar. Multiconductor transmission line in multilayered dielectric media. *IEEE Trans. Microwave Theory Tech.*, vol. MTT-32, pp. 439–450, Apr. 1984.

[26] R. F. Harrington and C. Wei. Losses on multiconductor transmission line in multilayered dielectric media. *IEEE Trans. Microwave Theory Tech.*, vol. MTT-32, pp. 705–710, July 1984.

[27] L. Venkatarman, S. M. Rao, A. R. Djordjevi, T. K. Sarkar, and Y. Naiheng. Analysis of arbitrary oriented microstrip transmission lines in arbitrarily shaped dielectric media over a finite ground plane. *IEEE Trans. Microwave Theory and Tech.*, vol. MTT-33, pp. 952–959, Oct. 1985.

[28] S. Fukuda, N. Shigyo, K. Kato, and S. Nakamura. A ULSI 2-D capacitance simulator for complex structures based on actual processes. *IEEE Trans. Computer-Aided Design of Integrated Circuits and Systems*, vol. CAD-9, pp. 39–47, Jan. 1990.

[29] L. F. Greengard. *The rapid evaluation of potential field in particle systems.* PhD thesis, Massachusetts institute of Technology, Cambridge, Massachusetts, 1988.

[30] A. E. Ruehli. Inductance calculations in a complex integrated circuit environment. *IBM J. Res. Develop.*, vol. 16, pp. 476–481, Sept. 1972.

[31] A. E. Ruehli and P. A. Brennan. Efficient capacitance calculation for three-dimensional multiconductor system. *IEEE Trans. Microwave Theory and Tech.*, vol. MTT-21, pp. 76–82, Feb. 1973.

[32] A. E. Ruehli, N. Kulasza, and J. Pivnichny. Inductance of nonstraight conductors close to a ground return plane. *IEEE Trans. Microwave Theory and Tech.*, vol. MTT-23, pp. 706–708, 1975.

[33] A. E. Ruehli. Survey of computer-aided electrical analysis of integrated circuit interconnection. *IBM J. Res. Develop.*, vol. 23, pp. 626–639, Nov. 1979.

[34] Ruey-Beei Wu, Chien-Nan Kuo, and K. Chang. Inductance and resistance computations for three-dimensional multiconductor interconnection. *IEEE Trans. Microwave Theory and Tech.*, vol. MTT-40, pp. 263–270, Feb. 1992.

[35] T.Y Chou, J. Cosentino, and Z. J. Cendes. High-Speed Interconnect Modeling and High-Accuracy Simulation Using SPICE and Finite Element Methods. *30th ACM/IEEE Design Automation Conference*, pp. 684–690, June 1993.

[36] L. T. Olson. Application of the finite element method to determine the electrical resistance, inductance, capacitance parameters for the circuit package environments. *IEEE Trans. Components, Hybrid, Manuf. Technol.*, vol. 5, pp. 486–492, Des. 1982.

[37] P. E. Cottrel and E. M. Buturla. VLSI wiring capacitance. *IBM J. Res. Develop*, vol. 29, pp. 277–288, May 1985.

[38] D. Nayak, L Hwang, and I. Turlik. Calculation of electrical parameters of a thin-film multichip package. *IEEE Trans. Components, Hybrid, Manuf. Technol.*, vol. 12, pp. 303–309, June 1989.

[39] K. Nabors. *Efficient three-dimensional capacitance calculation.* PhD thesis, Massachusetts institute of Technology, Cambridge, Massachusetts, 1993.

[40] C. D. Taylor, G. N. Elkhouri, and T. E. Wade. On the parasitic capacitances of multilevel parallel metalization lines. *IEEE Trans. Electron Devices*, vol. ED-32, pp. 2408–2414, Nov. 1985.

[41] Y. L. Chow, Y. F. Lan, and D. G. Fang. Capacitance and its upper and lower bounds by the method of optimized simulated images. *Journal of Applied Physics*, vol. 53, pp. 7144–7148, Nov. 1982.

[42] Y. L. Chow and M. M. Yovanovich. The shape factor of the capacitance of a conductor. *Journal of Applied Physics*, vol. 53, pp. 8470–8475, Dec. 1982.

[43] Y. L. Chow and K. D. Srivastava. Non-Uniform electrical field induced voltage calculations. Tech. Rep. CEA 117-T-317, Canadian Electrical Association, March 1985.

[44] P. S. Maruvada and N. Hytenca. Capacitance calculation for some basic high-voltage electrode configuration. *IEEE Trans. on Power Apparatus and Systems*, vol. PAS-94, pp. 1708–1713, Sept./Oct. 1975.

[45] R. Guerrier and A Sangiovanni-Vincentelli. Three-dimensional capacitance evaluation on a connection machine. *IEEE Trans. Computer-Aided Design of Integrated Circuits and Systems*, vol. CAD-7, pp. 1125–1133, Nov. 1988.

[46] M. E. Goldfarb and R. A. Pucel. Modeling via hole grounds in microstrip. *IEEE Microwave and Guided Wave Letters*, vol. 1, pp. 135–137, June 1991.

[47] B. M. Kolundzija and B. D. Popvic. Entire-domain Galerkin method for analysis of metallic antennas and scatterer. *IEE Proc. Part H*, vol. 140, pp. 1–10, Feb. 1993.

[48] J. S. Bagby, Ching-Her Lee, Y. Yuan, and D. P. Nyquist. Entire-domain basis MoM Analysis of coupled microstrip transmission lines. *IEEE Trans. Microwave Theory and Tech.*, vol. MTT-40, pp. 49–57, Jan. 1992.

[49] H. A. N. Hejase. Analysis of a printed wire loop antenna. *IEEE Trans. Microwave Theory and Tech.*, vol. MTT-42, pp. 227–233, Feb. 1994.

[50] G. Goubau, N. N. Puri, and F. Schwering. Diakoptic theory of multielement antennas. *IEEE Trans. Antenna and Propag.*, vol. AP-30, pp. 15–26, Jan. 1982.

[51] F. Schwering, N. N. Puri, and C. M. Butler. Modified diakoptic theory of multielement antennas. *IEEE Trans. Antenna and Propag.*, vol. AP-34, pp. 1273–1281, Nov. 1986.

[52] C. M. Butler. Diakoptic theory and the moment method. *IEEE AP-S Symposium Digest*, vol. 1, pp. 72–75, 1990.

[53] V. Amoruso and F. Lattarulo. Diakoptic for electrostatics. *IEE Proc. Science, Measurement and technology*, vol. 141, pp. 317–323, Sept. 1994.

[54] P. Naylor and C. Christopoulos. Comparison between the time-domain and frequency-domain diakoptic methods of solving field problems by Transmission-Line Modeling. *Inter Jour. of Numerical Modeling: Electronic Network, Devices and Fields*, vol. 2, pp. 17–30, 1989.

[55] K. R. Umshanker. Numerical analysis of electromagnetic wave scattering and interaction based on frequency domain integral equation and method of moments techniques. *Wave Motion*, vol. 10, pp. 493–425, 1988.

[56] K. R. Umshanker and S. Nimmagadda. Application of the integral equation method and method of moments for electrically very large scatterer using spatial decomposition technique. *IEEE AP-S Symposium Digest*, vol. 1, pp. 76–79, 1990.

[57] G. E. Howard. *Analysis of large microwave integrated circuits by the multilevel moment method.* PhD thesis, University of Waterloo, Ontario, Canada, 1991.

[58] B. Johnson, T. Quarles, A. Newton, D. Pederson, and A. Sangiovani-Vincentelli. SPICE3 Version 3e user's manual. *Department of EE and CS, Berkely, University of California*, 1992.

[59] C. R. Paul. *Analysis of Multiconductor Transmission lines.* John Willy & sons, New York, 1994.

[60] C. R. Paul and J. E. McKnight. Prediction of crosstalk involving twisted pairs of wires, Part I, A transmission-line model for twisted wire pairs. *IEEE Trans. on Electromagnetic Compatibility*, vol. EMC-21, pp. 92–105, May 1979.

[61] C. R. Paul and J. E. McKnight. Prediction of crosstalk involving twisted pairs of wires, Part II, A simplified low-frequency prediction model,. *IEEE Trans. on Electromagnetic Compatibility*, vol. EMC-21, pp. 105–114, May 1979.

[62] C. Yen, Z. Fazarinc, and R. L. Wheeler. Time-domain shin effect model for transient analysis of lossy transmission lines. *Proc. IEEE*, vol. 70, pp. 750–757, 1982.

[63] J. Poltz and A. Wexler. Transmission line analysis of PC boards. *VLSI Systems Design*, pp. 38–43, Mar. 1986.

[64] A. Ang, K. Ehn, J. Poltz, and A. Wexler. Analyzing PC board electrical performance using field theory. *In Automated Design and Eng. for Electronics West-Proc. Tech. Sessions*, pp. 21–30, 1986.

[65] R.L. Khan and G. I. Costache. Finite element method applied to modeling crosstalk problem on printed circuit boards. *IEEE Trans. on Electromagnetic Compatibility*, vol. 31, pp. 5–15, Feb. 1989.

[66] T. Vu Dinh, B. Cabon, and J. Chilo. New skin-effect equivalent circuit. *Electronic Letter*, vol. 26, pp. 1582–1584, Sept. 1990.

[67] T. Vu Dinh, B. Cabon, and J. Chilo. Time domain analysis of skin effect on lossy interconnection. *Electronic Letter*, vol. 26, pp. 1582–1584, Dec. 1990.

[68] D. N. Ladd and G. I. Costache. SPICE simulation used to characterize the cross-talk reduction effect of additional tracks ground with vias on printed circuit boards. *IEEE Trans. on Circuits and System-II:Analog and Digital Signal Processing*, vol. 39, pp. 342–347, June 1992.

[69] C. R. Paul. *Introduction to Electromagnetic Compatibility*. John Willy & sons, New York, 1992.

[70] A. Ahmadouche and J. Chilo. Optimum computation of capacitance coefficients of multilevel interconnecting lines for advanced package. *IEEE Trans. Components, Hybrid, Manuf. Technol.*, vol. 12, pp. 124–129, Mar. 1989.

[71] S. Mukherjee and M. Morjaria. On the efficiency and accuracy of the boundary element method and the finite element method. *Int. J. Numer. Meth. Eng.*, vol. 20, pp. 515–522, 1984.

[72] I. Stakgold. *Boundary value problem of mathematical physics*. volume 2. Macmillan, New York, 1968.

[73] M. Ouda and A. Sebak. Minimizing the computational cost and memory requirements for the capacitance calculation of 3-d multiconductor systems. *IEEE Trans. Components, Hybrid, Manuf. Technol.*, vol. 18, pp. 685–689, Sept. 1995.

[74] M. Ouda and A. Sebak. Efficient technique for the capacitance calculation of 3-d multiconductor systems. *Proce. ANTEM, Ottawa*, pp. 455–458, Aug. 1994.

[75] K. Mahadevan and H. A. Auda. Electromagnetic field of a rectangular patch of uniform and linear distributions of current. *IEEE Trans. Antenna and Propag.*, vol. AP-37, pp. 1503–1509, Dec. 1989.

[76] V. Rokhlin. Rapid solution of integral equation of classical potential theory. *J. of Computational Physics*, vol. 60, pp. 187–207, Sept. 1985.

[77] Y. Saad and A. Sameh. A parallel block stiefel method for solving positive definite system. In M.H. Schults, editor. *Elliptic problem solver*, pp. 405–412, Academic Press, New York, 1981.

[78] Y. Saad and M.H. Schults. GMRES: A generalized minimal residual algorithm for solving nonsymmetric linear systems. *SIAM J. on Scientific and Statistical Computing*, vol. 7, pp. 856–869, July 1986.

[79] M. Ouda and A. Sebak. Capacitance calculation and its application to integrated circuits interconnections. *Proce. ANTEM, Ottawa*, pp. 247–250, Aug. 1994.

[80] C.A. Brebbia and J. Dominguez. *Boundary elements an introductory course*. McGraw Hill, New York, 1992.

[81] C. A. Desoer. *Basic circuit theory*. McGraw-Hill, New York, 1969.

[82] M. Ouda and A. Sebak. Efficient method for frequency dependent inductance and resistance calculations. *Proce. WESCANEX*, vol. 2, pp. 473–477, May 1995.

[83] Charles S. Walker. *Capacitance, inductance and crosstalk analysis*. Artech House Inc., Boston, 1990.

[84] J.D. Jackson. *Classical electrodynamics*. second edition, Wiley, New York, 1975.

[85] W.T. Weeks, L.L. Wu, M.F. McAllistewr, and A. Singh. Resistive and inductive skin effect in rectangular conductors. *IBM J. Res. Develop*, vol. 23, pp. 652–660, Nov. 1979.

[86] R. Kamikawai, M. Nishi, K. Nakanishi, and A. Masaki. Electrical parameter analysis from three dimensional interconnection geometry. *IEEE Trans. Components, Hybrid, Manuf. Technol.*, vol. 8, pp. 269–274, June 1985.

[87] W. I. Bowman and J. M. McNamee. Development of equivalent Pi and T matrix circuits for long untransposed transmission lines. *IEEE Trans. on Power Apparatus and System.*, vol. PAS-85, pp. 625–632, 1964.

[88] R. F. German, H. W. ott, and C. R. Paul. Effect of an image plane on printed circuit board radiation. *IEEE EMC Int. Symp.*, pp. 282–291, Aug. 1990.

[89] C. R. Paul. Modeling electromagnetic interference properties on printed circuit boards. *IBM J. Res. Develop.*, vol. 33, pp. 33–50, Jan. 1989.